(12)

ALEX(01)-TR-78-09

LEVEL II

APPLICATION OF A COMBINED SOURCE MODEL FOR SEISMIC DISCRIMINATION

TECHNICAL REPORT NO. 21
VELA NETWORK EVALUATION AND AUTOMATIC PROCESSING RESEARCH

Prepared by
Helmut Y. A. Hsiao

TEXAS INSTRUMENTS INCORPORATED
Equipment Group
Post Office Box 6015
Dallas, Texas 75222

Prepared for

AIR FORCE TECHNICAL APPLICATIONS CENTER
Alexandria, Virginia 22314

Sponsored by

ADVANCED RESEARCH PROJECTS AGENCY
Nuclear Monitoring Research Office
ARPA Program Code No. 7F10
ARPA Order No. 2551

25 October 1978

Acknowledgment: This research was supported by the Advanced Research Projects Agency, Nuclear Monitoring Research Office, under Project VELA-UNIFORM, and accomplished under the technical direction of the Air Force Technical Applications Center under Contract Number F08606-77-C-0004.

ALEX(01)-TR-78-09

APPLICATION OF A COMBINED SOURCE MODEL FOR SEISMIC DISCRIMINATION

TECHNICAL REPORT NO. 21
VELA NETWORK EVALUATION AND AUTOMATIC PROCESSING RESEARCH

Prepared by
Helmut Y. A. Hsiao

TEXAS INSTRUMENTS INCORPORATED
Equipment Group
Post Office Box 6015
Dallas, Texas 75222

Prepared for

AIR FORCE TECHNICAL APPLICATIONS CENTER
Alexandria, Virginia 22314

Sponsored by

ADVANCED RESEARCH PROJECTS AGENCY
Nuclear Monitoring Research Office
ARPA Program Code No. 7F10
ARPA Order No. 2551

25 October 1978

Acknowledgment: This research was supported by the Advanced Research Projects Agency, Nuclear Monitoring Research Office, under Project VELA-UNIFORM, and accomplished under the technical direction of the Air Force Technical Applications Center under Contract Number F08606-77-C-0004.

UNCLASSIFIED

SECURITY CLASSIFICATION OF THIS PAGE (When Data Entered)

REPORT DOCUMENTATION PAGE		READ INSTRUCTIONS BEFORE COMPLETING FORM
1. REPORT NUMBER	2. GOVT ACCESSION NO.	3. RECIPIENT'S CATALOG NUMBER
4. TITLE (and Subtitle) (4) APPLICATION OF A COMBINED SOURCE MODEL FOR SEISMIC DISCRIMINATION.		5. TYPE OF REPORT & PERIOD COVERED (9) Technical rept. no. 21
		6. PERFORMING ORG. REPORT NUMBER (14) TI-ALEX(01)-TR-78-09
7. AUTHOR(s) (10) Helmut Y. A. Hsiao		8. CONTRACT OR GRANT NUMBER(s) F08606-77-C-0004
9. PERFORMING ORGANIZATION NAME AND ADDRESS Texas Instruments Incorporated Equipment Group Dallas, Texas 75222		10. PROGRAM ELEMENT, PROJECT, TASK AREA & WORK UNIT NUMBERS VELA T/8705/B/PMP
11. CONTROLLING OFFICE NAME AND ADDRESS Advanced Research Projects Agency Nuclear Monitoring Research Office Arlington, Virginia 22209		12. REPORT DATE (11) 25 Oct 1978
		13. NUMBER OF PAGES 101 (12) 102p.
14. MONITORING AGENCY NAME & ADDRESS (if different from Controlling Office) Air Force Technical Applications Center VELA Seismological Center Alexandria, Virginia 22314		15. SECURITY CLASS. (of this report) UNCLASSIFIED
		15a. DECLASSIFICATION/DOWNGRADING SCHEDULE

16. DISTRIBUTION STATEMENT (of this Report)

APPROVED FOR PUBLIC RELEASE, DISTRIBUTION UNLIMITED

17. DISTRIBUTION STATEMENT (of the abstract entered in Block 20, if different from Report)

(15) F08606-77-C-0004; ARPA Order-2551

18. SUPPLEMENTARY NOTES

ARPA Order No. 2551

19. KEY WORDS (Continue on reverse side if necessary and identify by block number)

Long-period teleseismic surface wave
Seismic source parameter estimation
Seismic source mechanism
Combined source
Moment versus m_b plot
Amplitude spectral fitting
Seismic discrimination

20. ABSTRACT (Continue on reverse side if necessary and identify by block number)

The purpose of this study has been to use the observed long-period teleseismic surface wave data of earthquakes and presumed underground explosions to determine the source mechanisms and to use these source mechanism estimates to discriminate between the two classes of events. In order to demonstrate this purpose, fifteen events have been selected and analyzed for the Russian Eastern Kazakh (EKZ) region, central and northern Eurasia, and the United States Nevada Test Site (NTS). → next page

DD FORM 1 JAN 73 1473 EDITION OF 1 NOV 65 IS OBSOLETE

4/05 076

UNCLASSIFIED

SECURITY CLASSIFICATION OF THIS PAGE (When Data Entered)

JOB

20. continued

The observation stations available for this study included the Seismic Research Observatories (SRO), Abbreviated Seismic Research Observatories (ASRO), the High Gain Long-Period (HGLP) stations (the same as the previous VLPE), and existing VELANET arrays.

For a fair comparison of explosion and earthquake events, both have been treated in the same way by using the combined source model which combines a point explosive source and a point double-couple source.

In order to cut down computer expenses and widen the searching range of some parameters, a binary exhaustive search method was applied to modify the amplitude spectral fitting process without any constraint. The results obtained from this modified process gave very good spectral fits for most events and lowered the minimum residual fitting error of each event.

The estimated seismic moment versus m_b plot has been found to be very promising for the purpose of discrimination between earthquakes and explosions. Taking the surface wave seismic moment to be a universal scaling parameter for sizing events, the average m_b of explosions is one magnitude greater than the average m_b of earthquakes. As expected, this indicates more efficient radiation of high frequency P-waves for explosions of equal moment. Since this criterion appears to apply equally to both Nevada Test Site and Eastern Kazakh presumed explosions, it suggests that surface wave moment estimates may be a more universal parameter than M_s for scaling the size of earthquakes and explosions. This inference from our results needs further investigation.

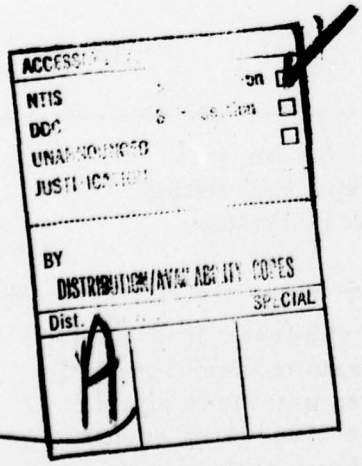

ABSTRACT

The purpose of this study has been to use the observed long-period teleseismic surface wave data of earthquakes and presumed underground explosions to determine the source mechanisms and to use these source mechanism estimates to discriminate between the two classes of events. In order to demonstrate this purpose, fifteen events have been selected and analyzed for the Russian Eastern Kazakh (EKZ) region, central and northern Eurasia, and the United States Nevada Test Site (NTS).

The observation stations available for this study included the Seismic Research Observatories (SRO), Abbreviated Seismic Research Observatories (ASRO), the High Gain Long-Period (HGLP) stations (the same as the previous VLPE), and existing VELANET arrays.

For a fair comparison of explosion and earthquake events, both have been treated in the same way by using the combined source model which combines a point explosive source and a point double-couple source.

In order to cut down computer expenses and widen the searching range of some parameters, a binary exhaustive search method was applied to modify the amplitude spectral fitting process without any constraint. The results obtained from this modified process gave very good spectral fits for most events and lowered the minimum residual fitting error of each event.

The estimated seismic moment versus m_b plot has been found to be very promising for the purpose of discrimination between earthquakes and explosions. Taking the surface wave seismic moment to be a universal scaling parameter for sizing events, the average m_b of explosions is one magnitude greater than the average m_b of earthquakes. As expected, this

indicates more efficient radiation of high frequency P-waves for explosions of equal moment. Since this criterion appears to apply equally to both Nevada Test Site and Eastern Kazakh presumed explosions, it suggests that surface wave moment estimates may be a more universal parameter than M_s for scaling the size of earthquakes and explosions. This inference from our results needs further investigation.

TABLE OF CONTENTS

TABLE OF CONTENTS
(continued)

LIST OF FIGURES

LIST OF FIGURES
(continued)

LIST OF TABLES

SECTION I
INTRODUCTION

The primary intention of this report is to obtain a better understanding of earthquake and explosion source mechanisms as determined from long-period surface wave spectra and to apply these results to discriminating between earthquakes and explosions. Tsai's method, an exhaustive comparison scheme between the observed and theoretical spectra, was used and modified by applying the binary method to search through the following three source parameters; depth, strike angle, and F value (F is the ratio of the point radial and double-couple source terms). The purpose of this modification is to economize computer expenses and to acquire more precise source parameter estimates over a wider range of the F value. In order to improve the source representation, a combined source model which consists of a point double-couple source and a point explosive source was utilized to analyze all the events selected. The following report represents the results of study on long-period surface waves of fifteen EKZ, Eurasian, and NTS events.

Section II offers a detailed description of the data selection, data processing, data availability and data quality of this study. In Section III, a brief summary of the theoretical source description, the procedures to obtain observed surface wave spectra, and the amplitude spectra fitting process is presented. The results of source mechanism and source discrimination are discussed in Section IV. Finally, in Section V, the directions this study expects to take in the future are discussed.

SECTION II
DATA BASE

A. DATA SELECTION

In the previous report (Sun, 1977), twenty-seven underground nuclear explosions from three different regions, the United States Nevada Test Site (NTS), the Russian eastern Kazahk (EKZ), and North Caspian Sea area, were selected by means of chronologically exhaustive search (starting from 1976 and progressing backward into 1975, 1974 and so on) through the Norwegian Seismic Array (NORSAR) bulletin and Preliminary Determination of Epicenters (PDE) bulletin. The availability and quality of NTS events data are much better than that of the EKZ events data. Therefore, in this year's study, only EKZ events as a group of presumed explosions were searched (covering 1976 to 1977) using the National Earthquake Information Service (NEIS) list and PDE bulletin. In the same way, an attempt was made to search and select as many recent Eurasian earthquakes as possible to satisfy the purpose of this study.

In the preliminary list, there were eighteen EKZ events (eight in 1976 and ten in 1977) and twenty-one Eurasian events (nine in 1976 and twelve in 1977). However, considerable numbers of those events were lost due to operational and recording problems, the details of which are discussed in Subsection C. Therefore, two processed earthquakes and five presumed underground nuclear explosions were selected from previous reports (Lambert et al., 1974 and Sun, 1977) to supplement the data base. Based on these processed events and the preliminary list, the availability of good quality long-period teleseismic surface wave data was examined and the final list of the selected events was obtained. This final list of events is depicted in Table II-1.

TABLE II-1

LIST OF THE SELECTED EVENTS AND THEIR DATA AVAILABILITY
(PAGE 1 OF 3)

(a) EKZ Events

	Event I. D. Date	Location		Origin Time	m_b	Sub. Region	Station I. D.														
		Lat. °N	Lon. °E				HGLP (VLPE)					SRO					ASRO				Array		
							5	6	7	8	9	30	35	36	38	41	50	51	52	53	A	L	N
	EKZ/03/20/76 03/20/76	50.0	77.3	04.03.39	5.1	329			B			B	B	B	B								
	EKZ/06/29/77 06/29/77	50.0	78.9	03.06.58	5.5	329							B	R	R								
	EKZ/09/05/77 09/05/77	50.1	78.9	03.02.57	5.9	329													B	B			
	EKZ/10/29/77 10/29/77	49.8	78.1	03.06.57	5.5	329							B						R	B			
*	EKZ/723/73 07/23/73	50.0	78.9	01.22.58	5.3	329															L	R	B
*	EKZ/1214/3 12/14/73	50.0	79.0	07.46.57	6.0	329															B	R	R
*	EKZ/427/75 04/27/75	50.0	79.0	05.36.57	5.6	329		R			R	R											R

B: Both Rayleigh and Love Wave R: Only Rayleigh Wave L: Only Love Wave

*: Event Selected from Previous Report (Use the same event names as before)

TABLE II-1

LIST OF THE SELECTED EVENTS AND THEIR DATA AVAILABILITY
(PAGE 2 OF 3)

(b) Eurasian Events

Event I. D. Date	Location		Origin Time	m_b	Sub. Region	Station I. D.														
	Lat. °N	Lon. °E				HGLP (VLPE)							SRO						ASRO			
						1	2	3	4	5	6	7	30	33	35	36	38	41	50	51	52	53
UZB/07/14/77 07/14/77	40.3	63.6	05.49.08	5.5	339										B		B			B	B	B
LBR/08/10/77 08/10/77	50.9	110.7	21.59.58	5.2	327													B			L	
NVZ/09/01/77 09/01/77	73.3	54.5	02.59.57	5.7	648								B	R			B	L			B	
* ECU/02/03/72 02/03/72	40.7	48.4	02.29.22	5.1	337			R	B		B	B										
* TZK/03/17/72 03/17/72	40.1	69.7	09.17.11	5.2	715			B	B		B											

B: Both Rayleigh and Love Wave R: Only Rayleigh Wave L: Only Love Wave

*: Event Selected from Previous Report

TABLE II-1

LIST OF THE SELECTED EVENTS AND THEIR DATA AVAILABILITY
(PAGE 3 OF 3)

(c) NTS Events

	Event I. D. Date	Location		Origin Time	m_b	Sub. Region	Station I. D.													
		Lat. °N	Lon. °W				HGLP (VLPE)									SRO				
							1	2	3	4	5	6	7	8	9	30	33	35	36	38	41
	NTS/02/07/76 02/07/76	37.2	116.4	07.36.55	4.3	41	B						B			B					
*	NTS/212/76 02/12/76	38.0	116.0	14.45.06	6.3	41				R		B		R	B						
*	NTI/317/76 03/17/76	38.0	115.0	14.15.04	6.1	41	R	R				B	B	R	B						

B: Both Rayleigh and Love Wave R: Only Rayleigh Wave L: Only Love Wave

*: Event Selected from Previous Report (Use the same event names as before)

B. DATA PROCESSING

After selecting the events, the next effort was to obtain the desired surface wave amplitude spectra from ten to fifty seconds for the estimation of the seismic source parameters. In order to obtain these amplitude spectra, the field tapes which contain the surface wave recordings for the selected events at all available observation stations were processed as follows:

- The desired surface wave recordings on the field tape were edited to yield the event signal which usually consists of 3·N signal traces, where N is the number of recording sites in a station, i. e. N= 1 for a single-site station. In general, the 3·N signal traces in the edited event signal were the vertical and two horizontal (oriented in N-S and E-W direction) recordings. The vertical Rayleigh wave signal was obtained from the vertical recording while the radial Rayleigh wave and transverse Love wave signals were obtained by properly rotating the two horizontal recordings. For the array stations, in addition to the rotation of horizontal recordings, the edited event signal was beamformed.

- The edited event signal with proper rotation of its traces (and beamforming for array stations) was reformatted to form the event files on 7 track tape to drive the processing programs in the PDP-15/50 computer.

- For each event signal in the event files, each component trace (Rayleigh or Love wave) was analyzed for evidence of multipathing by applying a series of narrowband filters (as discussed by Turnbull et al., 1974; Sun and Shaub, 1977). At each period, group velocities were determined for each multipath and were compared to the standard group velocity curves for the type of

travel path encountered (see example in Sun, 1976). Estimating the correct multipath from this comparison, the amplitude spectra were obtained. These raw observed amplitude spectra were then corrected for the station instrument response to yield the desired observed amplitude spectra for the estimation of the surface wave travel path attenuation. These raw observed amplitude spectra with appropriate instrument response correction were further corrected for geometrical spreading and travel path attenuation, to yield the corrected observed amplitude spectra. This corrected amplitude spectra was used for the examination of the surface wave spectra and the estimation of the seismic source parameters.

In the above described surface wave data reduction procedure, the two steps and the spectral correction in the third step are carried out by batch processing on the IBM 360/44 computer. The third step involving the narrowband filtering was accomplished using the Extended Interactive Seismic Processing System (ISPSE) developed by Texas Instruments using PDP-15/50 interactive graphics.

C. DATA AVAILABILITY AND QUALITY

According to the work statement of this year, it was requested that Texas Instruments use long-period surface wave data from the Seismic Research Observatories (SRO), Abbreviated Seismic Research Observatories (ASRO), the High Gain Long-Period (HGLP) stations (the same as the previous VLPE), and existing VELANET array data. The intention of including as many existing long-period recording stations as possible is understandable in that it provides better azimuthal coverage and better data availability. In this study, array data was not used because of the absence of useable signals caused by the distance from the source areas of interest, and in some cases recording

malfunctions. In part, the loss of data from the VELANET arrays was compensated by including ASRO data. For example, some of the KAA and MAJ ASRO data was substituted for the ILPA and KSRS data respectively. This substitution increased the azimuthal coverage to a level considered satisfactory in most cases. The criteria for azimuthal coverage will be covered later.

After checking the availability of the surface wave recordings and examining the results of the processed surface wave signals from all available recordings, the final list of the selected events was obtained as shown in Table II-1. Table II-1 gives the event name, date, origin time, location, and PDE m_b, together with the availability of good quality surface wave recordings indicated by the letter 'B', 'R', or 'L' under the 'STATION I. D.' heading. Stations are identified by the station number (1. 2. 3. . . .). 'B' means that both Rayleigh and Love wave recordings are useable, 'R' means that only the Rayleigh wave recording is useable, and 'L' means that only the Love wave recording is useable. The descriptions of the available observation stations are given in Table II-2, including station name, location, and identification number or letter. It can be seen that the final list of this year's selected events consists of eight events (three Eurasian events, four EKZ events, and one NTS event) instead of the thirty nine events in the preliminary list. The loss of events from the preliminary list was mainly caused due to the following:

- Bad field tapes which could not be edited for the desired events,
- Clipped data,
- Non-detectable data,
- Mixed events which contain more than one event in the desired signal gate,
- Malfunctions which could indicate any non-seismic occurrence which, occurring in the signal gate, would mask the seismic data under analysis. The types of malfunctions commonly ob-

TABLE II-2

DESCRIPTION OF OBSERVATION STATIONS

	Station I. D.		Station Location		
	#	Name	City and Country	Lat. °N	Lon. °E
HGLP (VLPE)	1	CTA	Charters Towers, Australia	-20.0	146.2
	2	CHG	Chiang Mai, Thailand	18.7	98.9
	3	FBK	Fairbanks, Alaska	64.9	-148.0
	4	TLO	Toledo, Spain	39.0	-4.0
	6	KON	Kongsberg, Norway	59.7	9.6
	7	OGD	Ogdensburg, New Jersey	41.1	-74.6
	8	KIP	Kipapa, Hawaii	21.4	-158.0
	9	ALQ	Albuquerque, New Mexico	34.9	-106.5
	10	ZLP	La Paz, Bolivia	-16.5	-68.1
SRO	30	ANMO	Albuquerque, New Mexico	34.9	-106.5
	33	CHTO	Chiang Mai, Thailand	18.7	98.9
	35	GUMO	Guam, Marianas Island	13.6	144.9
	36	MAIO	Mashhad, Iran	36.3	59.5
	38	NWAO	Narrogin, Western Australia	-32.9	117.24
	41	TATO	Taipei, Taiwan	25.0	121.5
ASRO	52	KAAO	Kabul, Afghanistan	34.5	69.04
	53	MAJO	Matsushiro, Japan	36.5	138.2
Array	A	ALPA	Alaska	65.2	-147.7
	L	LASA	Montana	46.7	-106.2
	N	NORSAR	Norway	60.8	10.9

served on the SRO, ASRO, and HGLP data were glitches, uncorrectable spikes, data dropouts, and calibration signals.

According to the above five criteria, only about twenty per cent of the event-stations corresponding to the twenty five events remained to be used. Fifteen per cent of total event-stations were lost due to bad field tapes, ten per cent due to malfunctions, twenty per cent due to mixed events, and thirty five per cent due to non-detectable data. In addition, nineteen of the twenty-seven events which had less than three good edited surface wave traces at two observation stations were discarded. This last condition for rejecting an event was based on the previous result that the source parameters of a given seismic event could be satisfactorily estimated with good quality surface wave recordings at two observation stations in two consecutive quadrants (Turnbull, et al., 1973). From the data availability indicated in Table II-1, it is obvious that the SRO and ASRO stations present more and better quality data than HGLP stations do.

In order to get better results, seven processed events (two from Eurasian events, two from NTS events, and three from EKZ events), as given in Table II-1, have been selected from previous reports to enlarge the data base of this task. Table II-3 presents the station azimuthal angles with respect to those event locations and the epicenter distances from those event locations to each observation station. In general, the station coverage for the selected events is thought to be satisfactory in terms of station azimuthal distribution and epicenter distances for the purposes of this study.

TABLE II-3

STATION AZIMUTHAL ANGLES AND EPICENTER DISTANCES FROM THE SELECTED EVENTS
(PAGE 1 OF 5)

(a) EKZ Events

	Station I. D.		EKZ/03/20/76 50.0N 77.3E		EKZ/06/29/77 50.0N 78.9E		EKZ/09/05/77 50.1N 78.9E		EKZ/10/29/77 49.8N 78.1E	
	#	Name	AZ	Δ	AZ	Δ	AZ	Δ	AZ	Δ
SRO	30	ANMO	3.1	95.2	4.4	95.1	4.4	95.0	3.7	95.4
SRO	35	GUMO	98.3	65.3	99.6	64.3	99.6	64.3	98.8	64.8
SRO	36	MAIO	-130.0	18.8	-126.9	19.6	-127.1	19.7	-128.1	19.0
SRO	38	NWAO	147.2	90.0	148.5	89.5	148.5	89.5	147.8	89.6
ASRO	52	KAAO	-155.5	16.6	-151.2	17.1	-151.3	17.1	-153.3	16.6
ASRO	53	MAJO	83.2	45.1	84.3	44.0	84.4	44.0	83.4	44.6
HGLP	7	OGD	-20.8	85.8	-19.7	86.2	-19.7	86.1	-20.3	86.2

AZ = Station Azimuth at Source (+ for NE)

Δ = Distance between Station and Source in degrees

TABLE II-3

LIST OF THE SELECTED EVENTS AND THEIR DATA AVAILABILITY
(PAGE 2 OF 5)

(a) EKZ Events (continued)

	Station I.D.		EKZ/723/73 50.0N 78.9E		EKZ/1214/3 50.0N 79.0E		EKZ/427/75 50.0N 79.0E	
	#	Name	AZ	Δ	AZ	Δ	AZ	Δ
Array	A	ALPA	20.8	59.4	20.8	59.4	20.8	59.4
	L	LASA	3.6	83.4	3.6	83.4	3.6	83.4
	N	NORSAR	-47.0	38.3	-47.0	38.3	-47.0	38.3
HGLP	6	KON	-47.4	40.4	-47.4	40.4	-47.4	40.4
	8	KIP	52.2	92.9	52.2	92.9	52.2	92.9
	9	ALQ	5.3	96.0	5.3	96.0	5.3	96.0

AZ = Station Azimuth at Source (+ for NE)

Δ = Distance between Station and Source in degree

TABLE II-3

STATION AZIMUTHAL ANGLES AND EPICENTER DISTANCES FROM THE SELECTED EVENTS
(PAGE 3 OF 5)

(b) Eurasian Events

	Station I. D.		UZB/07/14/77 40.3N 63.6E		LBR/08/10/77 50.9N 110.7E		NVZ/09/01/77 73.3N 54.5E	
	#	Name	AZ	Δ	AZ	Δ	AZ	Δ
SRO	30	ANMO	-8.4	104.4	29.7	88.3	-16.4	71.1
SRO	33	CHTO	114.7	37.2	-159.4	33.4	129.8	59.8
SRO	38	NWAO	137.2	88.3	174.5	83.8	125.0	114.1
SRO	41	TATO	89.1	50.2	158.2	27.2	104.6	59.6
ASRO	52	KAAO	141.3	7.2	-102.2	34.2	161.0	39.5

AZ = Station Azimuth at Source (+ for NE)

Δ = Distance between Station and Source in degrees

TABLE II-3

STATION AZIMUTHAL ANGLES AND EPICENTER DISTANCES FROM THE SELECTED EVENTS
(PAGE 4 OF 5)

(b) Eurasian Events (continued)

	Station I. D.		ECU/02/03/72 40.7N 48.4E		TZK/03/17/72 40.1N 69.7E	
	#	Name	AZ	Δ	AZ	Δ
HGLP (VLPE)	3	FBK	7.2	73.8	16.0	71.1
	4	TLO	-73.5	39.4	-64.5	54.8
	6	KON	-38.6	30.6	-41.4	41.6
	7	OGD	-39.5	83.4	-26.1	92.8

AZ = Station Azimuth at Source (+ for NE)

Δ = Distance between Station and Source in degrees

TABLE II-3

STATION AZIMUTHAL ANGLES AND EPICENTER DISTANCES FROM THE SELECTED EVENTS
(PAGE 5 OF 5)

(c) NTS Events

	Station I. D.		NTS/02/07/76		NTS/212/76		NTI/317/76	
			37.2N	116.4W	38.0N	116.0W	38.0N	115.0W
	#	Name	AZ	Δ	AZ	Δ	AZ	Δ
HGLP (VLPE)	1	CTA	-101.9	107.6	-101.4	108.1	-100.8	108.8
	2	CHG	-37.1	115.0	-36.5	114.5	-35.6	115.0
	4	TLO	45.9	81.2	46.2	80.4	46.8	79.9
	6	KON	25.3	73.6	25.5	72.7	25.9	72.4
	7	OGD	70.0	32.4	71.2	31.8	71.4	31.1
	8	KIP	-101.7	39.2	-102.4	39.7	-101.6	40.5
	9	ALQ	102.7	8.4	108.8	8.3	111.3	7.5
SRO	30	ANMO	102.7	8.4	108.8	8.3	111.3	7.5

AZ = Station Azimuth at Source (+ for NE)

Δ = Distance between Station and Source in degrees

SECTION III

THE PROCEDURE OF SOURCE PARAMETER ESTIMATION USING FAR-FIELD SURFACE WAVE DATA

Figure III-1 gives a schematical outline of the procedure to acquire the seismic source parameter estimation using long-period surface wave data. In this diagram, the following procedures are used after selecting events and before applying the amplitude spectra fitting process. The observed data are:

- The surface wave time traces were obtained by editing field tapes with satisfactory event signals.
- The edited time traces were analyzed using the ISPSE to obtain the demultipathed surface wave spectra (Sun and Shaub, 1977).
- The observed surface wave amplitude spectra are corrected for instrument response, geometric spreading, and travel path attenuation.

The theoretical data are:

- Earth models for calculation of the theoretical amplitude spectra.

The first two observed data listed above, were previously discussed in Section II. The third observed data and theoretical data listed above will be discussed in Subsections III-1 and III-3. Finally, the corrected observed spectra and the calculated theoretical spectra are input to an amplitude spectral fitting process to obtain estimates of the source parameters. This will be discussed in Subsection III-2.

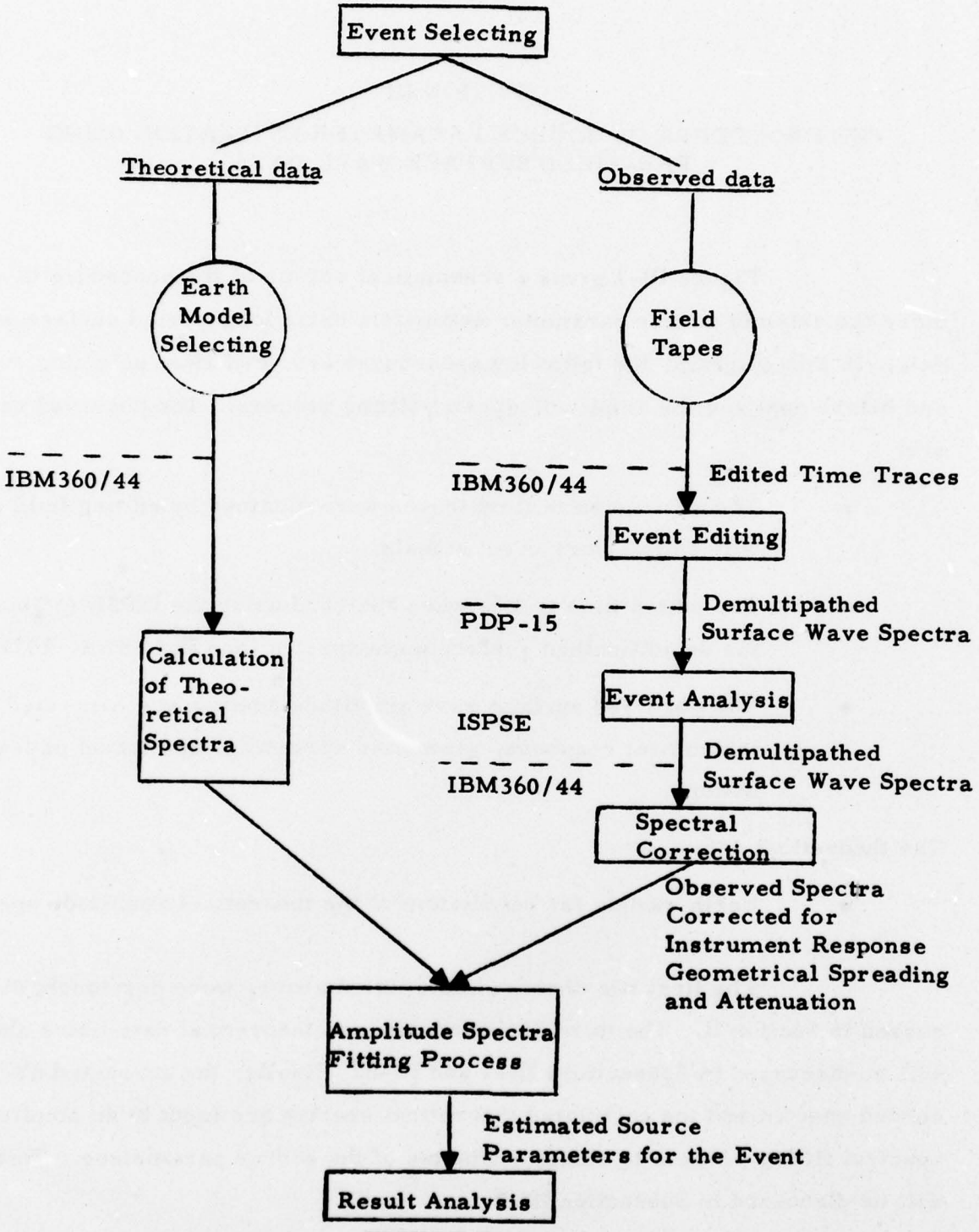

FIGURE III-1

SCHEMATIC DIAGRAM SHOWING A PROCEDURE TO OBTAIN THE SEISMIC SOURCE PARAMETER ESTIMATION USING FAR-FIELD SURFACE WAVE DATA

A. THE CORRECTIONS FOR THE INSTRUMENT RESPONSE, GEOMETRIC SPREADING, AND TRAVEL PATH ATTENUATION

For each event, the observed spectra are represented by spectral values at nine discrete periods, namely 10 to 50 seconds at 5 second increments. These spectra have been equalized at all observation stations in order to make direct comparison possible. Spectral equalization means that raw observed surface wave spectra have been corrected for the station's instrument response, geometric spreading, and travel path attenuation. Because these three corrections are well documented by Sun (1977), no detailed discussions of the theory will be given here.

The difficulty in correcting for the instrument response is not in the application, but in obtaining accurate instrument response curves for the different instruments used to measure the surface waves. An extreme example of the difficulty in obtaining accurate corrections is the HGLP network. During the initial assembly and installation of the HGLP (VLPE) systems, no attempt was made to standardize response characteristics. As a result, each component of each HGLP station had a unique response curve and unique digital sensitivity. Moreover, their response changes frequently, so that obtaining the correct instrument response for a specific time is a very difficult and tedious task. Fortunately, a standardized response curve for the HLGP system was initiated during 1976, and is now operating for the HGLP stations. Their instrumentation is calibrated daily with a step function input. A sine-wave calibration at a period of 30 seconds is applied once a month. Calibration constants and input levels can be obtained from the Albuquerque Seismological Laboratory. In ASRO and SRO systems, the response characteristics match the standard values to within plus or minus 10%. Digital recording sensitivity for the long-period data is set the same at all stations; 10,000 digital counts per micron of ground displacement at a period of 25 seconds for ASRO systems and 5,000 for SRO systems. Long-period channels are calibrated daily at

each station by a 25 second period sine-wave signal. Calibration constants and input levels also can be obtained from Albuquerque Seismological Laboratory.

The equation of correcting for geometrical spreading can be written as follows:

$$A_{cr_o} = A_{op}\left(\frac{Re \sin \Delta_p}{r_o}\right)^{1/2} \qquad \text{(III-1)}$$

where:

A_{cr_o} - amplitude corrected to reference point r_o

A_{op} - observed amplitude at observation station p

Δp - epicentral distance between source and p in degree

Re - radius of earth in kilometers

r_o - reference epicentral distance in kilometers.

According to this equation, it is obvious that all the observed data from different stations of the same event will be corrected to a standard distance one kilometer from the epicenter along different travel paths to reduce the effect of geometrical spreading.

The detailed geographic locations of the Eurasian events and the EKZ events are displayed in Figures III-2 and III-3, respectively. Figure III-4 shows the locations of the available observation stations in relation to the EKZ area together with the event-station travel paths. Observed Rayleigh wave amplitude spectra were available for nine sampled periods (T = 10 to 50 second, ΔT = 5 sec) of the seven events at most of the observation stations; while for the Love wave, the observed amplitude spectra were incomplete at almost half of the total stations. Figures III-5 and III-6 exhibit the locations of the available observation stations in relation to the Eurasian events and NTS area, together with the event-station travel paths. Except for the travel paths from

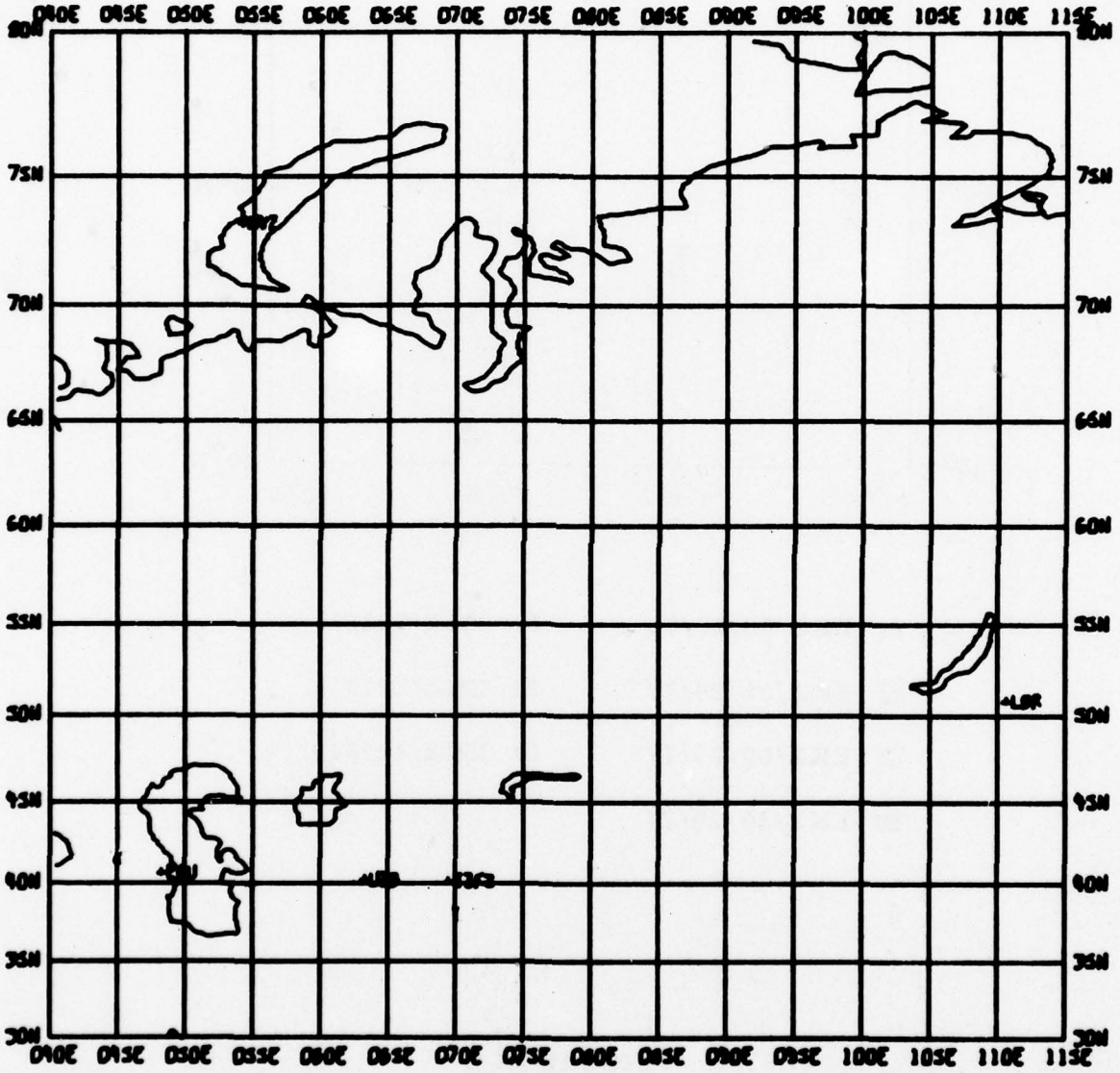

MILLER MODIFIED MERCATOR PROJECTION
MAP SCALE: 0.08000 INCHES/DEGREE LONGITUDE

FIGURE III-2

LOCATIONS OF THE SELECTED EURASIAN EVENTS

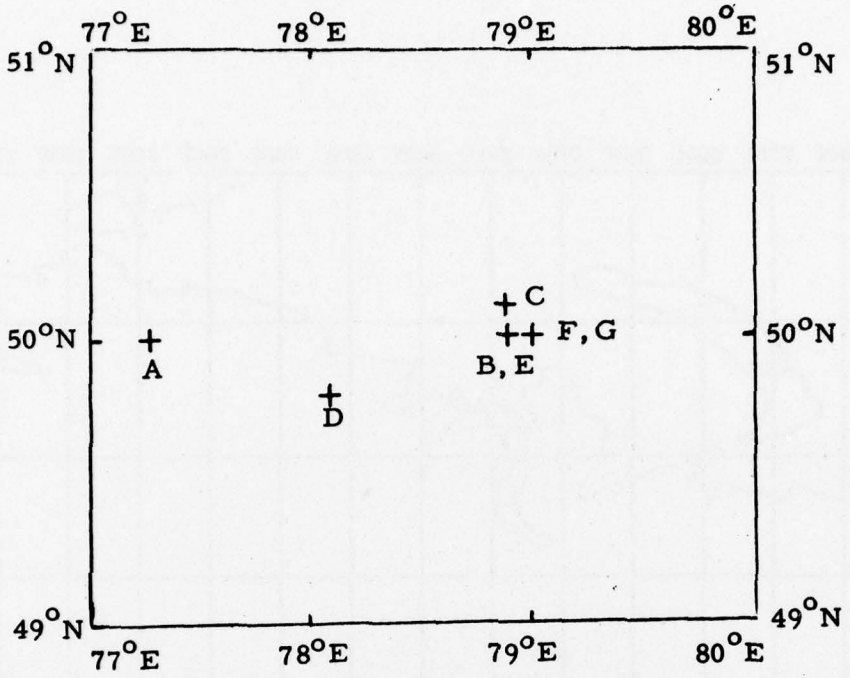

A: EKZ/03/20/76

B: EKZ/06/29/77

C: EKZ/09/05/77

D: EKZ/10/29/77

E: EKZ/723/73

F: EKZ/1214/3

G: EKZ/427/75

FIGURE III-3

LOCATIONS OF THE SELECTED EKZ EVENTS

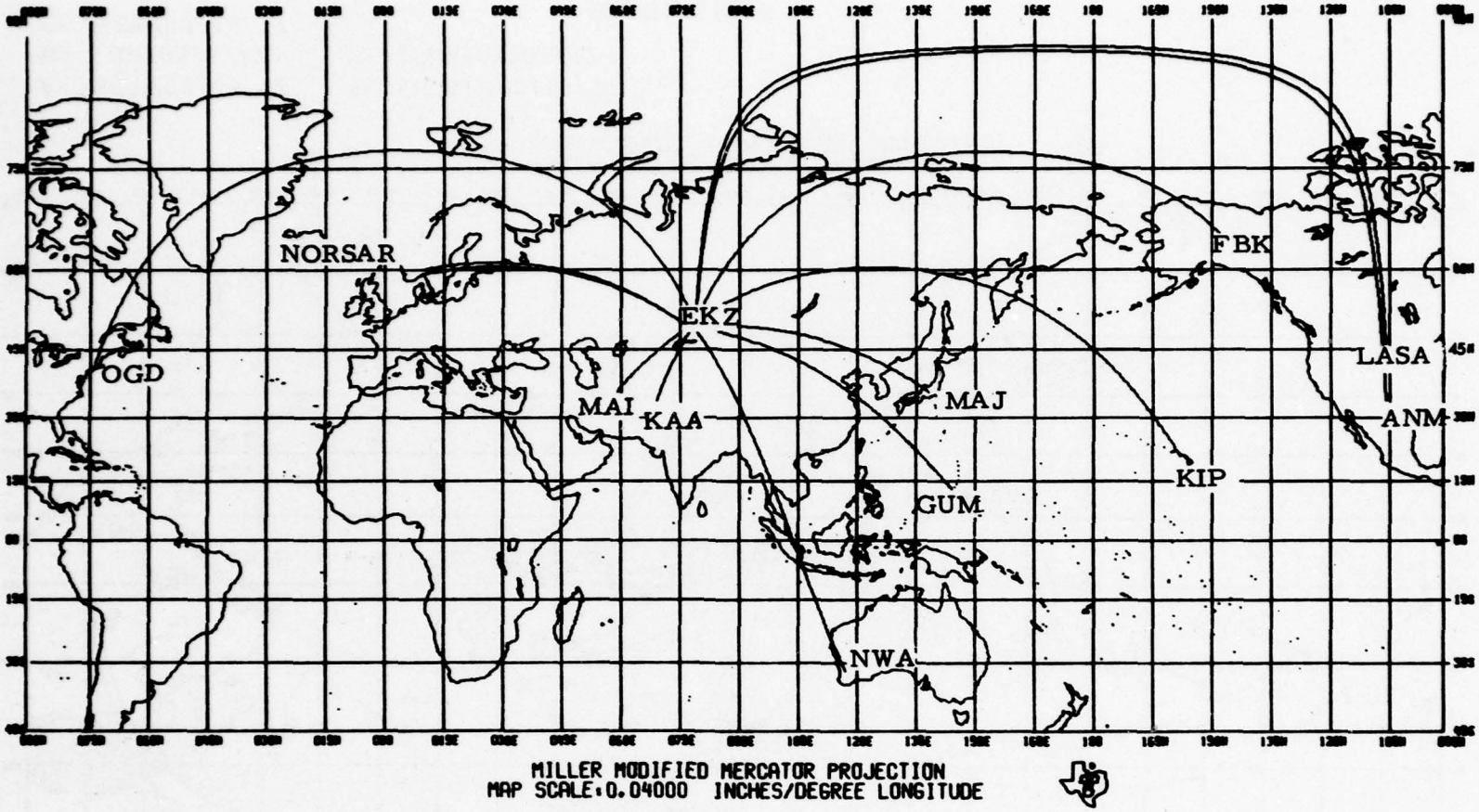

FIGURE III-4

LOCATIONS OF THE OBSERVATION STATIONS AND TRAVEL PATHS ENCOUNTERED TO THE EKZ

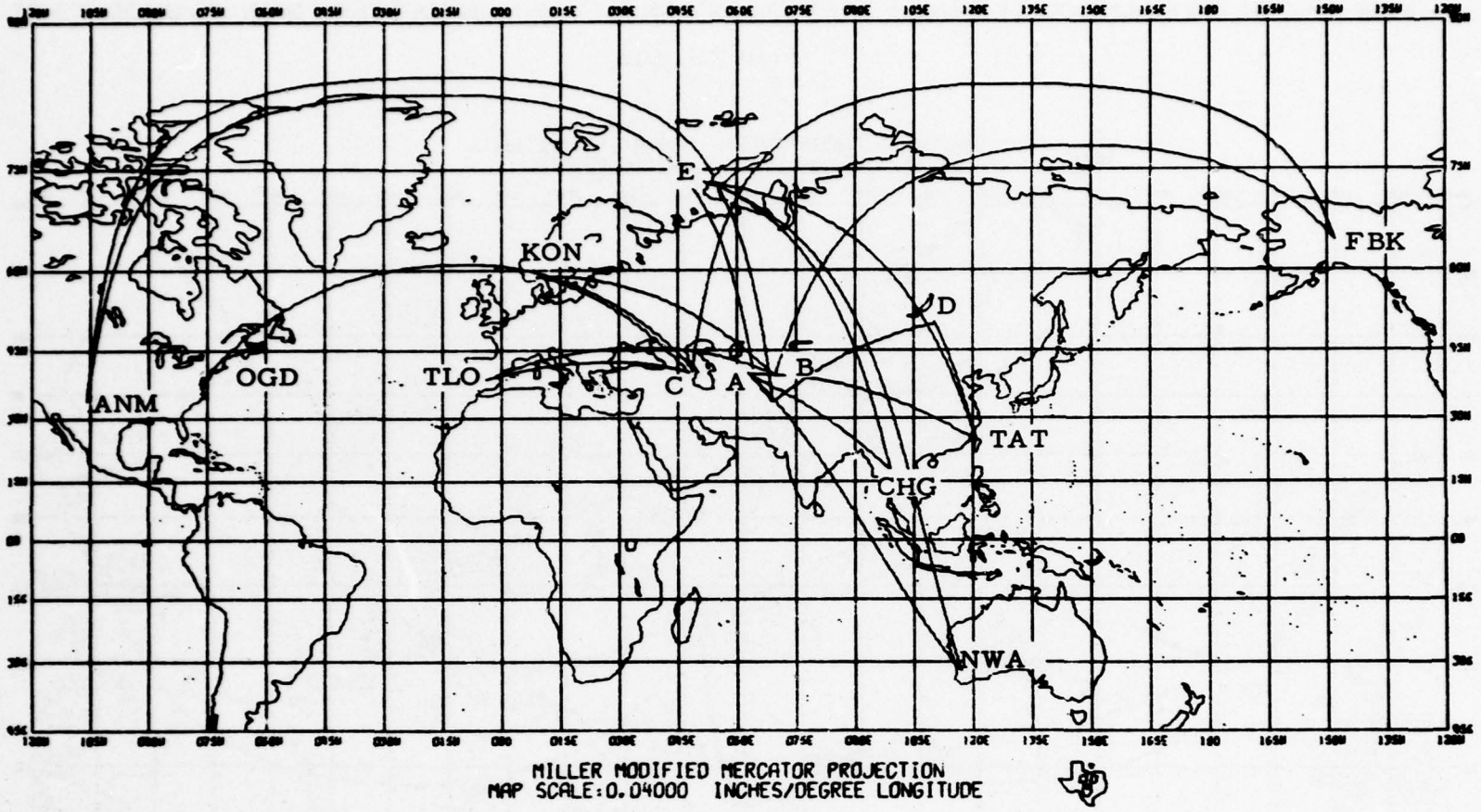

A: ECU/02/03/72
B: TZK/03/17/72
C: UZB/07/14/77
D: OLBR/08/10/77
E: NVZ/09/01/77

FIGURE III-5

LOCATIONS OF THE OBSERVATION STATIONS AND TRAVEL PATHS ENCOUNTERED TO THE EURASIAN EVENTS

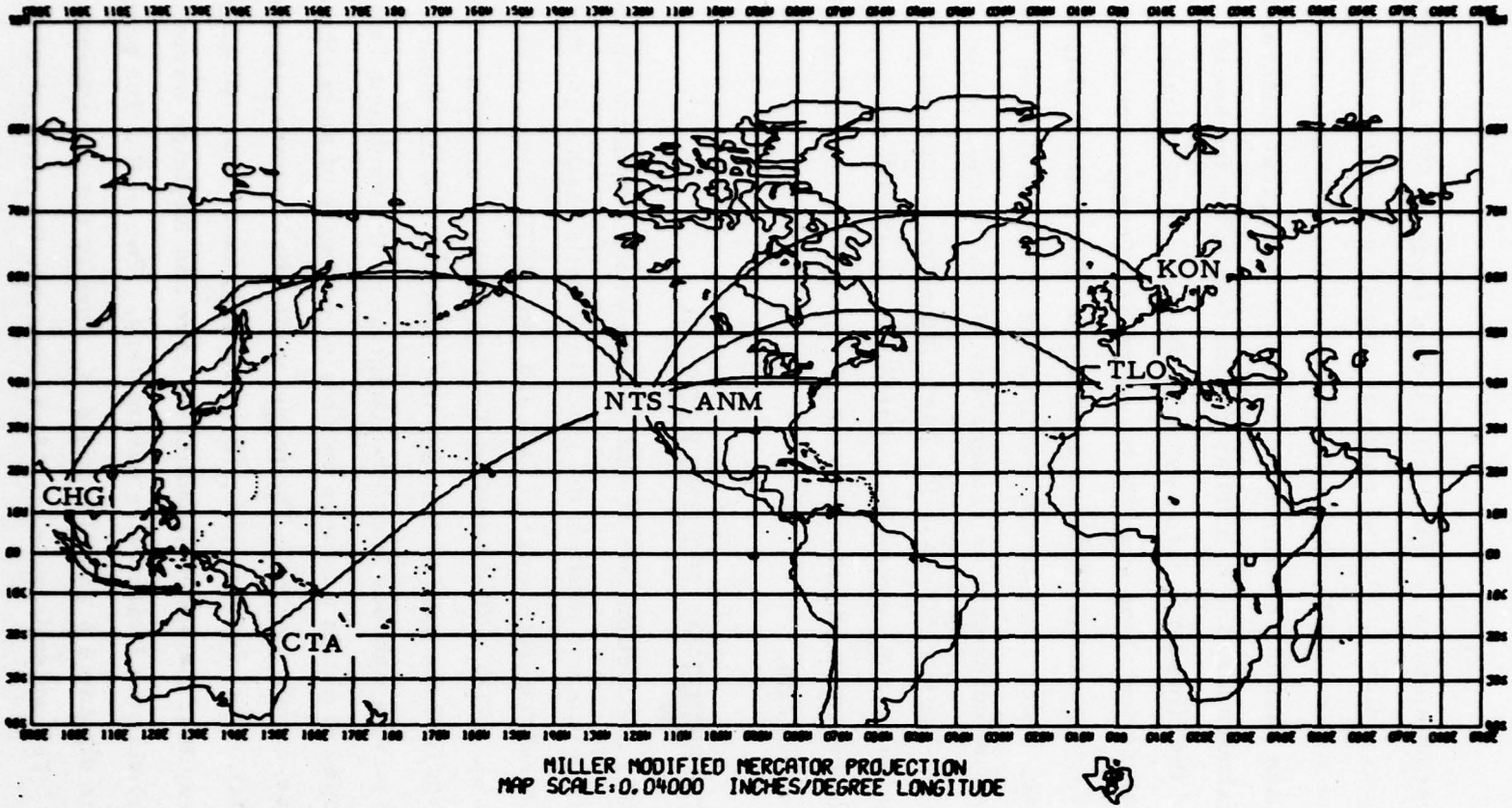

FIGURE III-6

LOCATIONS OF THE OBSERVATION STATIONS AND TRAVEL PATHS ENCOUNTERED TO THE NTS

NTS to the observation stations in the Pacific Ocean (such as KIP and CTA, which are entirely oceanic), the travel paths are either entirely continental or mixed. For the station, CHG, the spectral amplitudes are unusually small, indicating attenuation possibly caused by complicated geological features in central Eurasia; (abnormally thick crust approximately 60km thickness of the Tibet platform and the Himalayan fold system). Because of no reliable knowledge of energy attenuation along specific travel paths, Tryggvason's energy attenuation curve (Tryggvason, 1965) has been used. The general shape of Tryggvason's curve, which can affect the estimation of the focal depth and the source mechanism, is believed to be reasonable. Nevertheless, by using Tryggvason's attenuation correction in the past, the seismic moment estimates of numerous Eurasian seismic events have fitted very well with the seismic moment versus bodywave magnitude curve determined from the revised W^2-model given by Tsai (1972b).

B. AMPLITUDE SPECTRAL FITTING PROCESS

In this Subsection, we abstracted the whole amplitude spectral fitting process. This process utilizes the modified Tsai's method for the estimation of seismic source parameters (Tsai and Aki, 1970; Tsai and Shen, 1972; Turnbull, et al. 1973). The modified Tsai's method is an exhaustive searching scheme to find the best fit between the observed and the theoretically calculated surface wave amplitude spectra. Originally, the modified Tsai's method was developed to obtain a source parameter estimate of an earthquake modeled by a double-couple source. The model yields five source parameters; seismic moment (M), focal depth (h), dip (δ), slip (λ), and strike (ϕ) angle. It is sufficient to say that the spectral values of Love and Rayleigh waves of a given frequency depend on a total of five parameters. Two of the five parameters, namely the dip angle δ and slip angle λ, specify the orientation of the double-couple. The seismic moment M, represents the strength of the

double-couple. The parameter h, indicates the depth at which the equivalent point source of the earthquake dislocation is located in the layered half-space. For an explosion event with associated tectonic strain release, the theoretical source model which is used here combines a point explosive source and a point double-couple source. Theoretical surface wave spectra are generated by this combined source in a layered half-space earth. (Harkrider, 1964; Ben-Menahem and Harkrider, 1964; Toksöz, et al., 1965). The point explosive source models an ideal explosion and radiates only isotropic Rayleigh waves; while a point double-couple source models the explosion-associated tectonic strain release and radiates anisotropic Rayleigh and Love waves. Therefore, the resultant Rayleigh wave radiated from the combined source is the vector sum of the Rayleigh wave from the point explosion source and that from the point double-couple source. The resultant Love wave from the combined source comes entirely from the point double-couple source. The resultant amplitude spectra can be expressed as follows:

$$
\begin{aligned}
Y^R_{ij} &= \left| M_E \, LR_E(h, \delta, \lambda, \phi) + M_x \, LR_x(h) \right|_{ij} \\
&= M_E \left| LR_E + F \, LR_x \right|_{ij} \\
Y^L_{ij} &= M_E \left| LQ_E(h, \delta, \lambda, \phi) \right|_{ij}
\end{aligned}
\qquad \text{(III-2)}
$$

where

Y^R_{ij} and Y^L_{ij} are the theoretical Rayleigh and Love wave amplitude spectra of the combined source, respectively, for the i-th period at the j-th station,

LR_E and LQ_E are the theoretical Rayleigh and Love wave spectra of the double-couple source, respectively, for a seismic moment of one dyne-cm,

M_E and M_x are the moments of the double-couple source and the explosive source, respectively, and

F is the relative strength of the explosive source with respect to the double-couple source, i.e., $F = M_x/M_E$.

It is assumed here that the explosion-associated tectonic strain release takes place in the vicinity of the explosion, i.e., the depths of the explosion source and the double-couple source are the same. Therefore, for an explosion with tectonic strain release, there are six parameters involved in the theoretical source model. There are focal depth (h), dip angle (δ), slip angle (λ), strike angle (ϕ), seismic moment of the double-couple source (M_E), and the relative strength of the explosion (F). The geometry of the double-couple source which models the explosion-associated tectonic strain release is shown in Figure III-7.

Let $s_p\ (\delta, \lambda, \phi, h, F)$ be a member in a predefined set of source parameters $S\ (\delta, \lambda, \phi, h, F)$. The exhaustive search in the amplitude spectral fitting process tests each member in S and obtains the member which yields the best fit between the observed and the theoretically calculated surface wave amplitude spectra. The entire set of the source parameters S can be conveniently defined by the upper and lower bounds of each source parameter with discrete increment, that is:

$h_1 \le h \le h_m$ with increment of Δh

$\delta_1 \le \delta \le \delta_k$ with increment of $\Delta\delta$

$\lambda_1 \le \lambda \le \lambda_\ell$ with increment of $\Delta\lambda$

$\phi_1 \le \phi \le \phi_n$ with increment of $\Delta\phi$

$F_1 \le F \le F_q$ with increment of ΔF

where m, k, ℓ, n, and q are positive integers. Thus, the entire set S is a discrete set consisting of $m \cdot k \cdot \ell \cdot n \cdot q$ members. In order to cut down com-

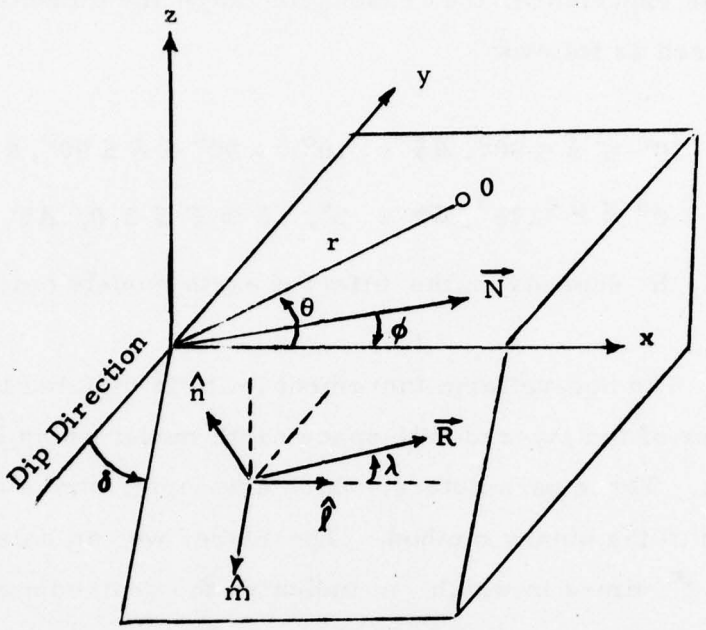

δ = Dip angle
λ = Slip angle
ϕ = Strike angle
θ = Azimuth angle with respect to strike direction
$\hat{n}$ = Surface normal
$\hat{m}, \hat{l}$ = Orthogonal vectors on the surface of fault plane
$\vec{R}$ = One force vector of double-couple force on the surface of fault plane
0 = Arbitrary observation station
$\vec{N}$ = Geographical north

FIGURE III-7

GEOMETRY OF THE DOUBLE-COUPLE SOURCE WHICH MODELS THE EXPLOSION-ASSOCIATED TECTONIC STRAIN RELEASE

puter expenses and widen the searching range of some parameters, a binary method was applied to modify the amplitude spectral fitting process. According to previous experience, the reasonable range and increment of each parameter were used as follows:

$$30^\circ \leq \delta \leq 90^\circ, \Delta\delta = 10^\circ; \quad -90^\circ \leq \lambda \leq 90^\circ, \Delta\lambda = 30^\circ;$$

$$0^\circ \leq \phi \leq 175^\circ, \Delta\phi = 5^\circ; \quad 0 \leq F \leq 3.0, \Delta F = 0.3;$$

h depends on the different earth models (see Table III-1).

The non-uniform increment in h is dictated by the individual layer thickness of the layered half-space earth model which is chosen for the source region. Three parameters, which are depth, strike angle and F value, were involved in the binary method. Therefore, we can enlarge the above increments by 2^n times in which n indicates the desired number of passes. The same search strategy was applied to all of the events analyzed; both earthquakes and explosions, were searched through the same kind of range and increment of each parameter to get final minimum error parameter estimations.

Let X_{ij}^R and X_{ij}^L denote the observed Rayleigh and Love wave spectral amplitudes, respectively, for the i-th period at the j-th station. The fitting error taken as the difference between the observed spectra and the corresponding theoretical spectra is referred to as the residual ϵ, defined as:

$$\epsilon(s_p) = \sum_j \sum_i \left[(X_{ij}^R - Y_{ij}^R)^2 + (X_{ij}^L - Y_{ij}^L)^2 \right]. \qquad \text{(III-3)}$$

Substituting equation (III-2) into equation (III-3), we have:

$$\epsilon(s_p) = \sum_j \sum_i \left[(X_{ij}^R - M_E \left| LR_E + F\, LR_x \right|_{ij})^2 + (X_{ij}^L - M_E \left| LQ_E \right|_{ij})^2 \right] . \qquad \text{(III-4)}$$

TABLE III-1

RANGES AND INCREMENTS OF THE SEARCHED DEPTH

*Earth Model / Depth	EKZ B-C Foldbelt	Eurasian G-B	NTS 35-CM^2
Depth (km)	0.5	0.5	0.5
	1.5	2.0	1.5
	2.5	4.0	2.5
	4.0	6.0	4.0
	6.0	8.0	6.0
	8.0	10.0	8.0
	9.5	12.0	10.0
	11.5	14.0	12.0
	14.0	16.0	14.0
	16.0	18.0	16.0
	18.0	19.5	18.0
	20.0	20.25	20.0
	21.5	22.5	22.5
	25.0	25.0	25.0
	30.0	27.25	27.5
	35.0	30.0	30.0
	40.0	32.5	32.5
	43.0	35.0	34.5
	45.0	37.5	37.5
	47.5	39.5	42.5
	49.5	42.0	47.0
		45.0	50.0
		47.5	
		49.5	

* Earth Model: details discussed in Section III-C

In the amplitude spectra fitting process, first the moment M_E is estimated by minimizing the residual $\epsilon(s_p)$ for all i and j, or explicitly:

$$M_E(s_p) = \frac{\sum_j \sum_i \left[X_{ij}^R \left| LR_E + F\, LR_x \right|_{ij} + X_{ij}^L \left| LQ_E \right|_{ij} \right]}{\sum_j \sum_i \left[\left| LR_E + F\, LR_x \right|_{ij}^2 + \left| LQ_E \right|_{ij}^2 \right]} \quad . \qquad \text{(III-5)}$$

In other words, for a particular member s_p in the set of source parameters S, the optimum moment is first found from equation (III-5). Then, the resultant $M_E(s_p)$ is used in equation (III-4) to compute the minimum residual (s_p) for this particular member s_p. The minimum residual $\epsilon(s_p)$ is computed for each of the members in S. This ϵ value is used as a convenient criterion for judging the goodness of the fit between the observed and the theoretically calculated spectra for each member s_p. In the end, the source parameter estimation of a given event will be the member $s_p^{optimal}$ whose theoretical surface wave spectra fits most closely the observed spectra; that is:

$$\epsilon_{min}^{all}\left(s_p^{optimal}\right) = \text{Minimum}\left[\epsilon(s_p)\right] \text{ for all } s_p \text{ in S.} \qquad \text{(III-6)}$$

In order to attain a greater degree of confidence in using the source parameter estimation based on the minimum residual criterion, a detailed knowledge of the residual distribution about the absolute minimum given by equation (III-6) would be helpful to guard against a possible spurious minimum generated by poor quality data. Therefore, in the amplitude spectral fitting process used here, distributions of $\epsilon(s_p)$ with respect to the source parameters are examined.

In the fitting process, the focal depth is varied last, because the focal depth (h) will have the most affect on the shape of the theoretical surface wave amplitude spectra, especially for Rayleigh waves (Turnbull, et al., 1974). There is one $\epsilon_{min}^{h_i}$ at one focal depth h_i, that is:

$$\epsilon^{h_i}_{min} = \text{Minimum} \left\{ \epsilon \left[s_p (\delta, \lambda, \phi, h_i, F) \right] \right\} \text{ for all } \delta, \lambda, \phi \text{ and } F \text{ at depth } h_i. \quad \text{(III-7)}$$

The variation of $\epsilon^{h_i}_{min}$ with respect to the focal depth is obtained and a standard value ϵ, say $\left[\epsilon^{h_i}_{min}\right]_{standard}$, is determined from those $\epsilon^{h_i}_{min}$ for the purpose of picking appropriate members in the set of source parameters S to form a sample set Sd. In the entire set of source parameters S, those members whose $\epsilon(s_p)$'s are less than $\left[\epsilon^{h_i}_{min}\right]_{standard}$ are included in the sample set Sd. These form the distributions of $\epsilon(s_p)$ with respect to the source parameters. These residual distributions for the various source parameters will be more easily understood from the results which will be presented later for the source parameter estimations of the selected events.

C. EARTH MODEL

From the theoretical part of Figure III-1, it is obvious that a layered half-space earth model (which describes the source region earth structure) has to be obtained first in order to generate theoretical spectra. Then, we can use earth models to calculate theoretical surface wave amplitude spectra which are needed in the amplitude spectral fitting process. In this task, three earth models, as shown in Figure III-8, are selected for the EKZ, NTS, and Eurasian events.

Both groups of EKZ events and NTS events employed the same earth models that were used in the previous report (Sun, 1977). For the EKZ events, the earth model is constructed from a representative subsurface crustal structure of the Balkhash-Chingiz Foldbelt, (see Figure III-8a). Since these crustal cross sections only extend to a depth of approximately 50 km, this model was created by merging the crustal cross section with the Gutenberg-Bullen model (Turnbull, et al., 1974) at a depth of 50 km. For the NTS events,

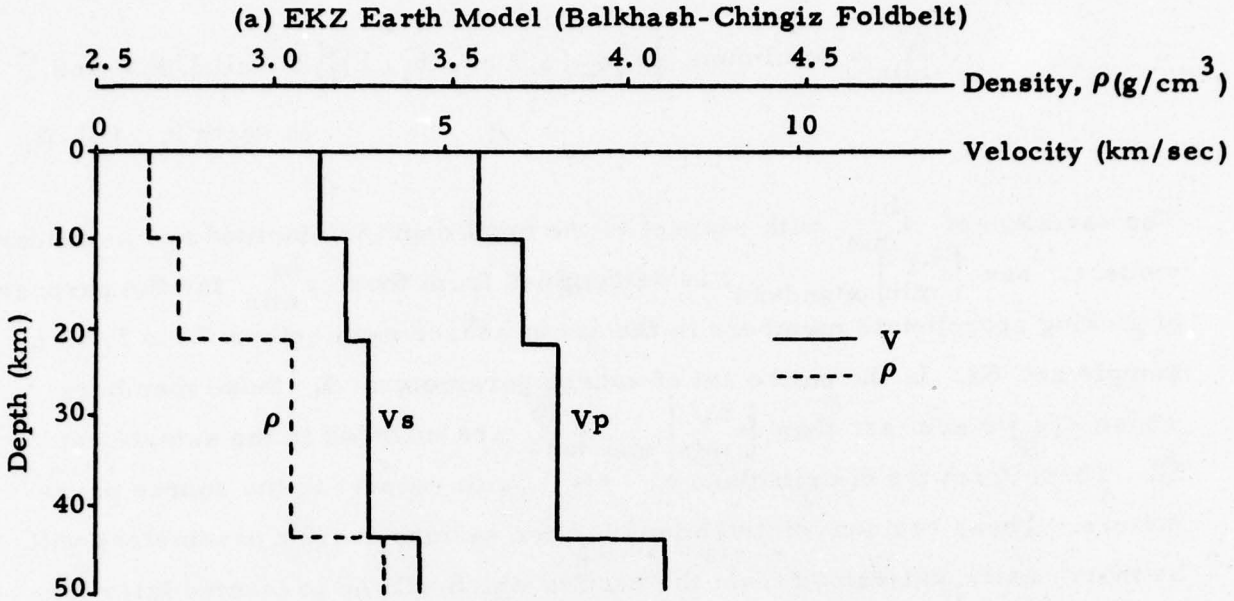

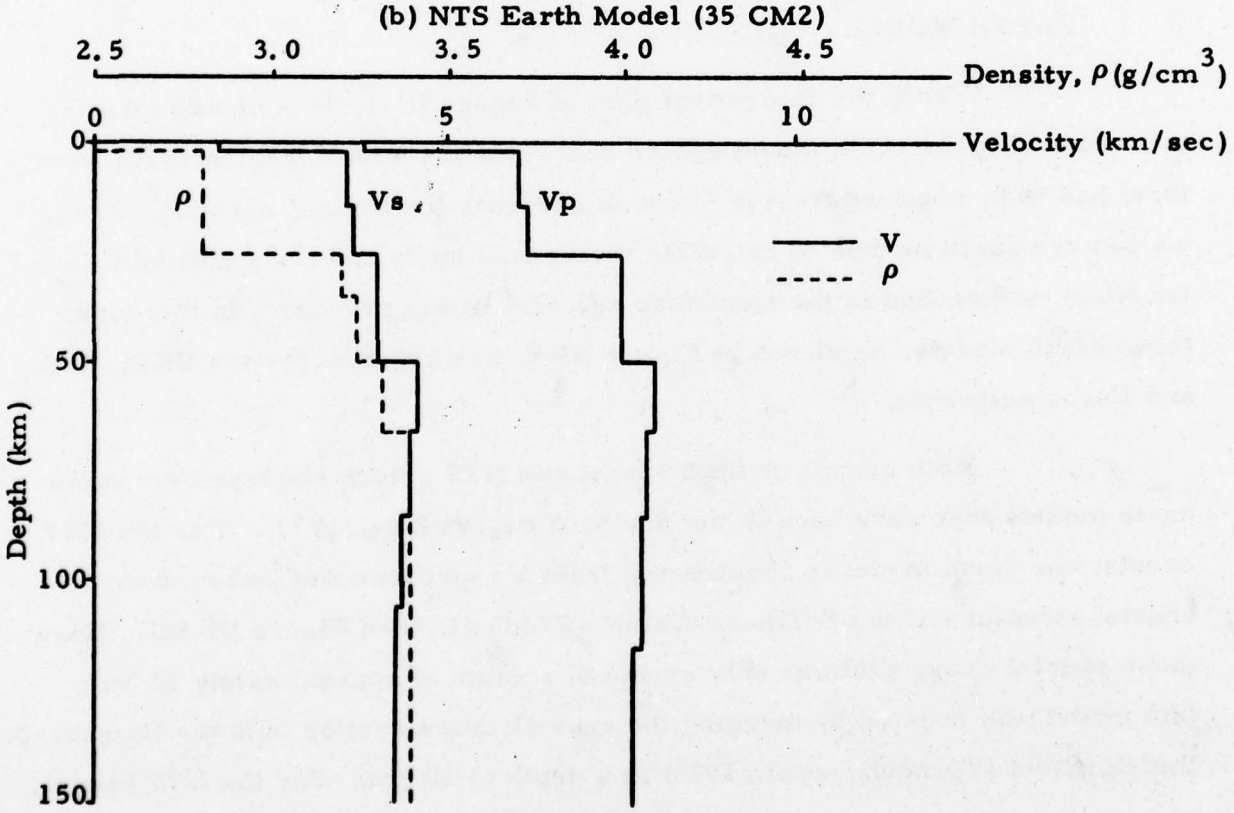

FIGURE III-8

EARTH MODELS
(PAGE 1 OF 2)

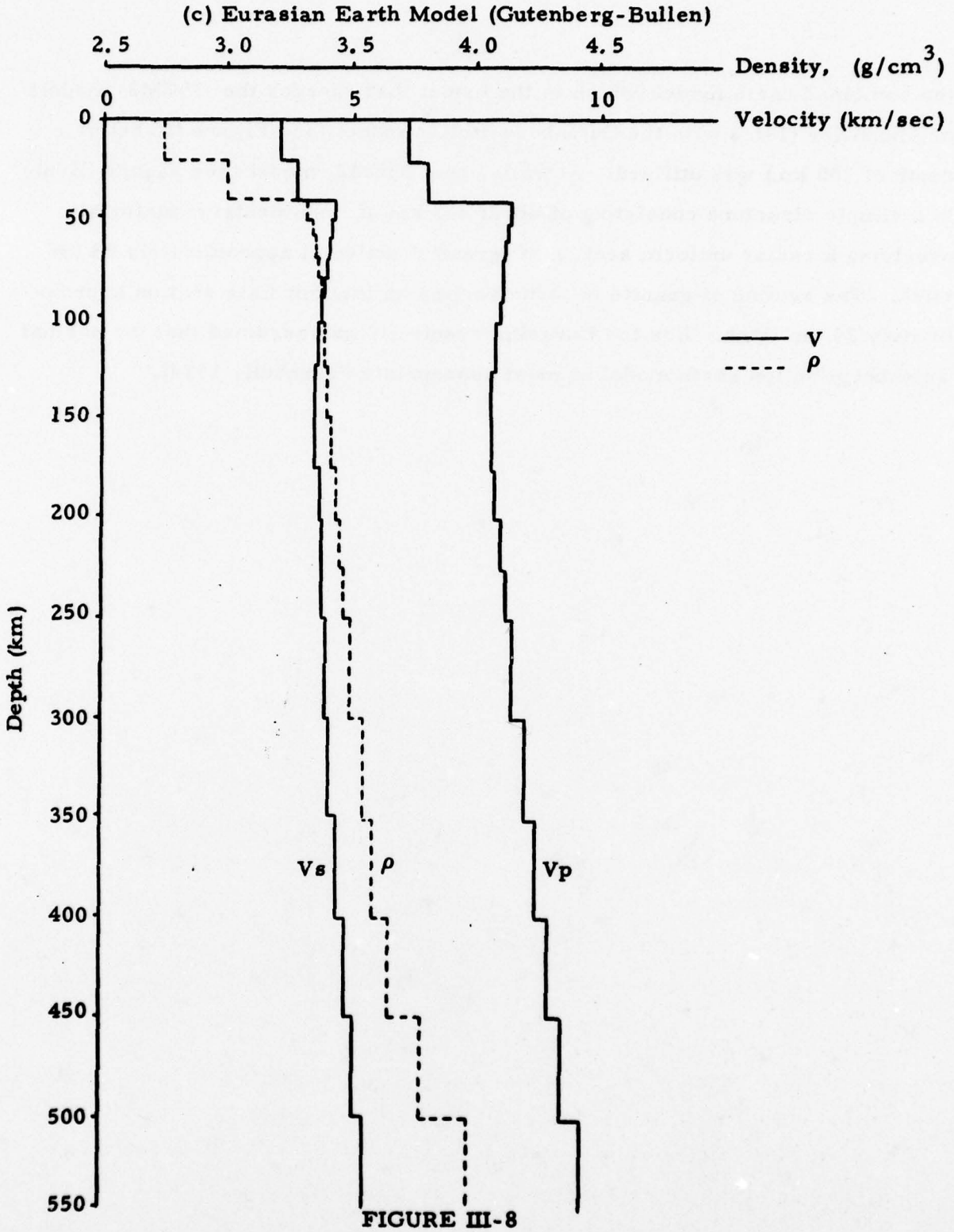

FIGURE III-8

EARTH MODELS
(PAGE 2 OF 2)

the combined earth model (which is the model that merges the 35CM2 models of Alexander (1963) with the Gutenberg-Bullen model (see Figure III-8c) at a depth of 150 km) was utilized. Actually, the 35CM2 model (see Figure III-8b) is a simple structure consisting of about 2-3 km of 'sedimentary' material overlying a rather uniform section of 'granite' material approximately 23 km thick. The section of granite in turn overlies an intermediate section approximately 25 km thick. For the Eurasian events, it was assumed that the normal Gutenberg-Bullen earth model is most appropriate (Turnbull, 1974).

SECTION IV

RESULTS AND CONCLUSIONS OF SOURCE PARAMETER ESTIMATIONS FOR EKZ, EURASIAN, AND NTS EVENTS

In the previous section, we discussed the procedures to obtain the theoretical amplitude spectra and the observed amplitude spectra from earth models and measured seismic waveforms. Also, we described the modified amplitude spectra fitting process which is utilized to get seismic source estimations. In this section, the results of the seismic source parameter estimation will be presented separately for EKZ, Eurasian and NTS events. The results of using these source parameter estimates for discrimination between earthquakes and explosions will be examined. Finally, a brief discussion of all the results also will be given.

A. THE EKZ EVENTS

For EKZ events, observed surface wave data are available for both Rayleigh and Love waves at most stations, except for the event EKZ/427/75 in which only Rayleigh wave data are used at all available stations. However, Sun (1976) compared the results obtained from spectral fittings using both Rayleigh and Love waves to spectral fittings using Rayleigh waves only. He reported no significant difference in the source parameter estimations. Therefore, the event EKZ/427/75 is still in our final event list.

The optimal solution of source parameters based on the minimum-residual criterion are listed in Table IV-1. The residual distributions with respect to the estimated depth, dip angle, slip angle, and strike angle are given in Figure IV-1 through Figure IV-7 with the spectral fits for each event. As described in more detail by Sun (1976), the residual distribution for one particular

TABLE IV-1

ESTIMATIONS OF SOURCE PARAMETERS OBTAINED BY AMPLITUDE SPECTRAL FITTING BASED ON THE MINIMUM-RESIDUAL CRITERION: SELECTED EKZ EVENTS

Event I. D.	Optimal Solution						
	Depth h km	Dip Angle δ^o	Slip Angle λ^o	Strike N ϕ^oE	Moment M_E 10^{25} dyne-cm	M_x	F
EKZ/03/20/76	8.0	60	90	95	0.182E-01	0	0
EKZ/06/29/77	2.5	40	60	5	0.489E-01	0	0
EKZ/09/05/77	2.5	40	90	145	0.102E-01	0.712E-02	0.6
EKZ/10/29/77	4.0	50	-30	150	0.979E-02	0.294E-02	0.3
EKZ/723/73	0.5	90	-90	0	0.232E 00	0	0
EKZ/1214/3	8.0	40	90	95	0.175E-01	0.440E-02	0.25
EKZ/427/75	2.5	30	-30	30	0.733E-02	0.183E-02	0.25

(a) Residual Distributions

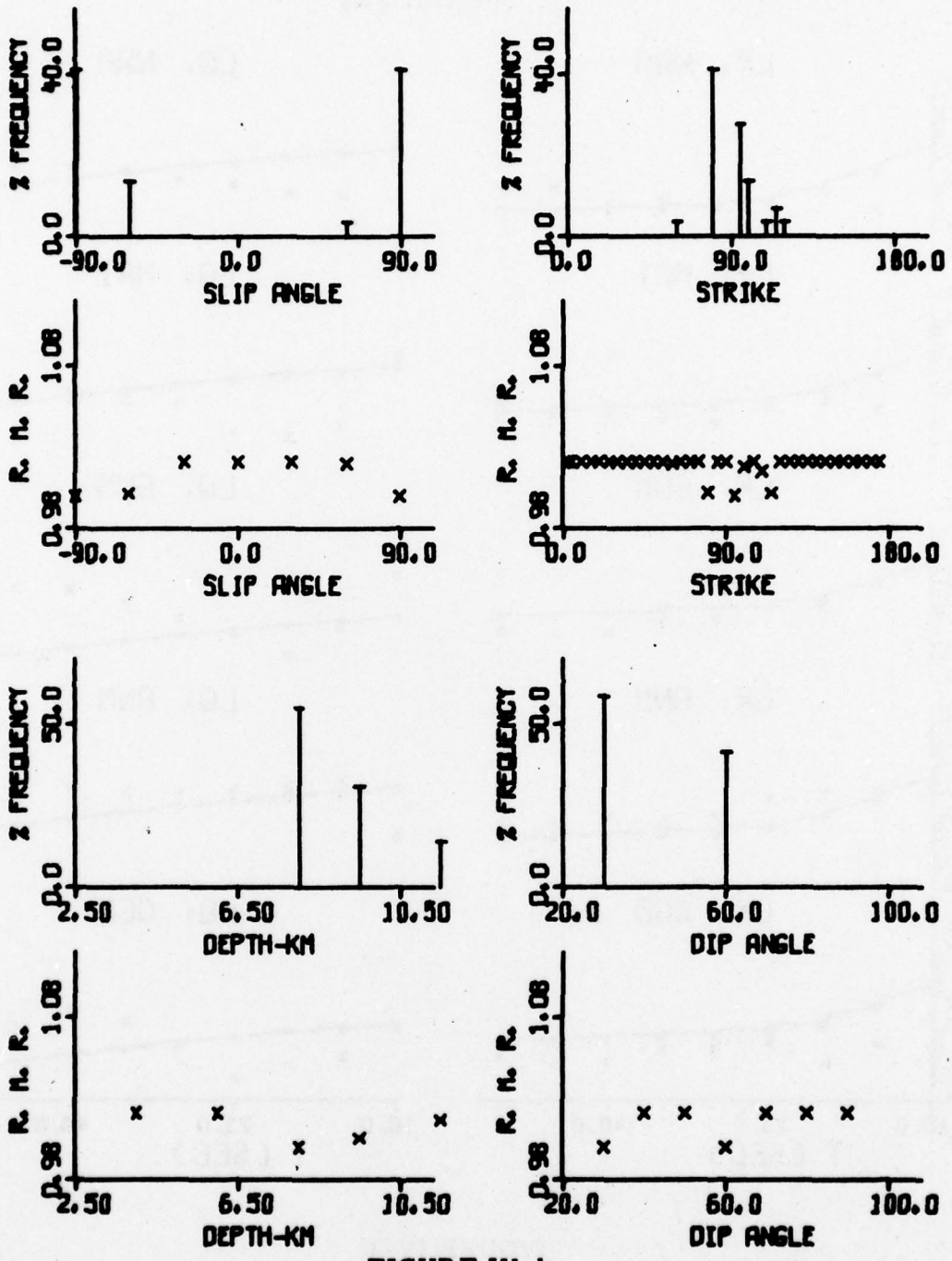

FIGURE IV-1

RESULTS FROM AMPLITUDE SPECTRAL FITTING: EKZ/03/20/76
(PAGE 1 OF 2)

(b) Spectral Fits

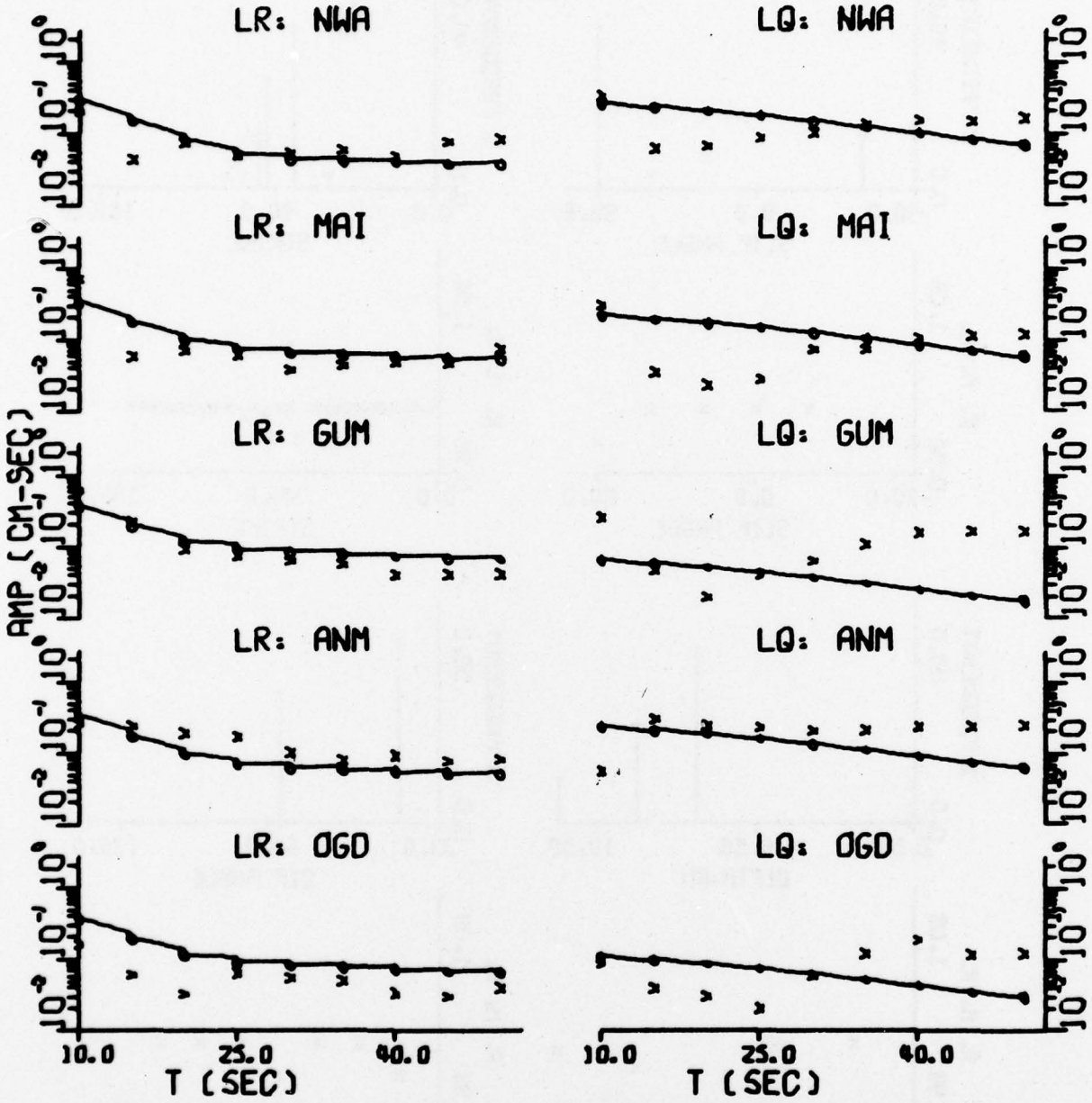

FIGURE IV-1

RESULTS FROM AMPLITUDE SPECTRAL FITTING: EKZ/03/20/76
(PAGE 2 OF 2)

(a) Residual Distribution

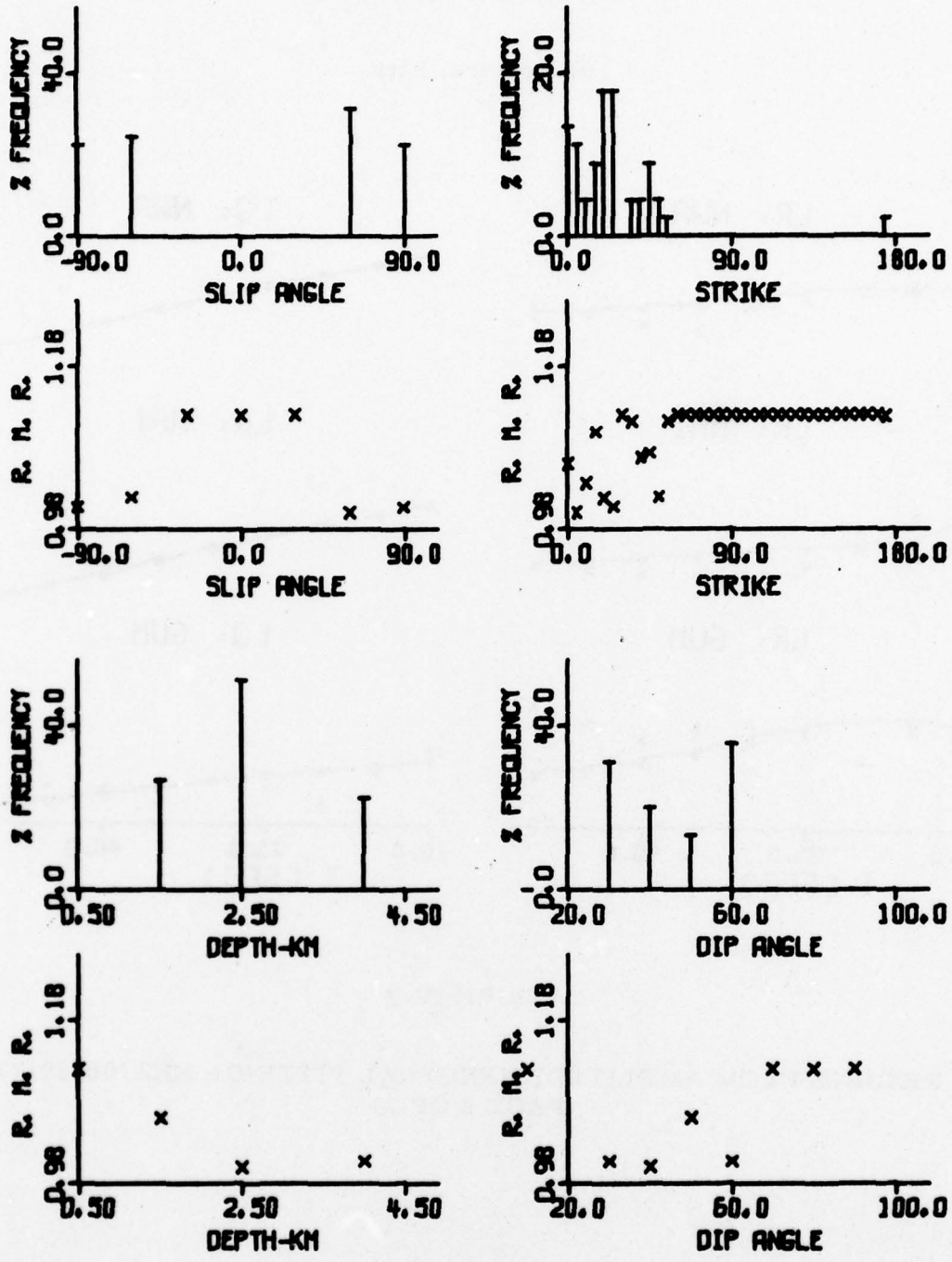

FIGURE IV-2

RESULTS FROM AMPLITUDE SPECTRAL FITTING: EKZ/06/29/77
(PAGE 1 OF 2)

(b) Spectral Fits

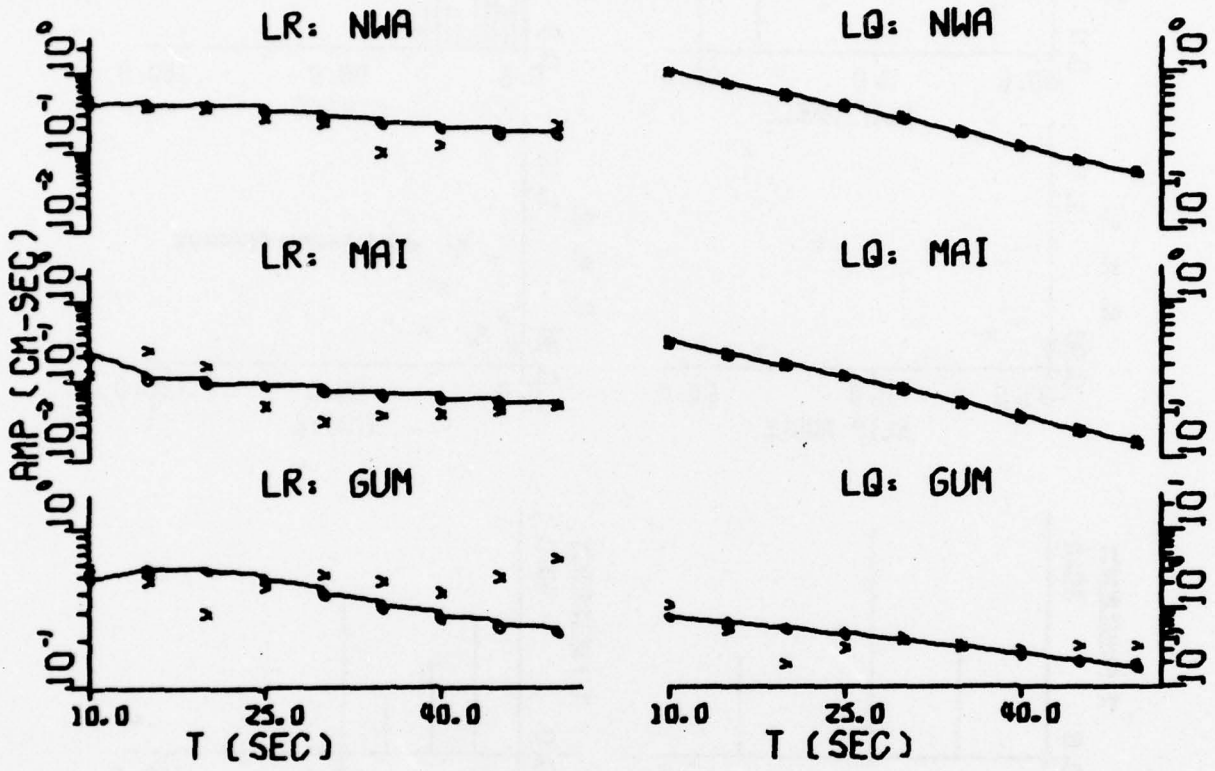

FIGURE IV-2

RESULTS FROM AMPLITUDE SPECTRAL FITTING: EKZ/06/29/77
(PAGE 2 OF 2)

(a) Residual Distribution

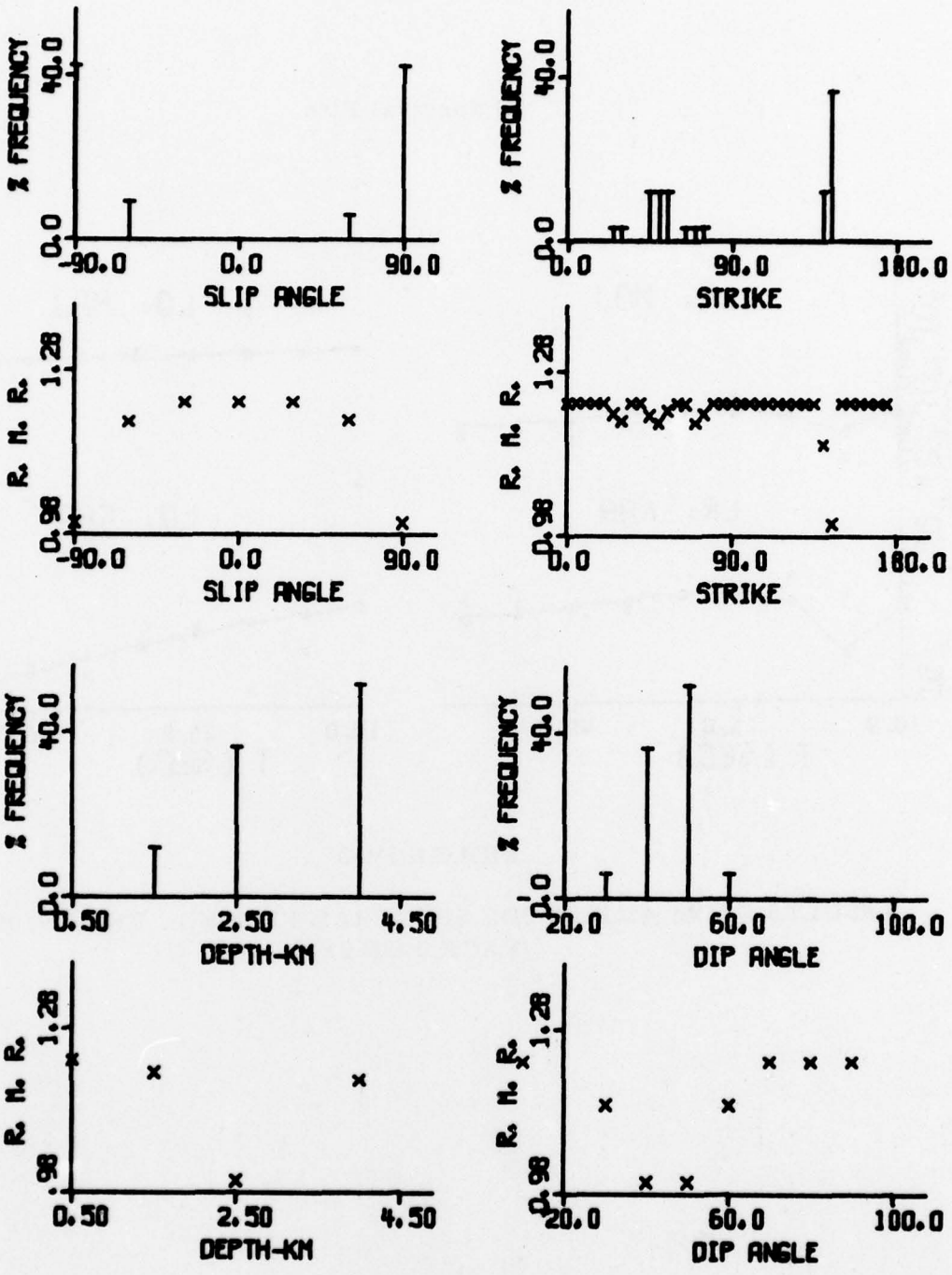

FIGURE IV-3

RESULTS FROM AMPLITUDE SPECTRAL FITTING: EKZ/09/05/77
(PAGE 1 OF 2)

(b) Spectral Fits

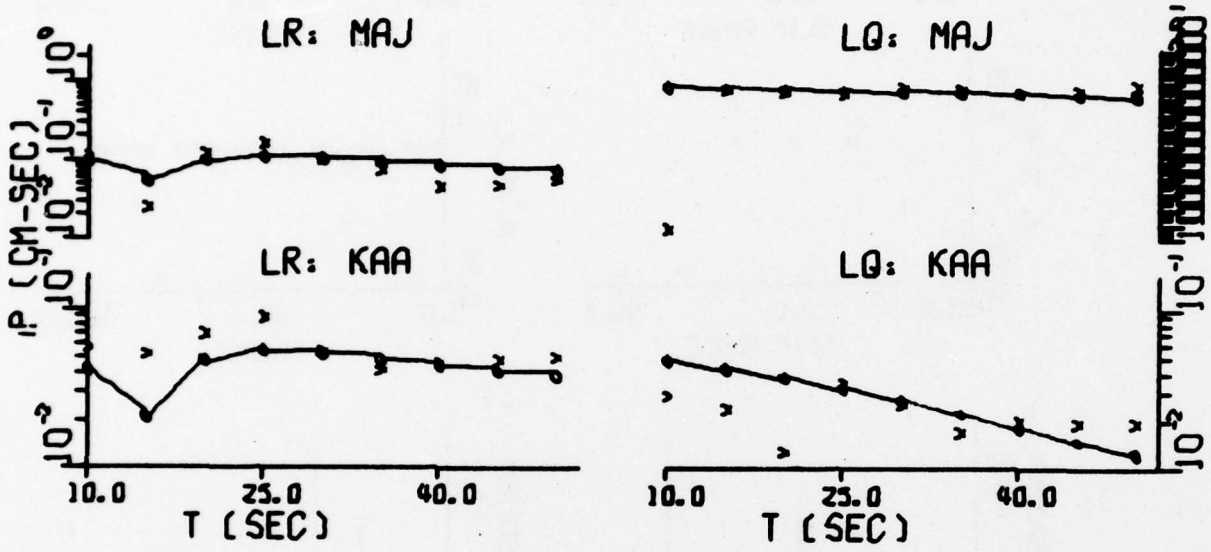

FIGURE IV-3

RESULTS FROM AMPLITUDE SPECTRAL FITTING: EKZ/09/05/77
(PAGE 2 OF 2)

(a) Residual Distribution

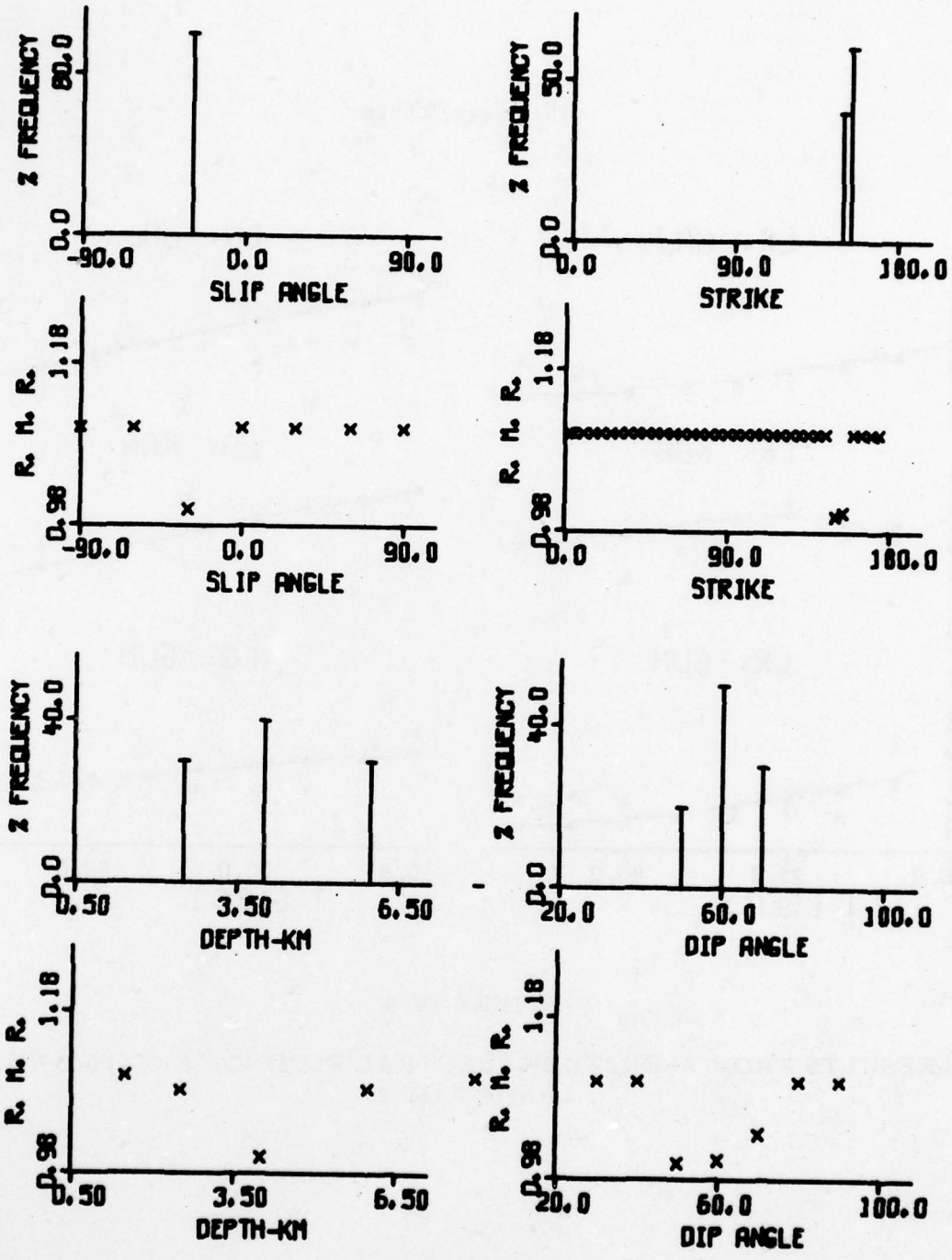

FIGURE IV-4

RESULTS FROM AMPLITUDE SPECTRAL FITTING: EKZ/10/29/77
(PAGE 1 OF 2)

(b) Spectral Fits

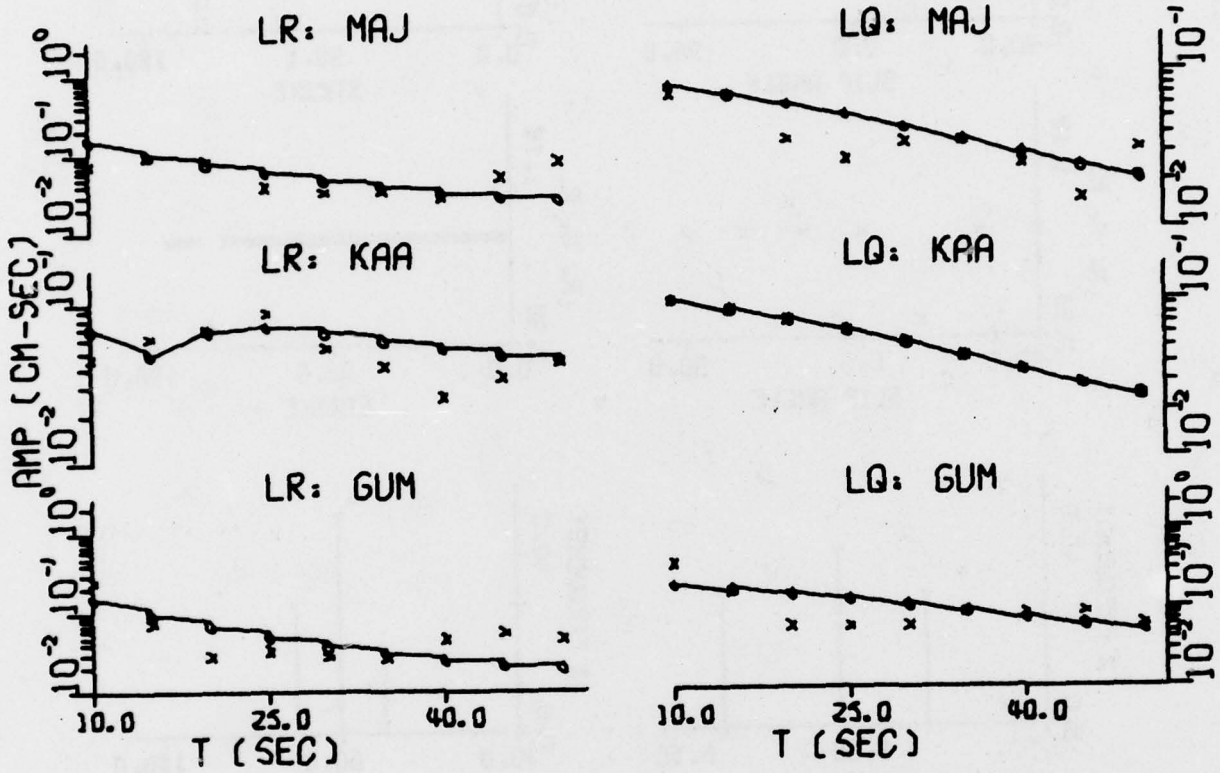

FIGURE IV-4

RESULTS FROM AMPLITUDE SPECTRAL FITTING: EKZ/10/29/77
(PAGE 2 OF 2)

(a) Residual Distribution

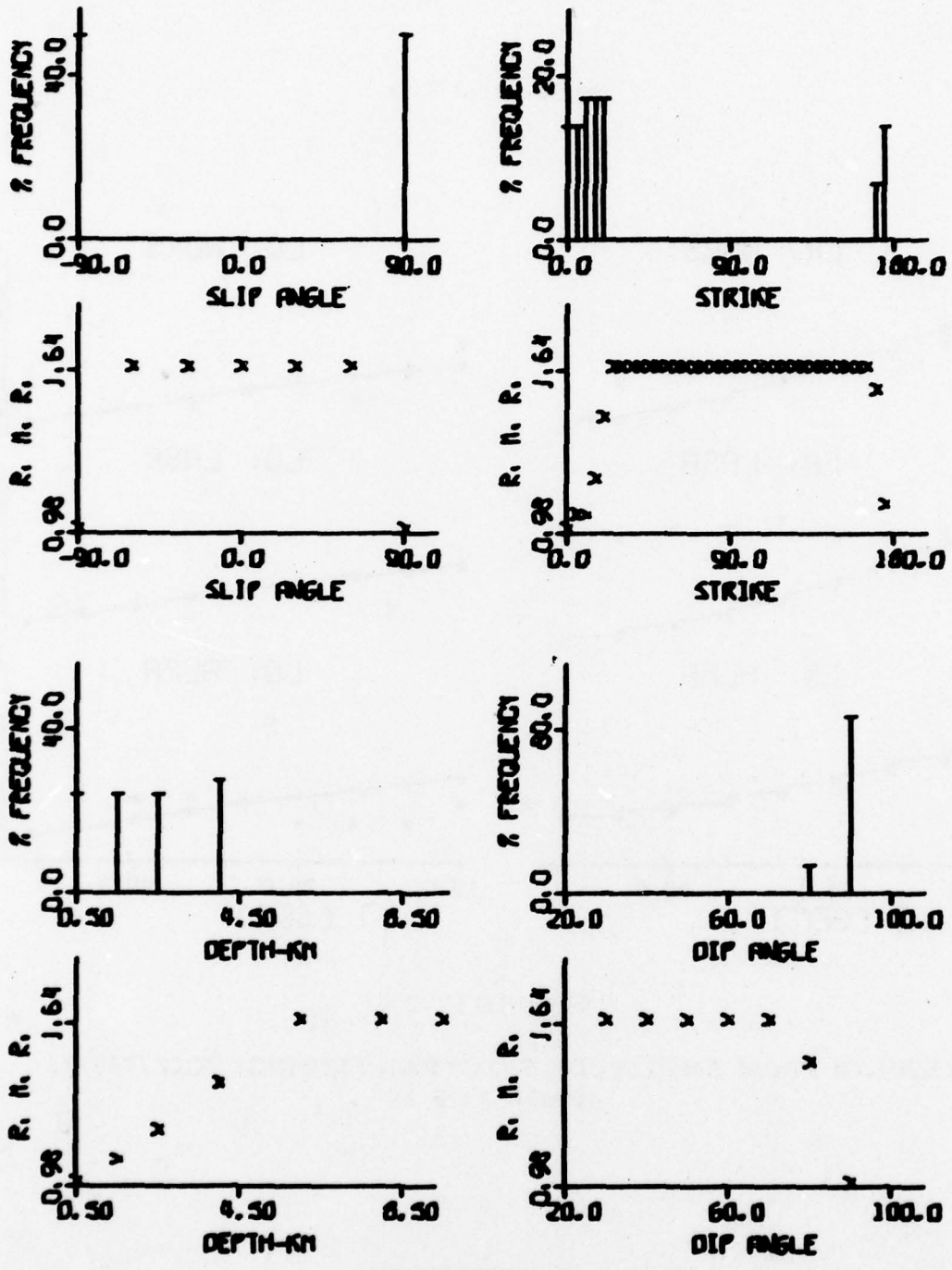

FIGURE IV-5

RESULTS FROM AMPLITUDE SPECTRAL FITTING: EKZ/723/73
(PAGE 1 OF 2)

(b) Spectral Fits

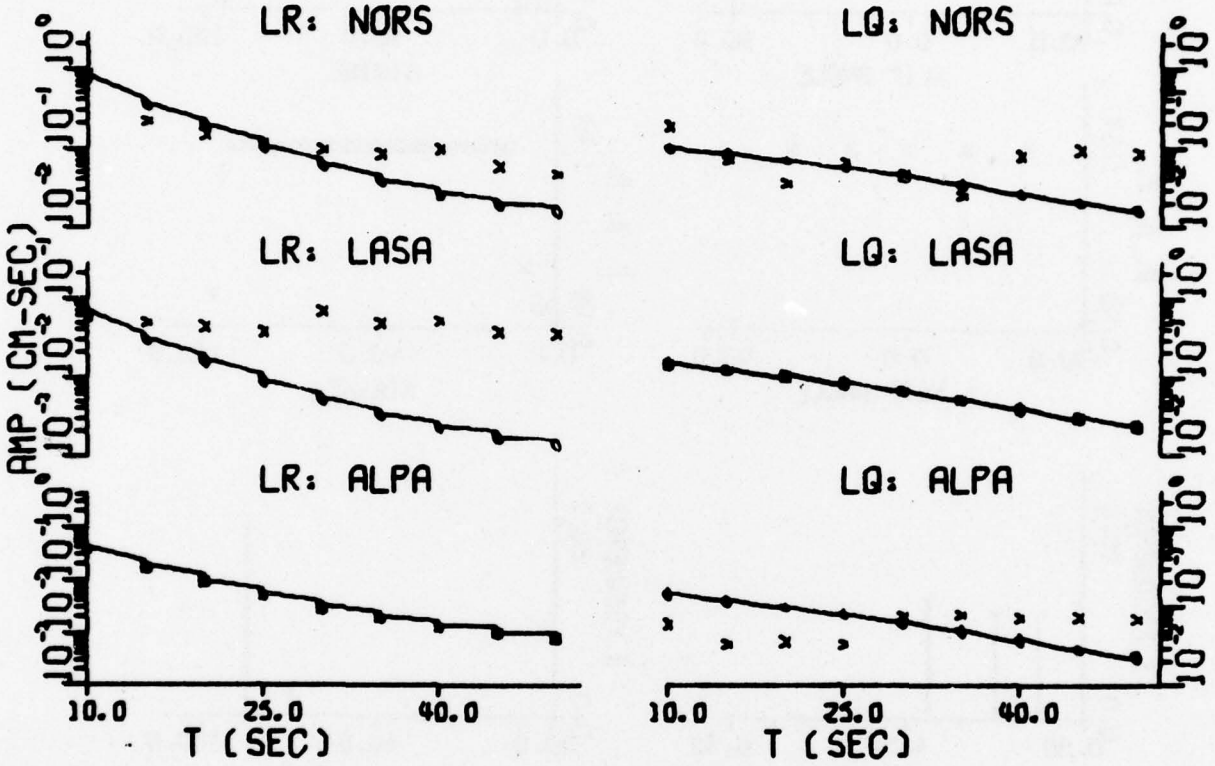

FIGURE IV-5

RESULTS FROM AMPLITUDE SPECTRAL FITTING: EKZ/723/73
(PAGE 2 OF 2)

(a) Residual Distribution

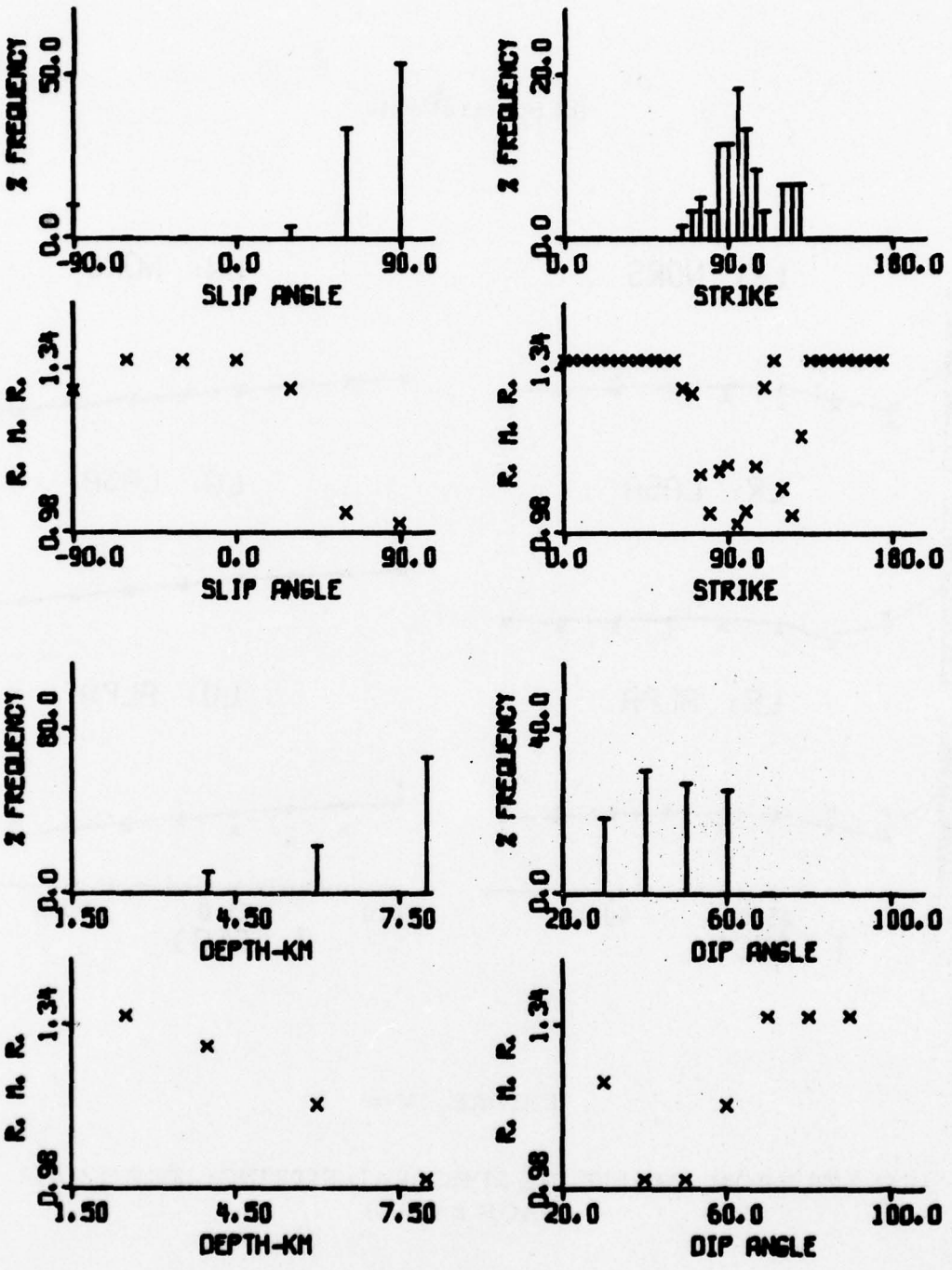

FIGURE IV-6

RESULTS FROM AMPLITUDE SPECTRAL FITTING: EKZ/1214/3
(PAGE 1 OF 2)

(b) Spectral Fits

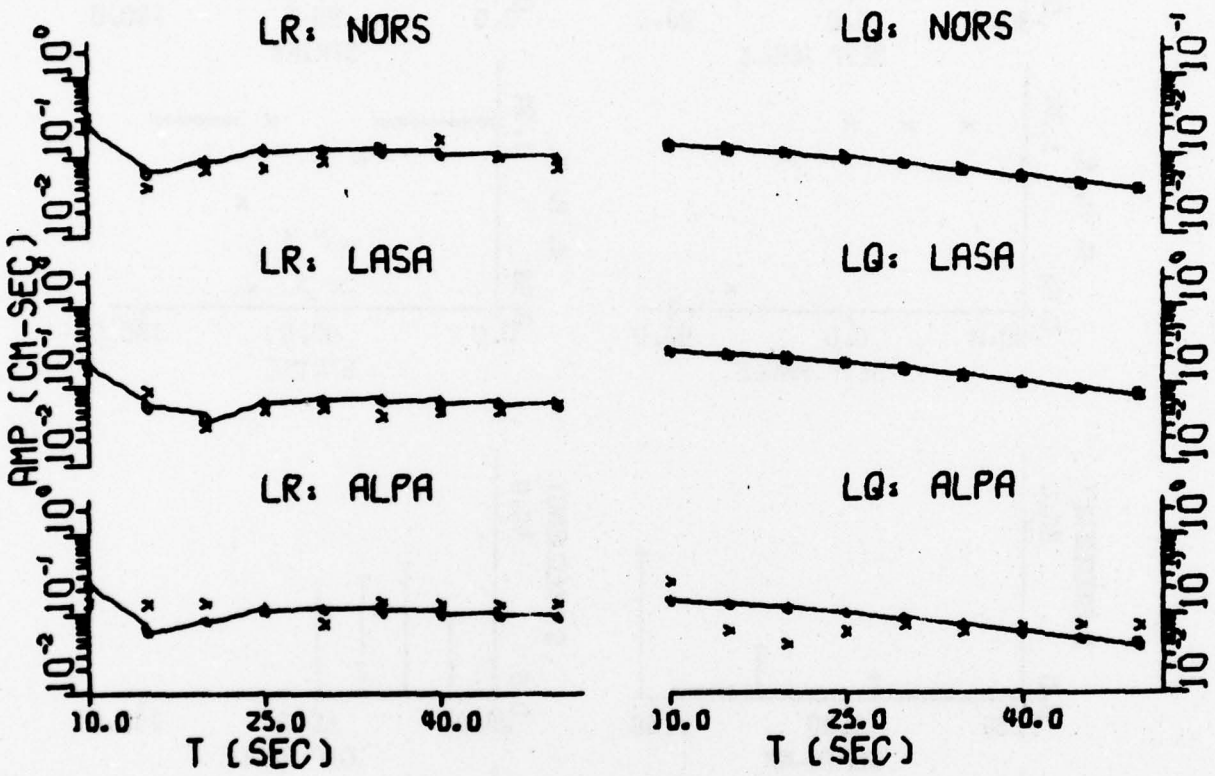

FIGURE IV-6

RESULTS FROM AMPLITUDE SPECTRAL FITTING: EKZ/1214/3
(PAGE 2 OF 2)

(a) Residual Distribution

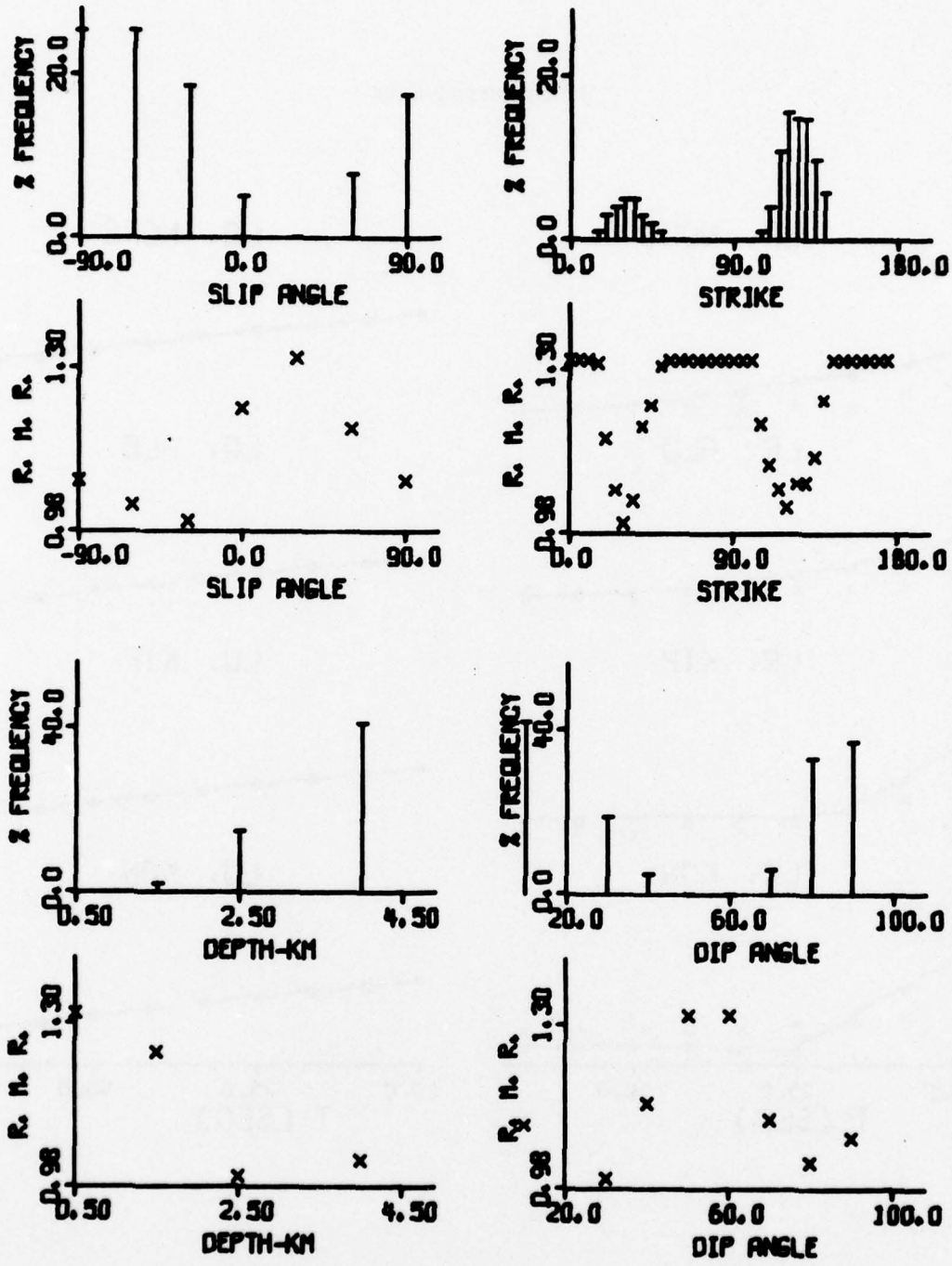

FIGURE IV-7

RESULTS FROM AMPLITUDE SPECTRAL FITTING: EKZ/427/75
(PAGE 1 OF 2)

(b) Spectral Fits

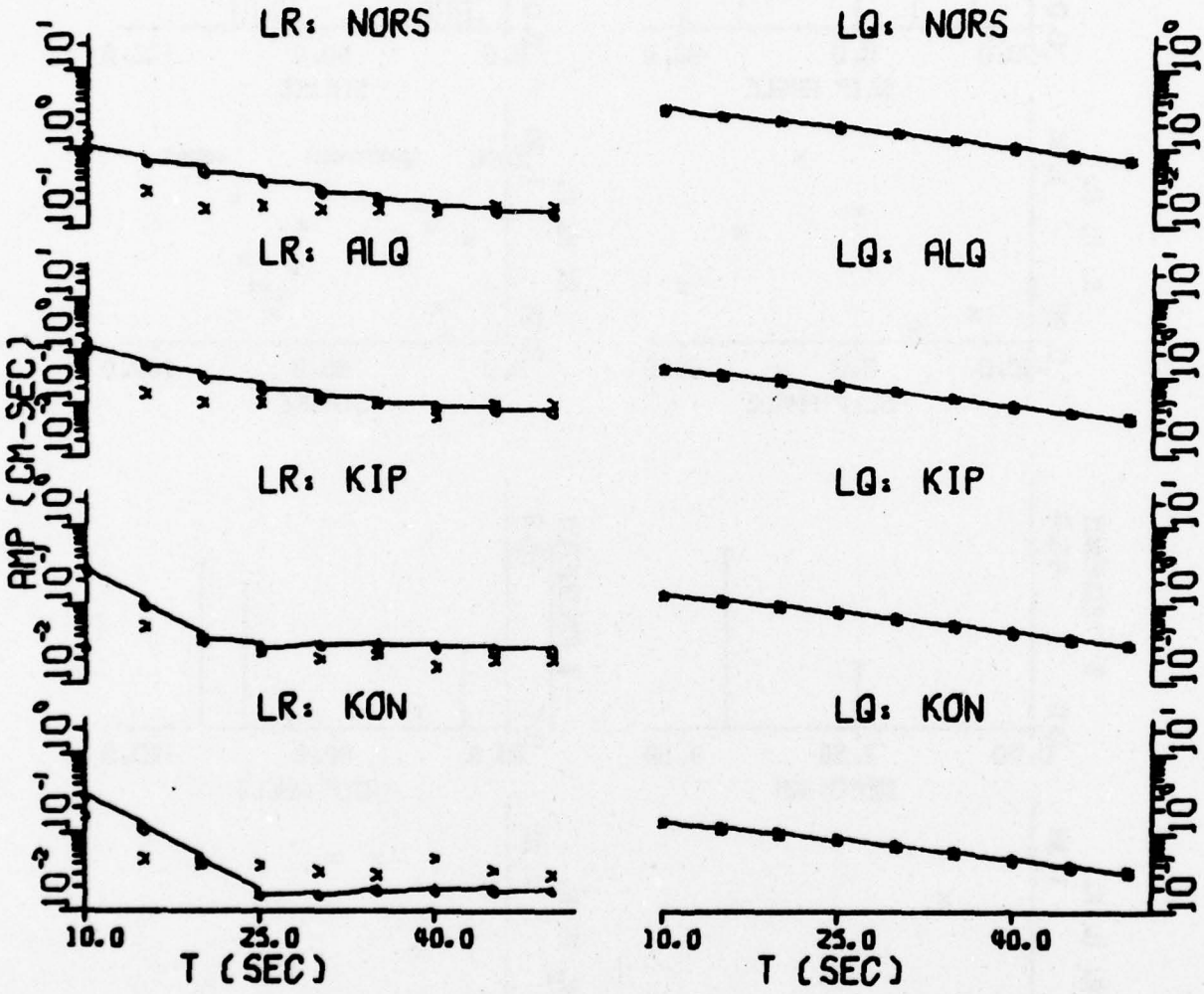

FIGURE IV-7

RESULTS FROM AMPLITUDE SPECTRAL FITTING: EKZ/427/75
(PAGE 2 OF 2)

source parameter, for example, depth, consists of the variation of the minimum-residual values with respect to the depths tested in the spectra fitting process and the percentage of occurrence of minimum-residual values at the various tested depths. For each event, the residual distributions are given in part (a) of Figure IV-1 through Figure IV-7. The best spectral fits of Rayleigh and Love waves (as defined by equation (III-6)) are shown in part (b) of Figure IV-1 through Figure IV-7. In these figures, the residual values are normalized with respect to the residual error of the optimal minimum variance solution which most closely fits the observed spectra. These are indicated as the relative minimum residuals (R.M.R.). The observed spectra are indicated by crosses (x) and the best fit theoretical spectra are represented by open circles (o) connected by straight lines. When there are no observed spectra for either the Rayleigh or Love wave, the crosses are plotted on top of the corresponding open circles. From the residual distributions shown in part (a) of Figures IV-1 through Figure IV-7, the estimates of the source parameters of each event can be represented in terms of the probable range of the estimate and the percentage frequency of that probable range. The estimations of source parameters based on the residual distributions are listed in Table IV-2. To give a clearer explanation of Table IV-2, consider the event EKZ/03/20/76. It has a depth estimate of 8.0 km indicated in Table IV-1; while Table IV-2 indicates that 100% of the members in the sample set s_p of the tested source parameters (as described in Subsection III-3) indicate that the probable range of the depth estimate is from 8.0 km to 11.5 km.

Referring to Table IV-1, these seven events can be divided into two groups according to the dip and slip angle estimates of the tectonic strain release associated with these events. The first group is nearly dip-slip for one event and purely dip-slip for four events, and the second group is nearly strike-slip for two events. These results correspond to those of Sun (1977). The estimated dip angles are quite consistent from event to event, except for

TABLE IV-2

ESTIMATIONS OF SOURCE PARAMETERS OBTAINED BY AMPLITUDE SPECTRAL FITTING BASED ON THE RESIDUAL DISTRIBUTIONS: SELECTED EKZ EVENTS

Event I. D.	Source Parameters							
	Depth h km		Dip Angle δ^{o}		Slip Angle λ^{o}		Strike N ϕ^{o}E	
	Probable Range	% Frequency	Probable Range	% Frequency	Probable Range	% Frequency	Probable Range	% Frequency
EKZ/03/20/77	8~11.5	100	30~60	100	60~90	45	80~100	83
EKZ/06/29/77	1.5~4.0	100	30~60	100	60~90	53	0~30	73
EKZ/09/05/77	1.5~4.0	100	40~60	86	60~90	52	145~150	55
EKZ/10/29/77	2.5~4.0	70	50~70	100	-30	100	150~155	100
EKZ/723/73	0.5~4.0	100	60~90	100	60~90	50	0~30	75
EKZ/1214/3	4.0~8.0	100	40~60	82	60~90	87	80~110	70
EKZ/427/75	1.5~4.0	60	30~40	25	-90~-30	70	0~50	24

the event EKZ/723/73. The reason for this variation may be caused by the poor spectral fits for the Rayleigh wave data of LASA station. The probable range of dip angles, as given in Table IV-2, are approximately 40° to 60°. For the estimated strike angles, there is no consistency among the seven events. The majority of the depth estimates of these events are shallow; from 0.5 km to 4.0 km except 8.0 km for both events EKZ/03/20/76 and EKZ/12 14/3 . The shallow depths are coincident with the fact that those events are presumed underground explosions. For the event EKZ/03/20/76, (one of the two events of 8.0 km depth), Strauss (1977) reported that the M_s values for this event as recorded at ANMO, GUMO, MAZO, and NWAO all fall in the earthquake population, indicating this event is an earthquake. In our M_E versus m_b plot, which is discussed later, this event also falls in the earthquake population. These descriptions might explain the 8.0 km depth of this event. The probable reason for the other anomalous event EKZ/1214/3 will be discussed in Subsection IV-E. The F-values vary from 0.0 to 0.6 among these seven events. This indicates that the double-couple source is for the most part responsible for the observed surface waves of these events. On physical grounds, this might be expected due to the expected order of magnitude drop in the amplitude of compressional waves emitted from a shallow explosion source and possibly from such a shallow strain release source due to the free surface reflection.

Judging the spectral fits visually, these seven events are fairly good at most available stations. In general, the Rayleigh wave amplitude spectral fits are better than those of the Love wave.

B. THE EURASIAN EVENTS

For the selected Eurasian events, the estimations of source parameters based on the minimum-residual criterion are listed in Table IV-3.

TABLE IV-3

ESTIMATIONS OF SOURCE PARAMETERS OBTAINED BY AMPLITUDE SPECTRAL FITTING BASED ON THE MINIMUM-RESIDUAL CRITERION: SELECTED EURASIAN EVENTS

Event I. D.		Optimal Solution					
	Depth h km	Dip Angle δ^o	Slip Angle λ^o	Strike $N\phi^oE$	Moment M_E 10^{25} dyne-cm	Mx	F
ECU/02/03/72	45.0	80	-30	15	0.219E00	0.165E00	0.75
TZK/03/17/72	19.5	40	90	55	0.304E-01	0.456E-01	1.5
UZB/07/14/77	8.0	50	90	40	0.290E00	0.870E-01	0.3
LBR/08/10/77	4.0	40	-60	120	0.252E-01	0.151E-01	0.6
NVZ/09/01/77	4.0	70	-90	15	0.221E-01	0.331E-02	0.15

Those based on the residual minima frequency of occurrence distributions are listed in Table IV-4. The residual distributions with respect to the estimated depth, dip angle, slip angle, and strike angle are given in Figure IV-8 through Figure IV-12 with the spectral fit for each event.

Referring to Table IV-3, these five Eurasian events may be divided into two groups according to their focal depth. In group 1, ECU/02/03/72 and TZK/03/17/72 have the deeper focal depth in the range of 20 to 45 km and in group 2, the other three have shallow focal depths of approximately 4.0 km to 8.0 km. In the first group, it is interesting to note the larger F-values of the two deeper events. The larger F-values may suggest that more energy is released from the dilatational point source than from that of the double-couple point source in the deeper earthquakes. In the second group, event NVZ/09/01/77 would be classified as an explosion due to its special origin time and its seismic moment falling into the explosion population of our M_E versus m_b plot.

For event ECU/02/03/72, the spectral fits yielded a focal depth in the range of 42 to 47.5 km with the best fit at 45 km. Comparing this result with the depth of 39 km indicated in the NEIS list, the difference is not significant. The best fit dip and slip angles suggested an oblique-slip source mechanism with a strike direction of N15°E. The estimated F-value is 0.75.

For event TZK/03/17/72, the optimal solution showed a dip-slip fault mechanism with an approximate strike direction of N55°E. The estimated focal depth lies in the range of 18 to 22.5 km with the best fit of depth at 19.5 km. The difference between this estimated depth and the depth of 26 km (indicated in the NEIS list) might be caused by the poor quality of the amplitude spectral fit at 10-second periods, because the variation of the amplitude spectra at shorter periods (less than 25 seconds) will affect the estimation of focal depth mostly. The estimated F-value is 1.6.

TABLE IV-4

ESTIMATIONS OF SOURCE PARAMETERS OBTAINED BY AMPLITUDE SPECTRA FITTING BASED ON THE RESIDUAL DISTRIBUTIONS: SELECTED EURASIAN EVENTS

Event I. D.	Source Parameters							
	Depth h km		Dip Angle δ^o		Slip Angle λ^o		Strike $N\phi^oE$	
	Probable Range	% Frequency	Probable Range	% Frequency	Probable Range	% Frequency	Probable Range	% Frequency
ECU/02/03/72	42 ~ 47.5	82.5	60 ~ 80	65	-30 ~ 30	100	10 ~ 20	85
TZK/03/17/72	18 ~ 22.5	90	40 ~ 60	80	90	100	45 ~ 55	90
UZB/07/14/77	6 ~ 8	75	40 ~ 60	95	30 ~ 90	91	5 ~ 40	84
LBR/08/10/77	2 ~ 4	100	40 ~ 60	86	-90 ~ -60	71	120 ~ 135	71
NVZ/09/01/77	2 ~ 6	79	60 ~ 80	57	-90	36	5 ~ 20	79

(a) Residual Distribution

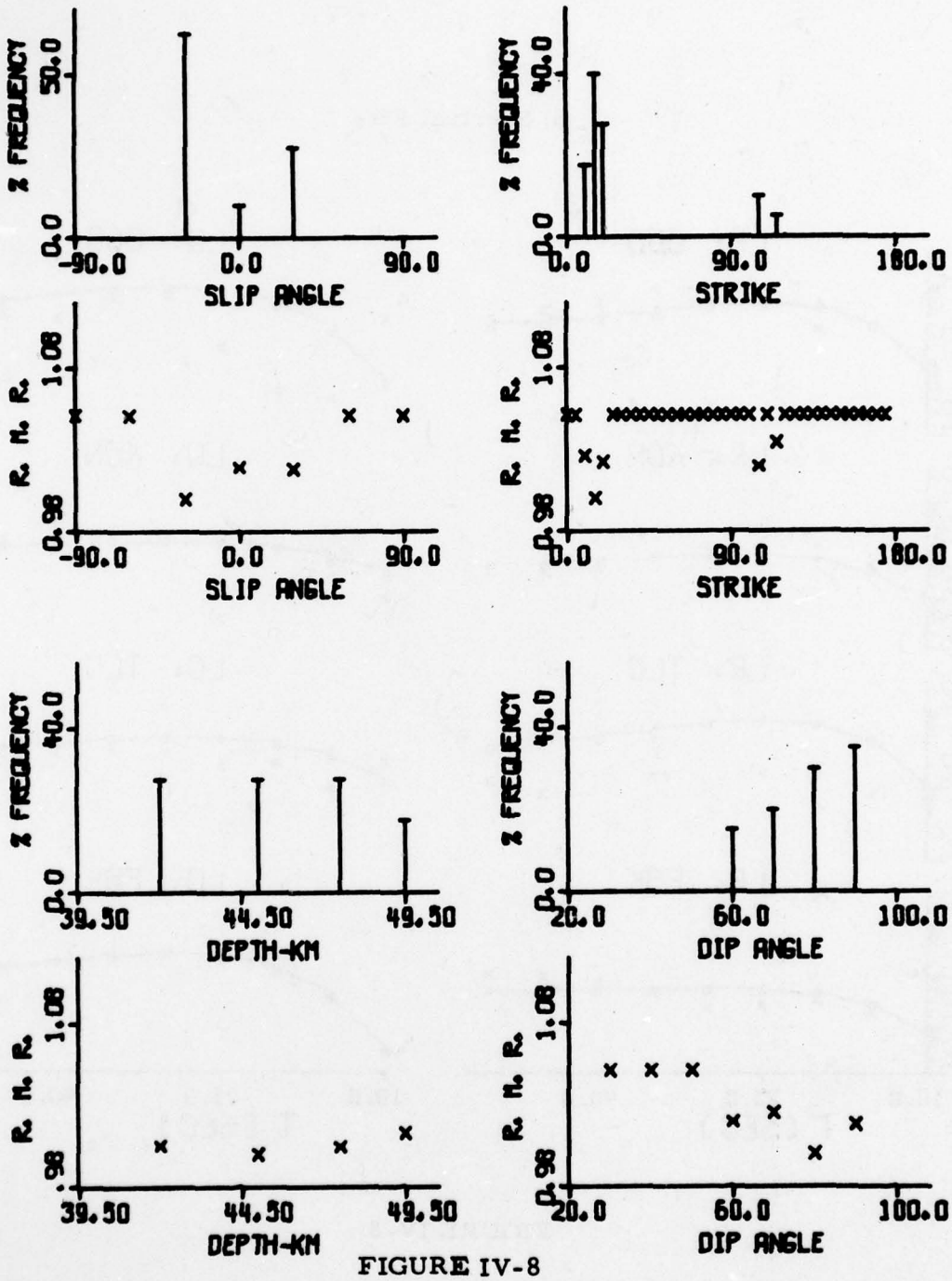

FIGURE IV-8

RESULTS FROM AMPLITUDE SPECTRAL FITTING: ECU/02/03/72
(PAGE 1 OF 2)

(b) Spectral Fits

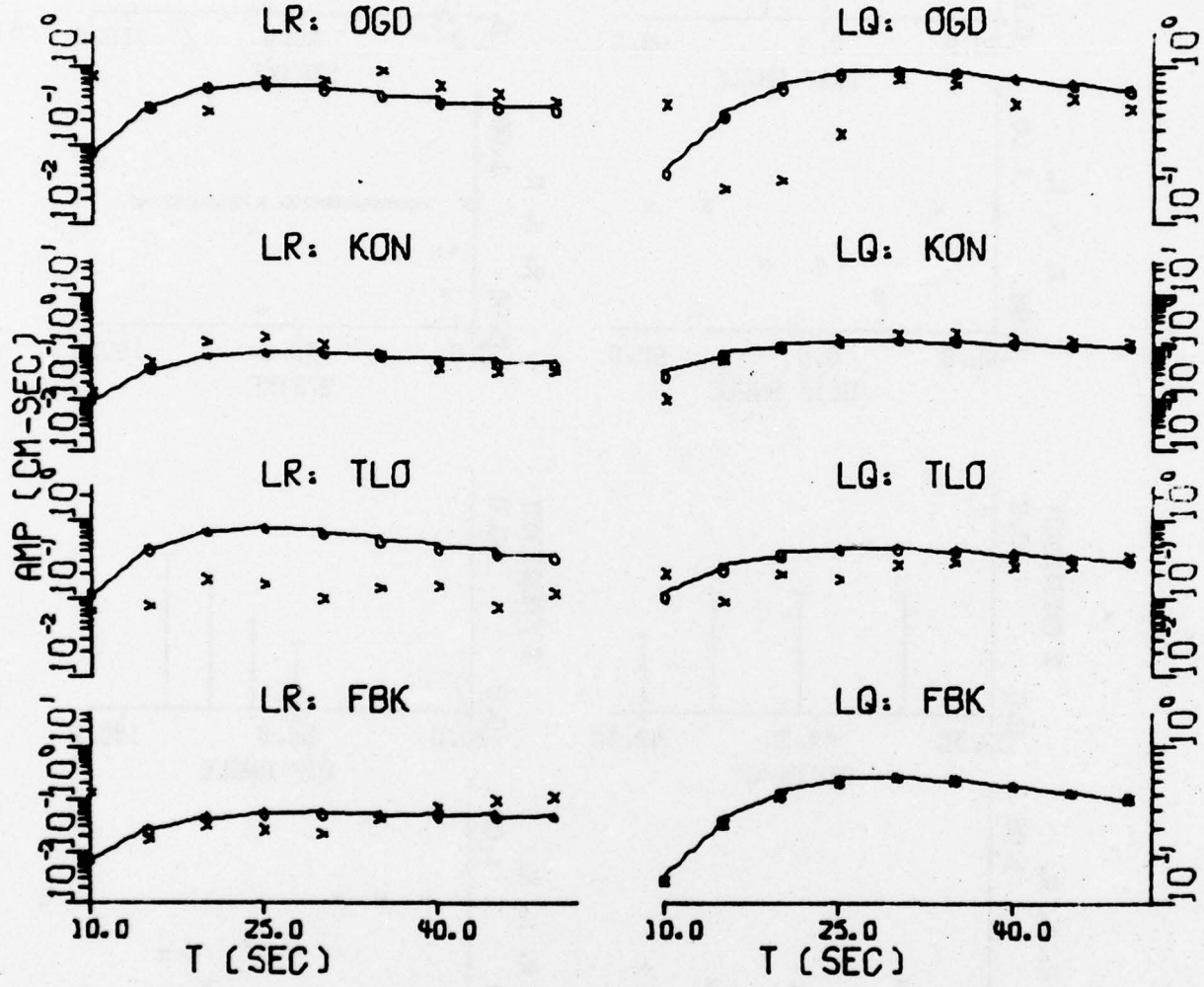

FIGURE IV-8

RESULTS FROM AMPLITUDE SPECTRAL FITTING: ECU/02/03/72
(PAGE 2 OF 2)

(a) Residual Distributions

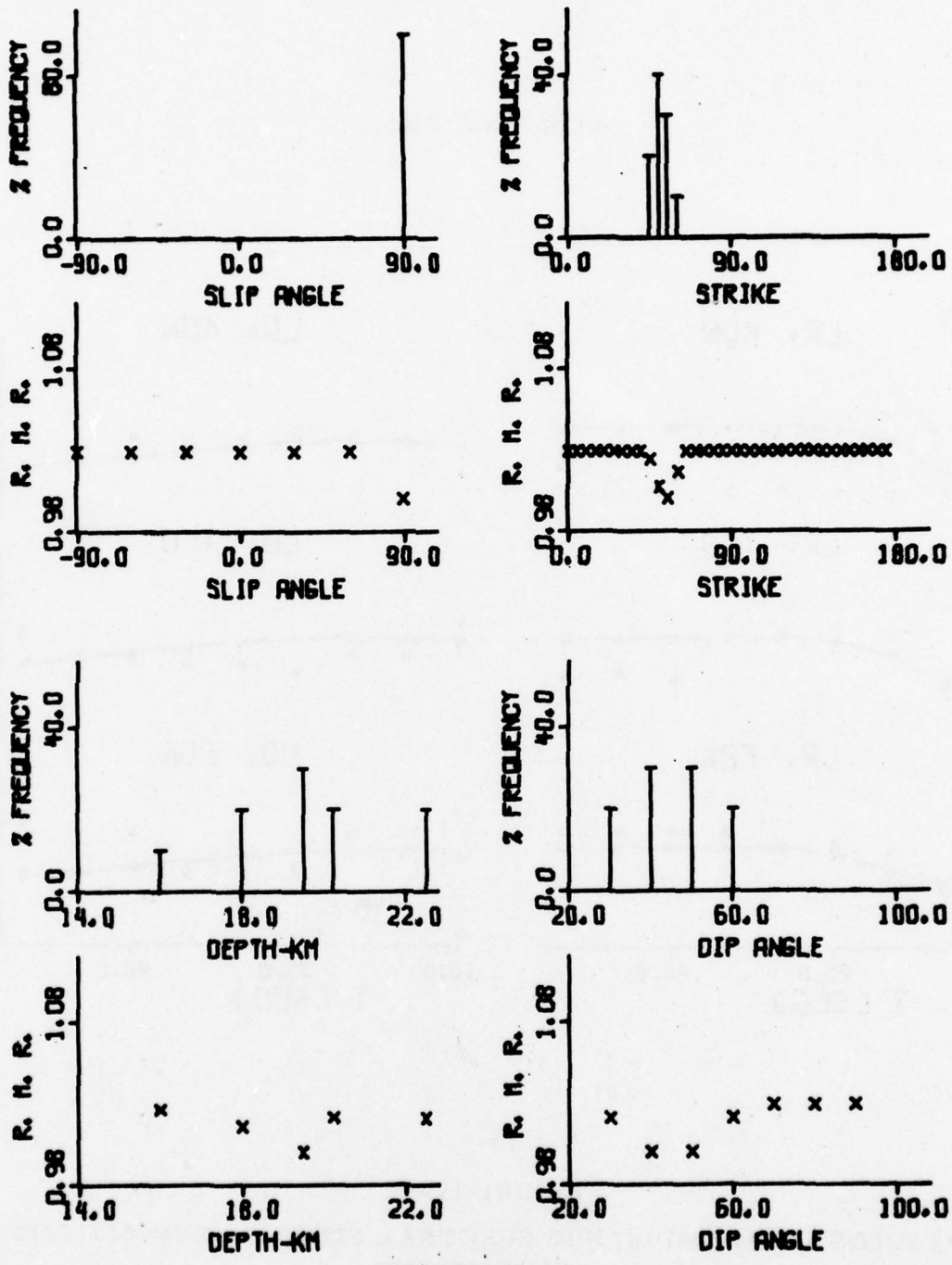

FIGURE IV-9

RESULTS FROM AMPLITUDE SPECTRAL FITTING: TZK/03/17/72
(PAGE 1 OF 2)

(b) Spectral Fits

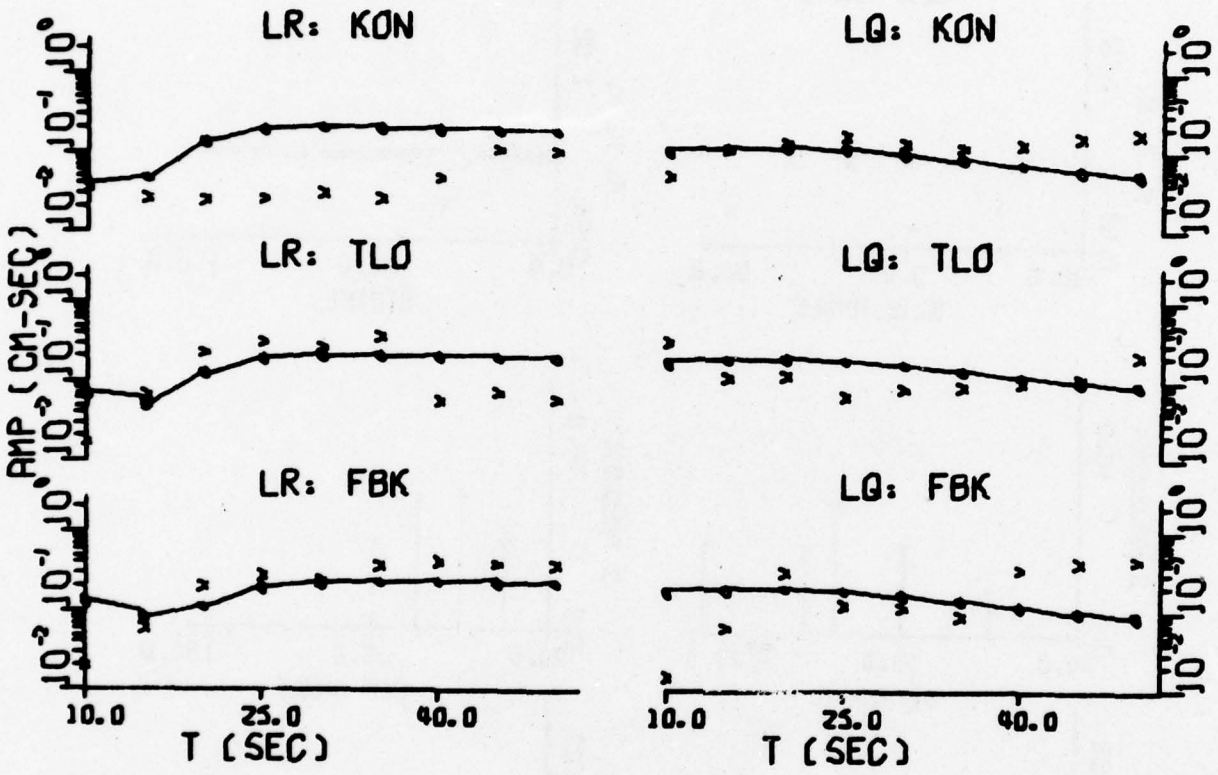

FIGURE IV-9

RESULTS FROM AMPLITUDE SPECTRAL FITTING: TZK/03/17/72
(PAGE 2 OF 2)

(a) Residual Distribution

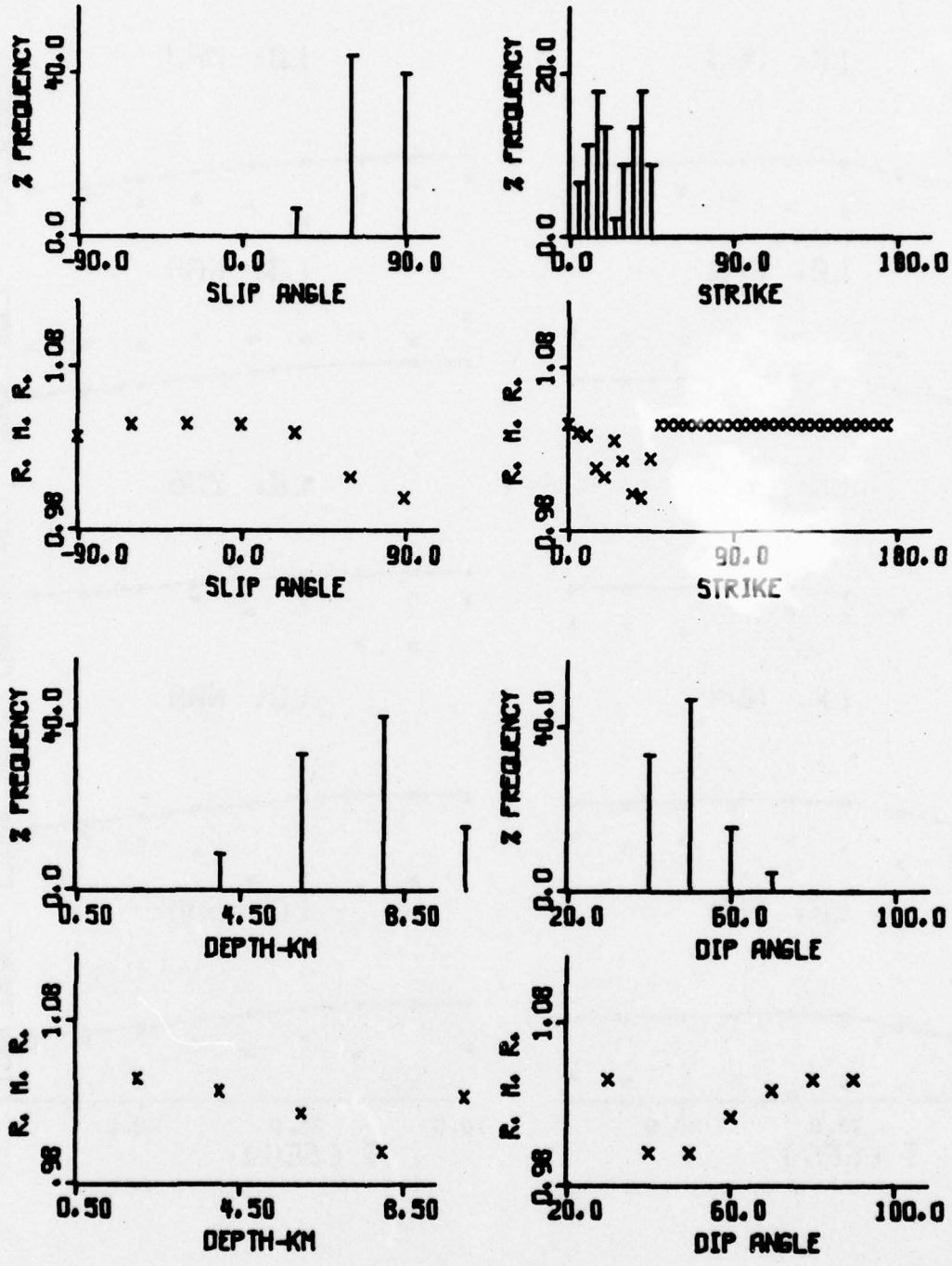

FIGURE IV-10

RESULTS FROM AMPLITUDE SPECTRAL FITTING: UZ[illegible]/07/14/77
(PAGE 1 OF 2)

(b) Spectral Fits

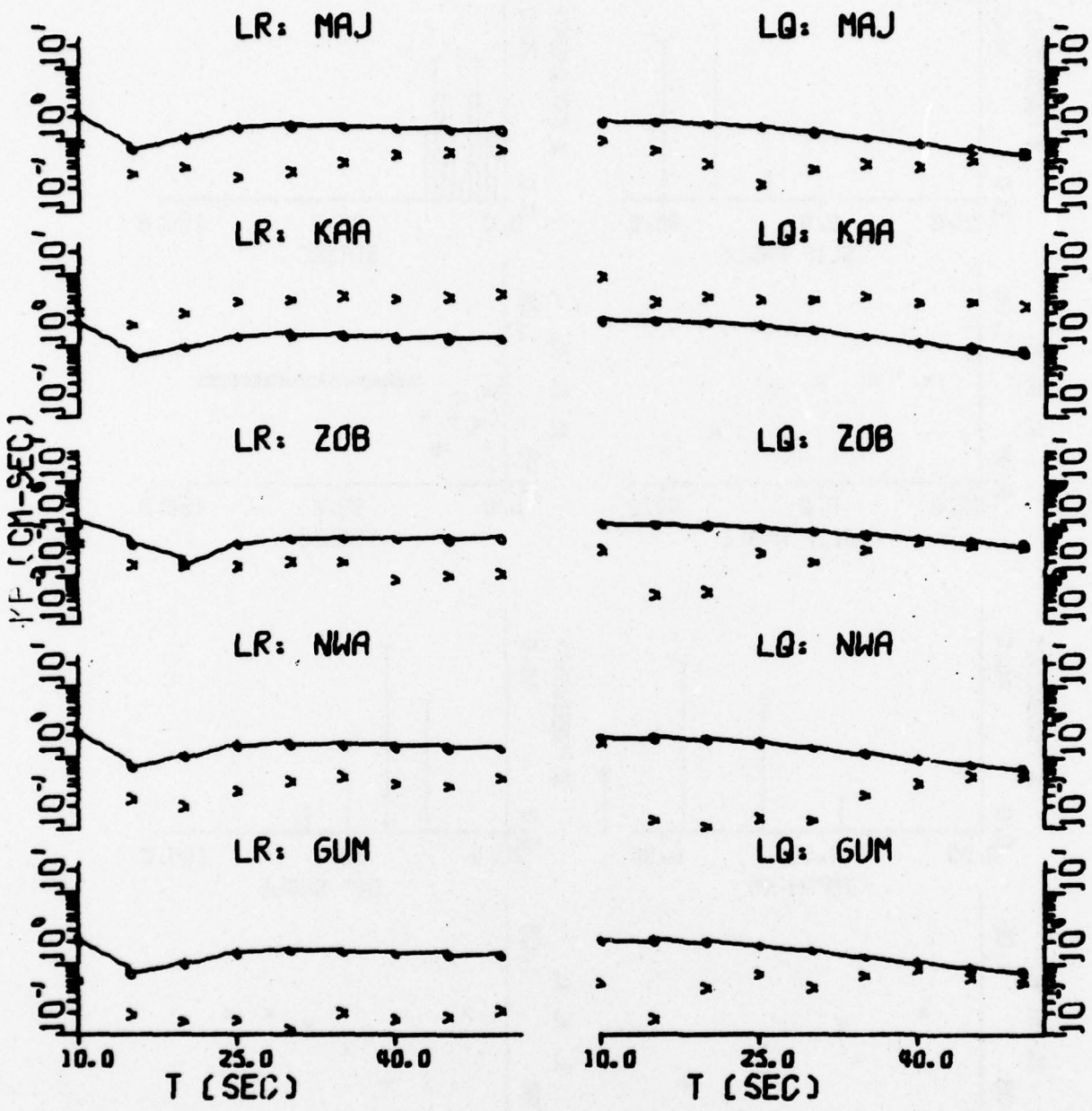

FIGURE IV-10

RESULTS FROM AMPLITUDE SPECTRAL FITTING: UZB/07/14/77
(PAGE 2 OF 2)

(a) Residual Distribution

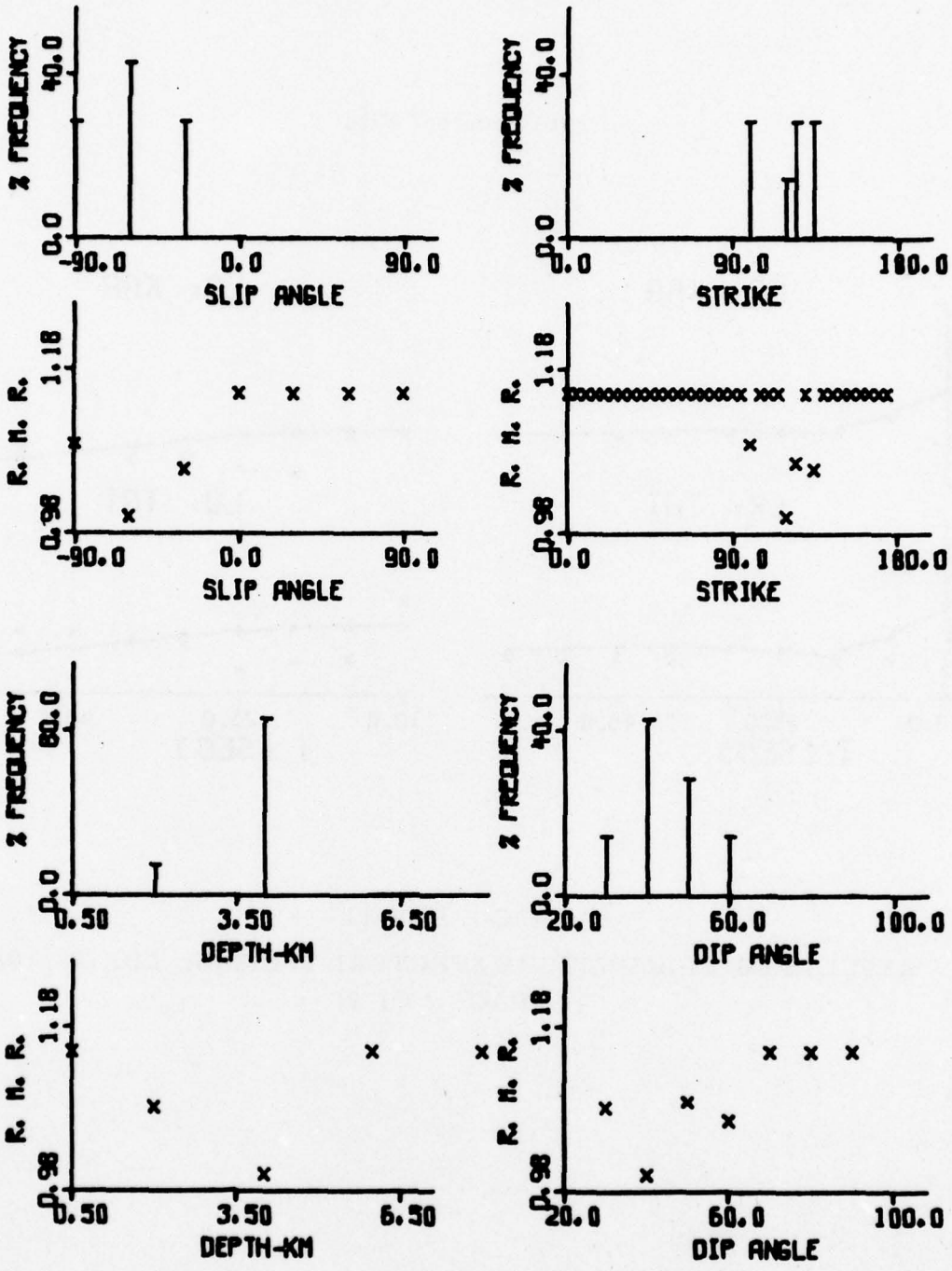

FIGURE IV-11

RESULTS FROM AMPLITUDE SPECTRAL FITTING: LBK/08/10/77
(PAGE 1 OF 2)

(b) Spectral Fits

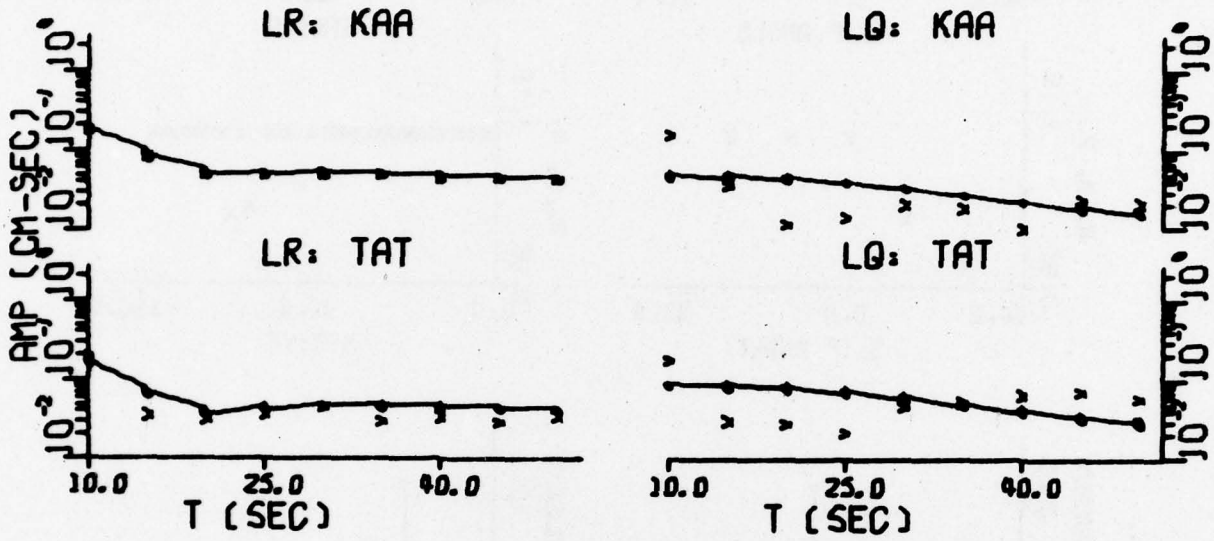

FIGURE IV-11

RESULTS FROM AMPLITUDE SPECTRAL FITTING: LBK/08/10/77
(PAGE 2 OF 2)

(a) Residual Distribution

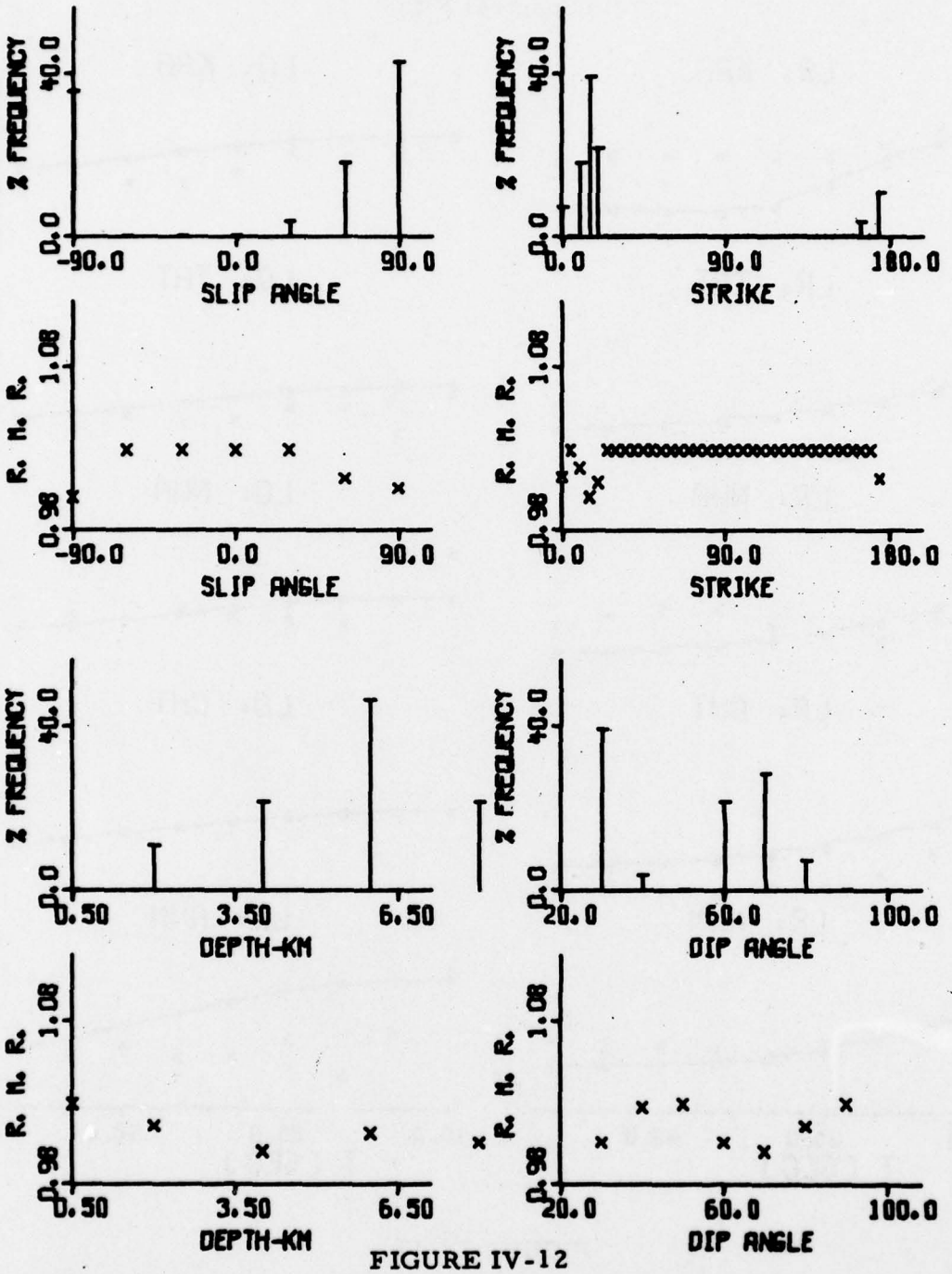

FIGURE IV-12

RESULTS FROM AMPLITUDE SPECTRAL FITTING: NVZ/09/01/77
(PAGE 1 OF 2)

(b) Spectral Fits

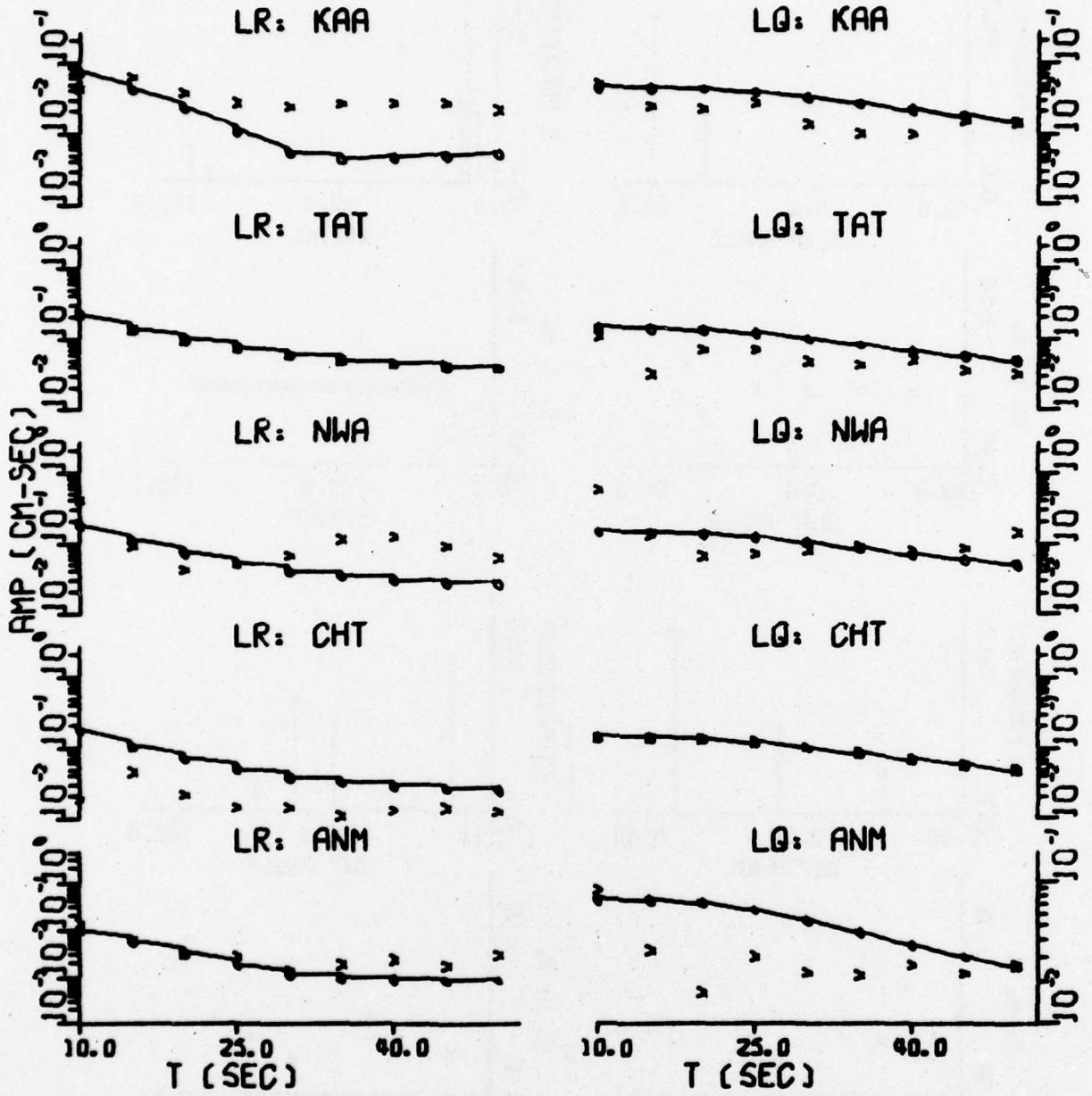

FIGURE IV-12

RESULTS FROM AMPLITUDE SPECTRAL FITTING: NVZ/09/01/77
(PAGE 2 OF 2)

For event LBR/08/10/77, the focal depth is located in the range of 2.0 to 4.0 km with the greatest possibility at 4.0 km. The focal depth obtained from bodywave depth phases is 2.0 km. Only two observation stations were available for this event; the best fit theoretical spectra followed quite closely the general shapes of their observed counterparts. And this yielded an oblique-slip fault mechanism with a strike direction of N120°E. The F-value is 0.6.

For event UZB/07/14/77, 8.0 km depth is given in Table IV-3. The spectral fits suggested a dip-slip mechanism with a strike angle of N40°E.

For event NVZ/09/01/77, as discussed previously, this event might be an explosion from Novaya Zemlya. The estimated focal depth is 4.0 km. The spectral fits yielded a dip-slip fault mechanism with a strike direction of N15°E. The estimated F-value is 0.1.

C. THE NTS EVENTS

For the selected NTS events, the estimations of source parameters based on the minimum-residual criterion are listed in Table IV-5. Those based on the residual minima frequency of occurrence distribution are listed in Table IV-6. The residual distributions with respect to estimated depth, dip angle, slip angle, and strike angle are given in Figure IV-13 to IV-15 with the spectral fit for each event.

According to Table IV-5, a dip-slip fault mechanism was suggested for these three events. The estimated focal depths are very shallow at 1.5 km for events NT1/317/76 and NTS/02/07/76. The strike angle estimates are quite close to the N-S direction as assumed by some authors (Toksöz, et al., 1965; Lambert, et al., 1972; Sun, 1977). From the estimated seismic moment, the event NTS/02/07/76 would be classified as an earthquake, and the reason for this is twofold. First, this event fell into the earthquake population of our M_E versus m_b plot, and secondly, the 4.5 km depth is indicated in the

TABLE IV-5

ESTIMATIONS OF SOURCE PARAMETERS OBTAINED BY AMPLITUDE SPECTRAL FITTING BASED ON THE MINIMUM-RESIDUAL CRITERION: SELECTED NTS EVENTS

Event I. D.	Optimal Soltuion						
	Depth h km	Dip Angle δ^o	Slip Angle λ^o	Strike $N\phi^oE$	Moment M_E 10^{25} dyne-cm	M_X	F
NTS/02/07/76	1.5	70	-90	25	0.133E00	0.665E-01	0.5
NTS/212/76	6.0	70	-90	160	0.419E00	0.105E00	0.25
NT1/317/76	1.5	40	-90	135	0.163E-01	0.203E-01	1.25

TABLE IV-6

ESTIMATIONS OF SOURCE PARAMETERS OBTAINED BY AMPLITUDE SPECTRAL FITTING BASED ON THE RESIDUAL DISTRIBUTIONS: SELECTED NTS EVENTS

Event I. D.	Source Parameters							
	Depth (h km)		Dip Angle (δ^{o})		Slip Angle (λ^{o})		Strike (Nϕ^{o}E)	
	Probable Range	% Frequency	Probable Range	% Frequency	Probable Range	% Frequency	Probable Range	% Frequency
NTS/02/07/76	0.5~1.5	100	60~90	60	-90~-30	67	20~50	75
NTS/212/76	2.5~6.0	100	50~70	60	-90~-30	40	150~160	60
NT1/317/76	0.5~1.5	100	40~60	84	-90~-60	100	130~135	100

(a) Residual Distribution

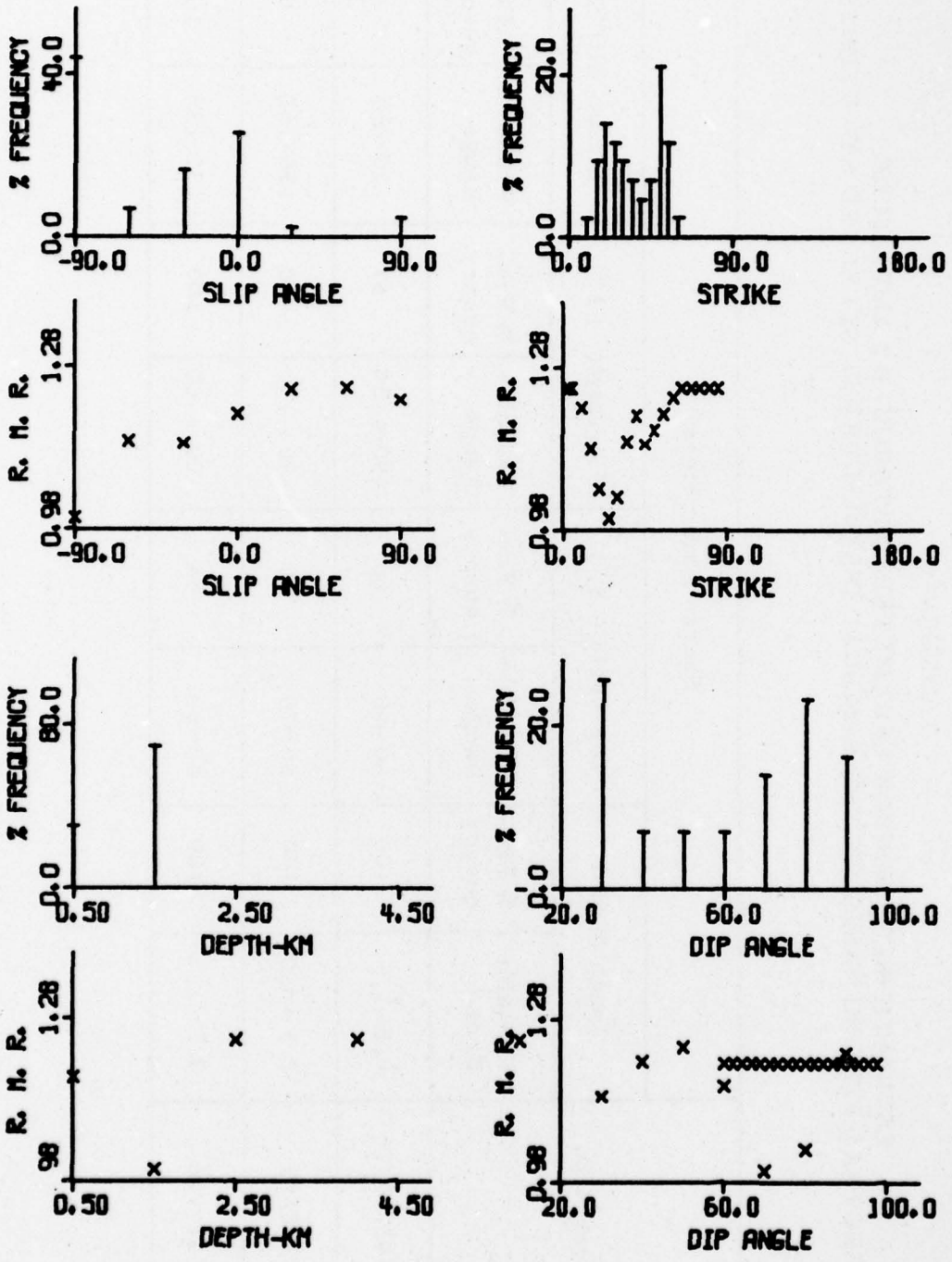

FIGURE IV-13

RESULTS FROM AMPLITUDE SPECTRAL FITTING: NTS/02/07/76
(PAGE 1 OF 2)

(b) Spectral Fits

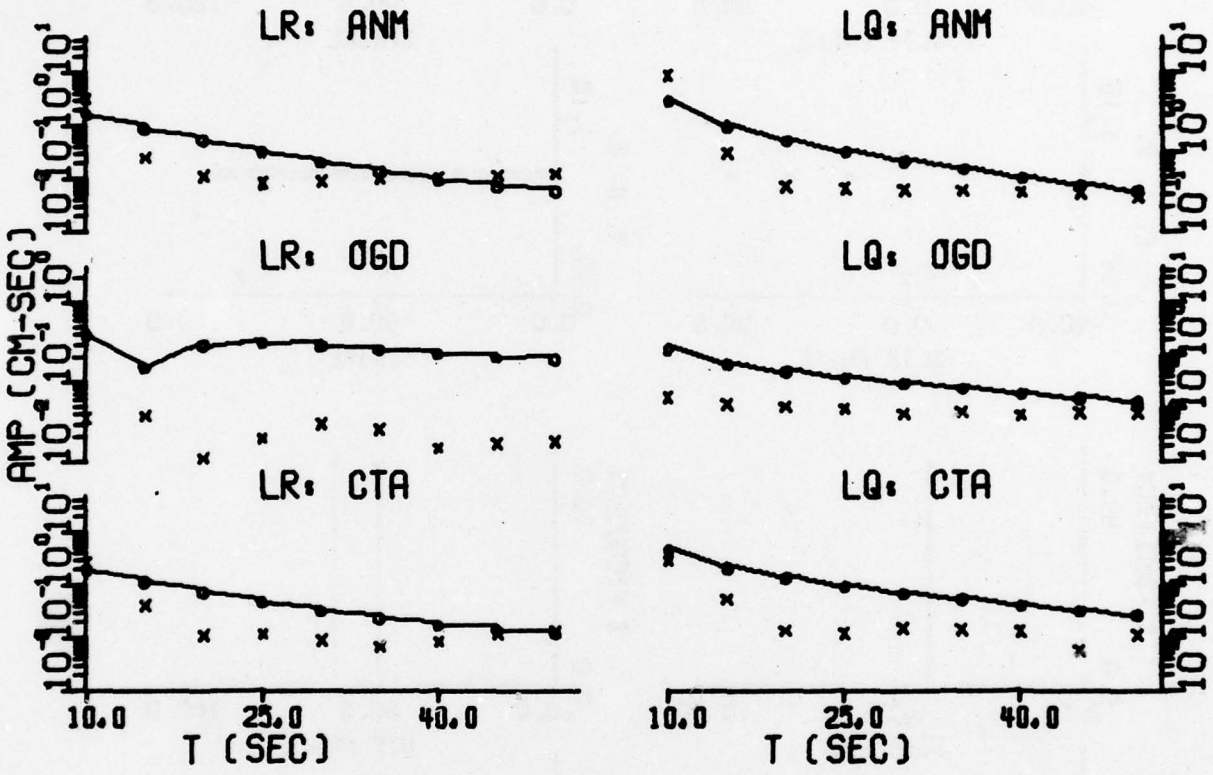

FIGURE IV-13

RESULTS FROM AMPLITUDE SPECTRAL FITTING: NTS/02/07/76
(PAGE 2 OF 2)

(a) Residual Distribution

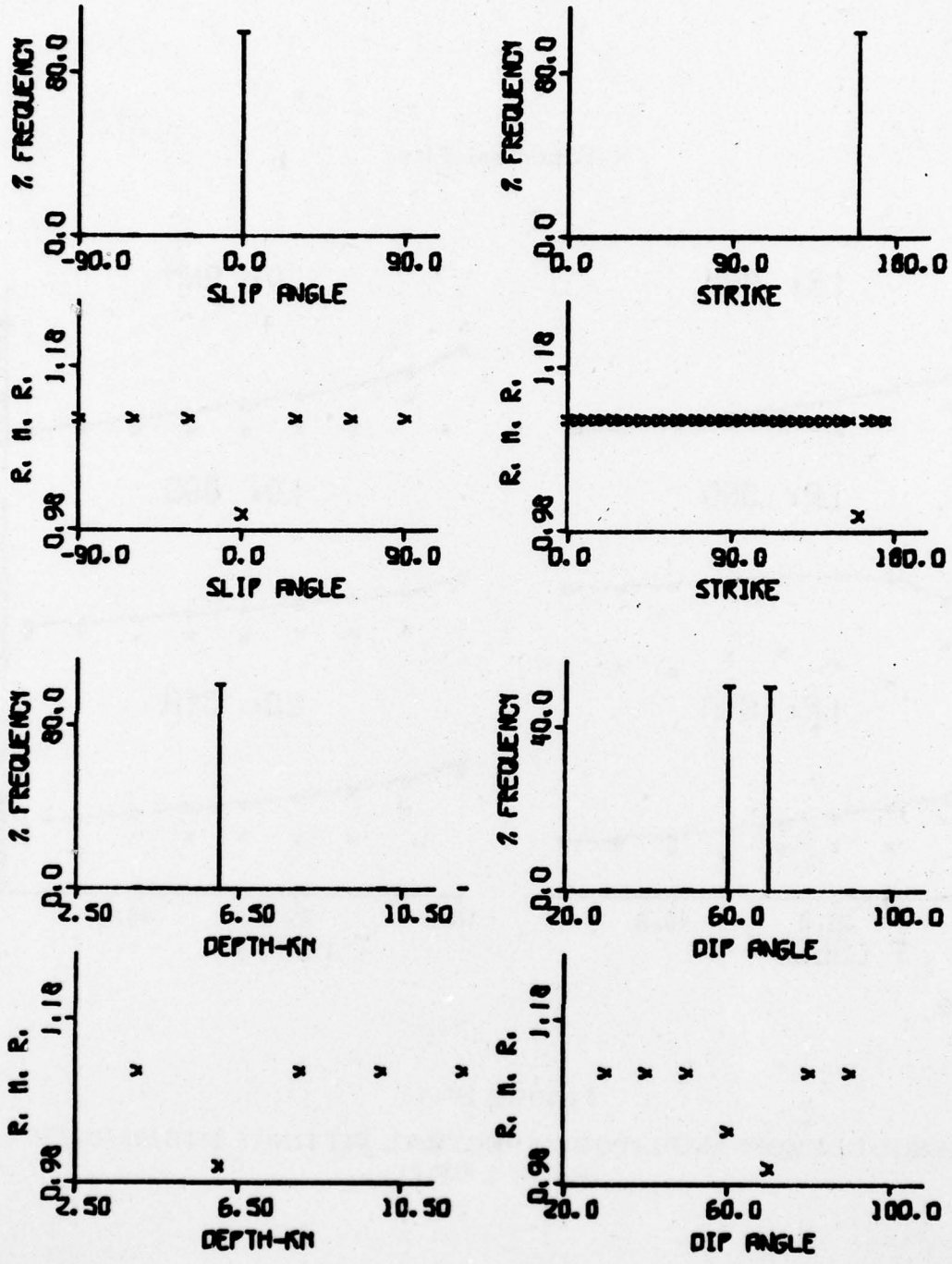

FIGURE IV-14

RESULTS FROM AMPLITUDE SPECTRAL FITTING: NTS/212/76
(PAGE 1 OF 2)

(b) Spectral Fits

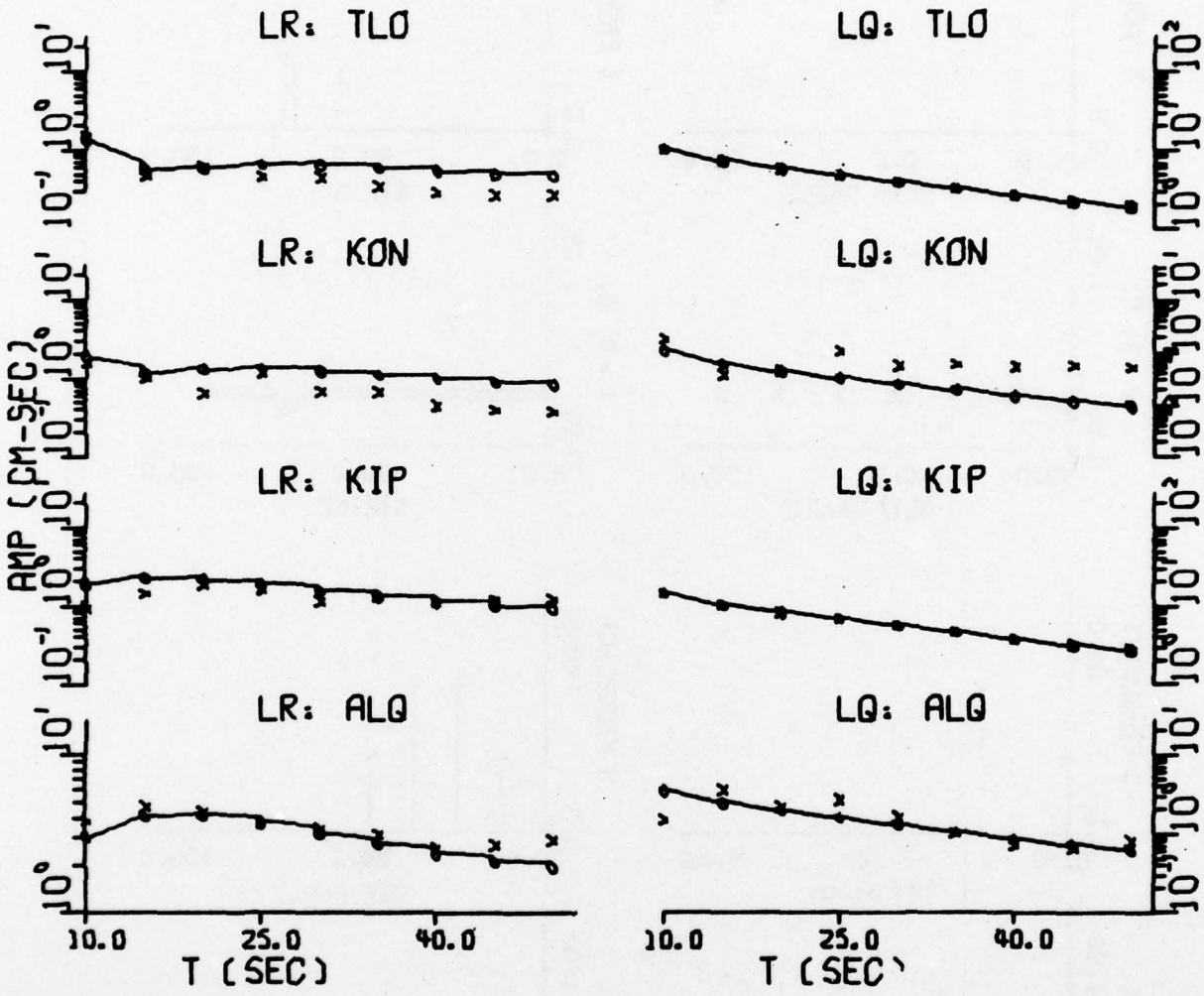

FIGURE IV-14

RESULTS FROM AMPLITUDE SPECTRAL FITTING: NTS/212/76
(PAGE 2 OF 2)

(a) Residual Distribution

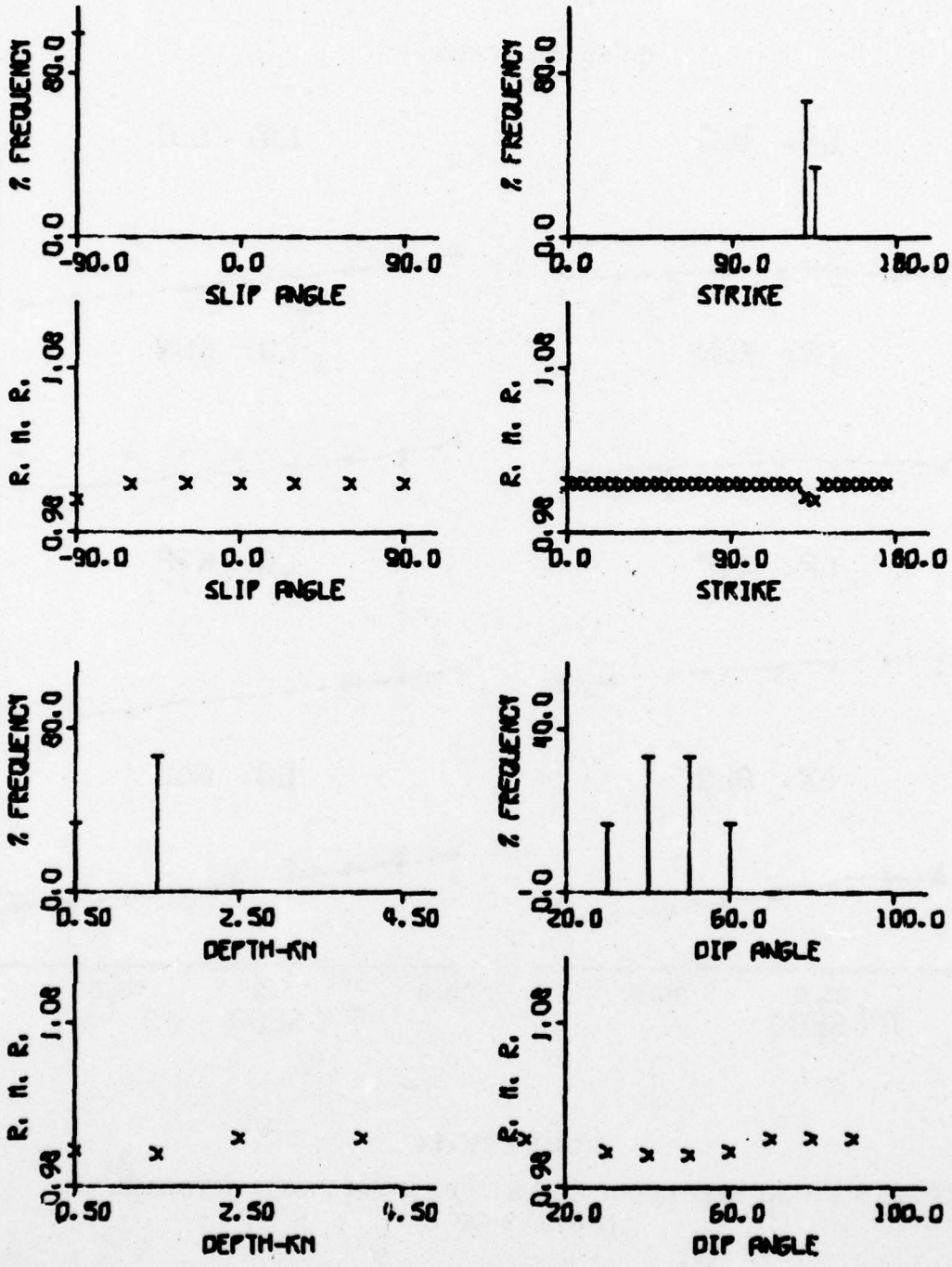

FIGURE IV-15

RESULTS FROM AMPLITUDE SPECTRAL FITTING: NT1/317/76
(PAGE 1 OF 2)

(b) Spectral Fits

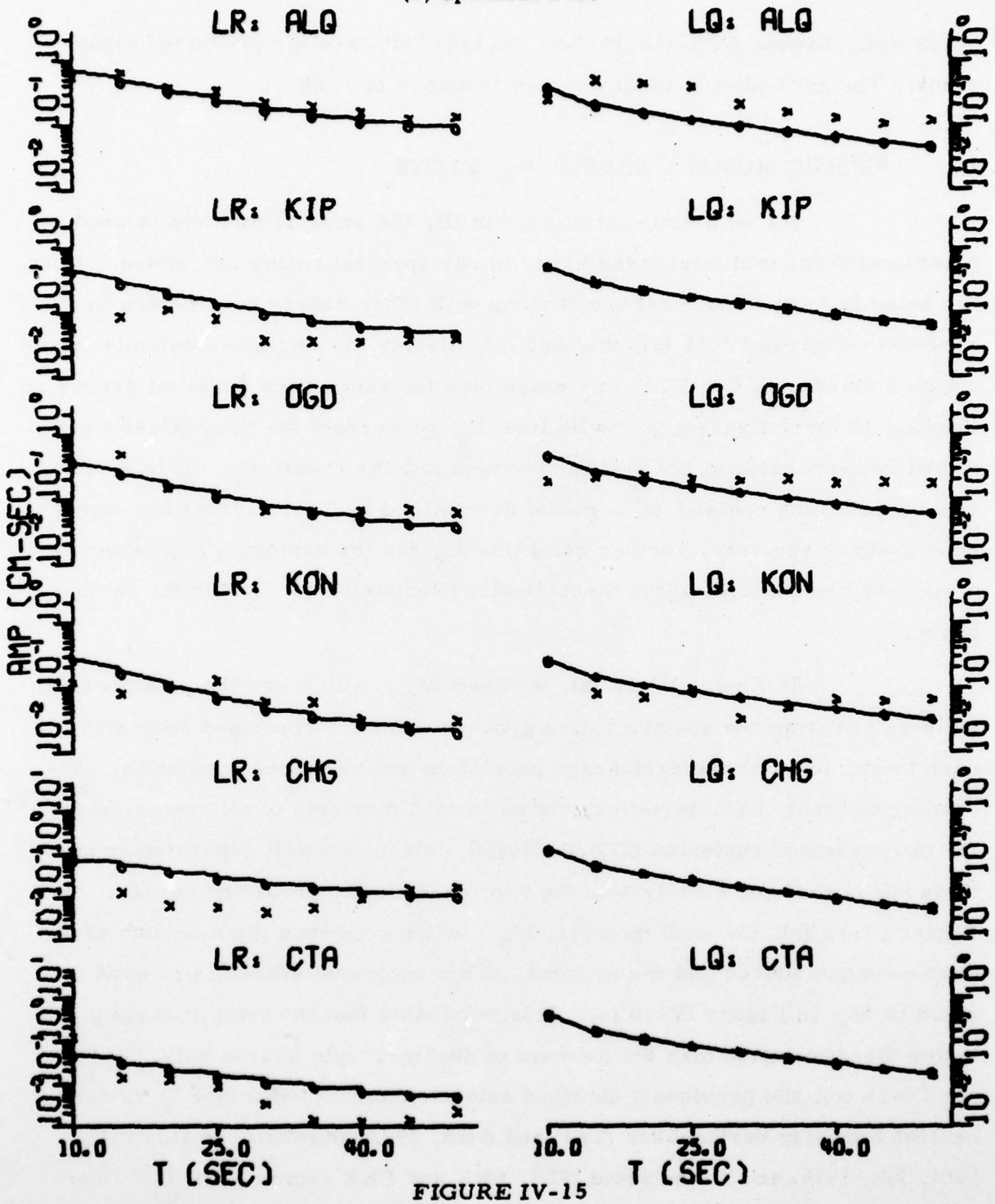

FIGURE IV-15

RESULTS FROM AMPLITUDE SPECTRAL FITTING: NT1/317/76
(PAGE 2 OF 2)

NEIS list. Events NTS/212/76 and NT1/317/76 are the presumed explosions. The estimated F-values varied from 0.5 to 1.25.

D. SEISMIC MOMENT VERSUS m_b PLOTS

As we mentioned in Section III, the seismic moment is used as a parameter for minimizing the error in our spectral fitting procedure. Thus, the seismic moment is determined along with other source parameters in the process. Figures IV-16 (a), (b), and (c), display the estimated seismic moment as a function of the NEIS m_b magnitude for each of the different groups of events. In these figures, the solid line L_E represents the theoretically predicted relation between the seismic moment and the event m_b. This relation was based on the revised ω^2 - model determined by Tsai (1972a) for earthquake source spectra. Another solid line L_X for the explosion population is a straight line parallel to the theoretically predicted line L_E for the earthquake.

In Figure IV-16 (a), we used M_E, which was the seismic moment obtained from the spectra fitting process using the combined source for each event, for both the earthquake population and explosion population. According to event characteristics, the estimated moments of all events except for the presumed explosion EKZ/06/29/77, fell in two well separated populations and correlated closely with the two theoretically predicted curves. In Figure IV-16 (b), the total moment, M_T, which combined the moment of the double-couple source and the moment of the explosive source, was used in stead of M_E in Figure IV-16 (a). It is noticeable that the total moment gives better discrimination than the moment of double-couple source only. In Figure IV-16 (c), the previously obtained seismic moment estimates of various central Eurasian earthquakes (Tsai and Shen, 1972; Turnbull, et al., 1973, 1974; Sun, 1976) and the selected NTS, EKZ and PNE events (Sun, 1977) were merged into Figure IV-16 (a) to yield this plot. The legend on the left corner

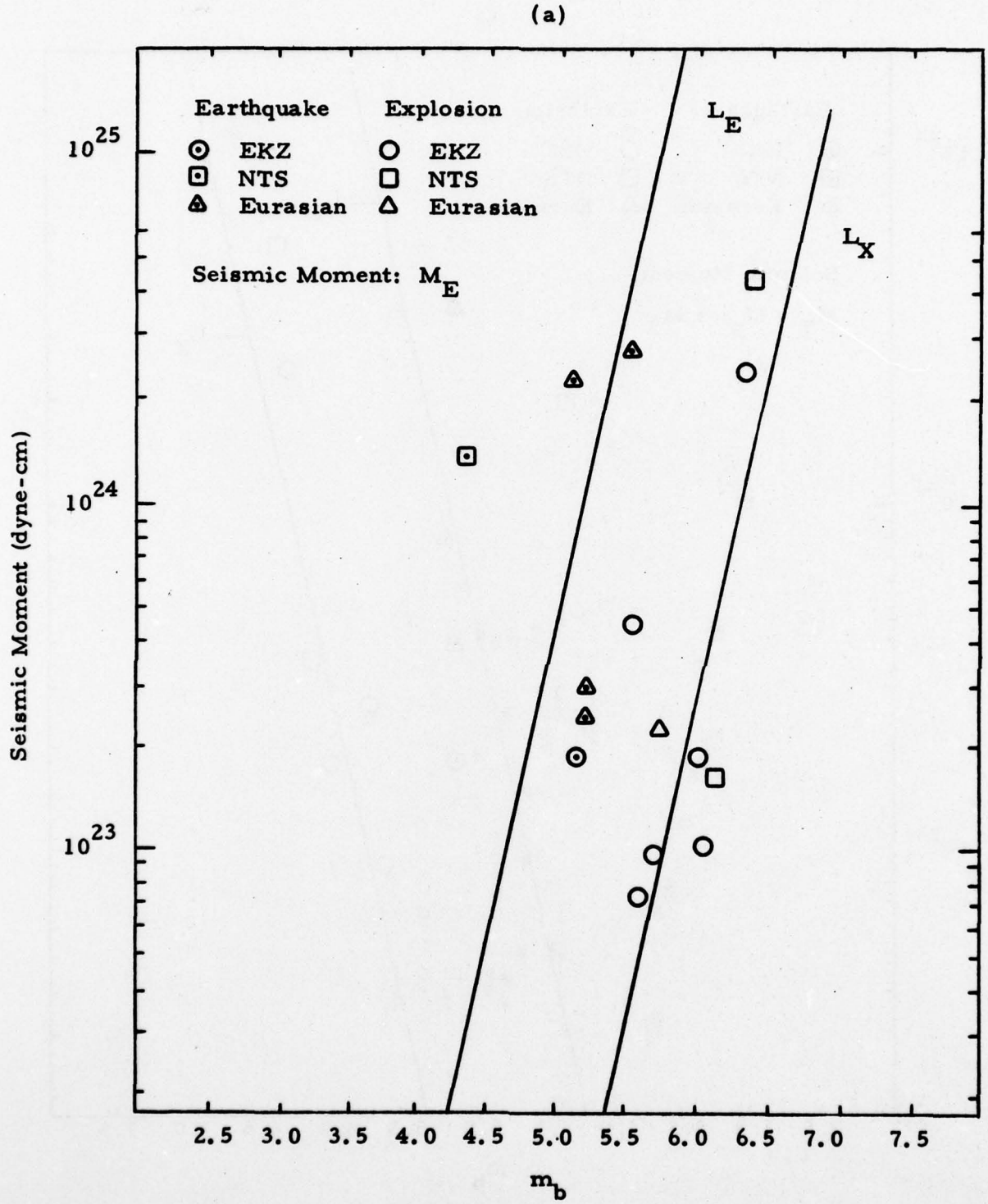

FIGURE IV-16

SEISMIC MOMENT VERSUS m_b PLOT
(PAGE 1 OF 3)

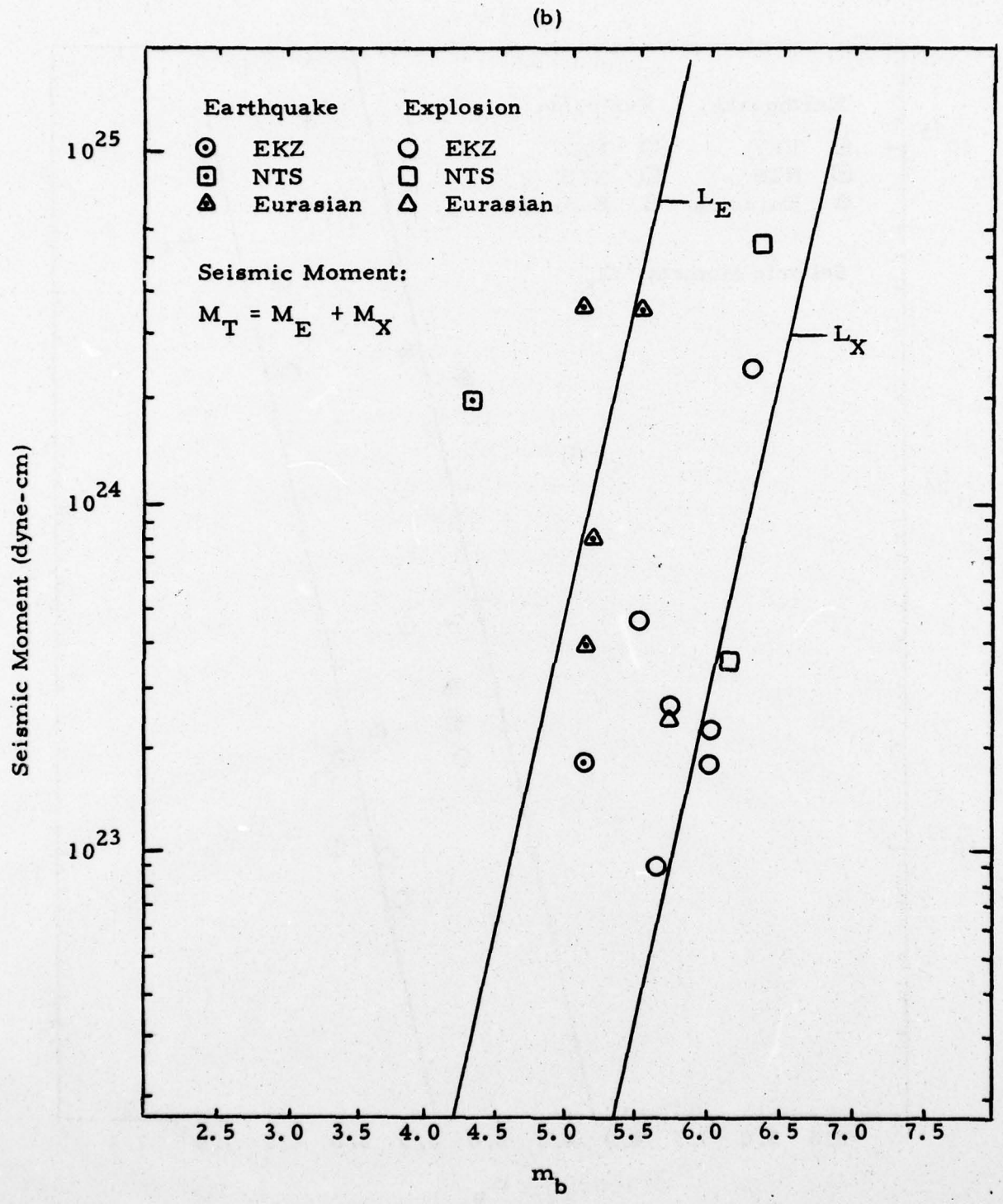

FIGURE IV-16

SEISMIC MOMENT VERSUS m_b PLOT
(PAGE 2 OF 3)

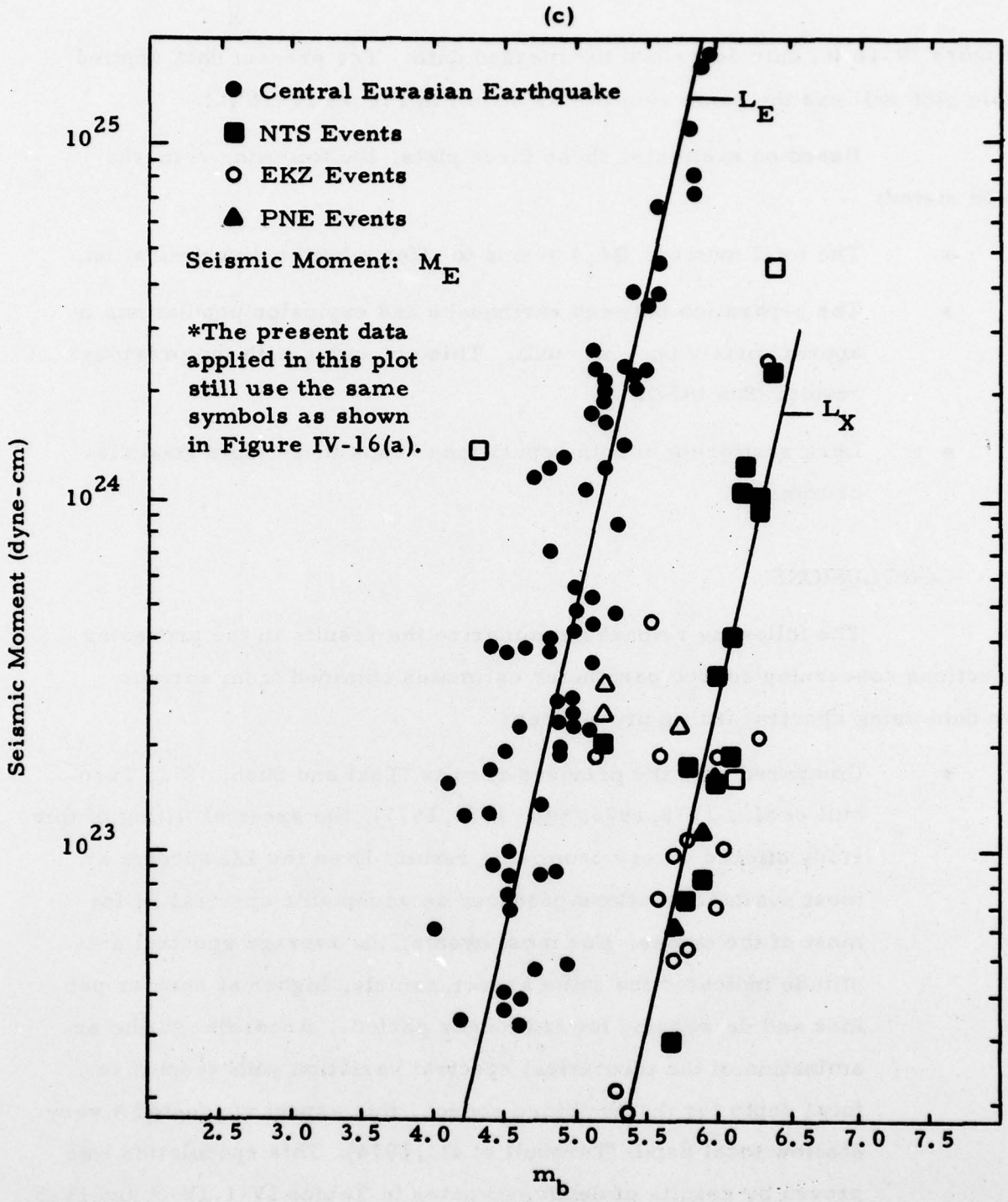

FIGURE IV-16

SEISMIC MOMENT VERSUS m_b PLOT
(PAGE 3 OF 3)

of Figure IV-16 (c) only described the merged data. The present data applied in this plot still use the same symbols as shown in Figure IV-16 (a).

Based on examining these three plots, the following remarks can be stated:

- The total moment (M_T) seems to offer a better discrimination.
- The separation between earthquake and explosion populations is approximately one m_b unit. This coincides with the previous results (Sun 1977).
- Less scattering in both populations keeps these plots good discriminants.

E. CONCLUSIONS

The following remarks summarize the results in the preceding subsections concerning source parameter estimates obtained from surface wave data using spectral fitting procedures:

- Compared with the previous results (Tsai and Shen, 1972; Turnbull et al., 1973, 1974; Sun, 1976, 1977), the spectral fitting of this study offered a very promising result. Even the LQ spectra at most available stations produced an acceptable spectral fit for most of the events. For most events, the average spectral amplitude indicated the same aspect, namely, higher at shorter periods and decreasing toward longer periods. According to the examination of the theoretical spectral variation with respect to focal depth for the combined source, this aspect suggested a very shallow focal depth (Turnbull et al., 1974). This speculation was proven by results of depth estimates in Tables IV-1, IV-3, and IV-5.
- Figure IV-17 shows the percentage of events occurring at each estimated slip angle of the double-couple source of tectonic

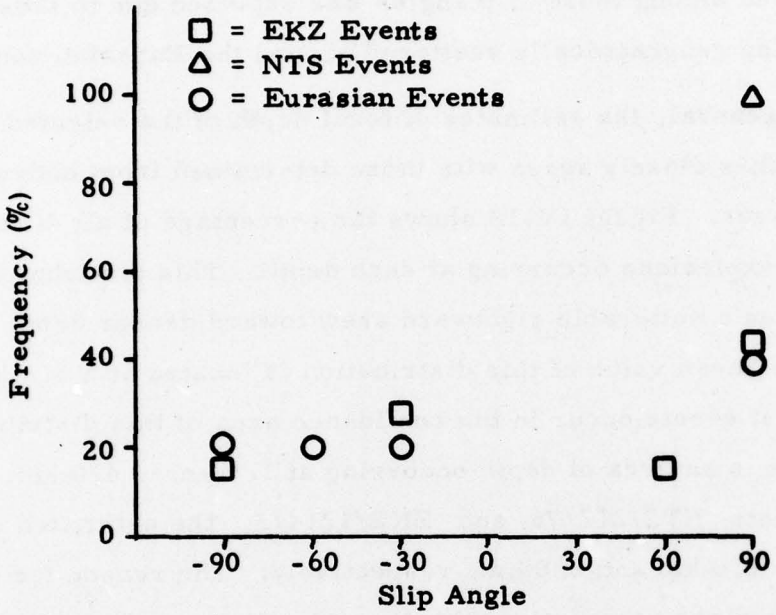

FIGURE IV-17

THE FREQUENCY DISTRIBUTIONS OF THREE GROUPS OF EVENTS AT EACH SLIP ANGLE

strain release. All three of the NTS events were indicated as dip slip. For the EKZ events and Eurasian events, the results are mixed with no difference of mechanism discernable between both sets of events. For Eurasian events, obviously no general trend among those slip angles was expected due to these events being geographically scattered around the Eurasian continent.

- In general, the estimates of focal depth of the selected earthquakes closely agree with those determined from bodywave depth phases. Figure IV-18 shows the percentage of all of the presumed explosions occurring at each depth. This distribution indicates a noticeable rightward skew toward deeper depth estimates. The mean value of this distribution is located at a 3.5 km depth. Most events occur in the confidence area of this distribution; that is an area of depth occurring at 1.5 km to 4.0 km. For events NTS/212/76 and EKZ/1214/3, the estimated depths are 6.0 km and 8.0 km, respectively. The reason for this might be a close association with irregularities in crustal structure and hence, with anomalous crustal rigidity or strength right beneath the shot point.

- Figure IV-19 shows the percentage of total events, total explosions, and EKZ events occurring at each dip angle. The mean values and standard deviations of these three distributions are shown in Table IV-7. According to Table IV-7 and Figure IV-19, the estimates of dip angle of nine explosions most likely occur between 40° to 50°. This kind of consistency might imply that the explosion can induce structure rupture along the planes of maximum shear stress which usually are oriented around 45°.

- Figure IV-20 shows the percentage of explosions and earthquakes at each F-value. No consistency between the explosion population

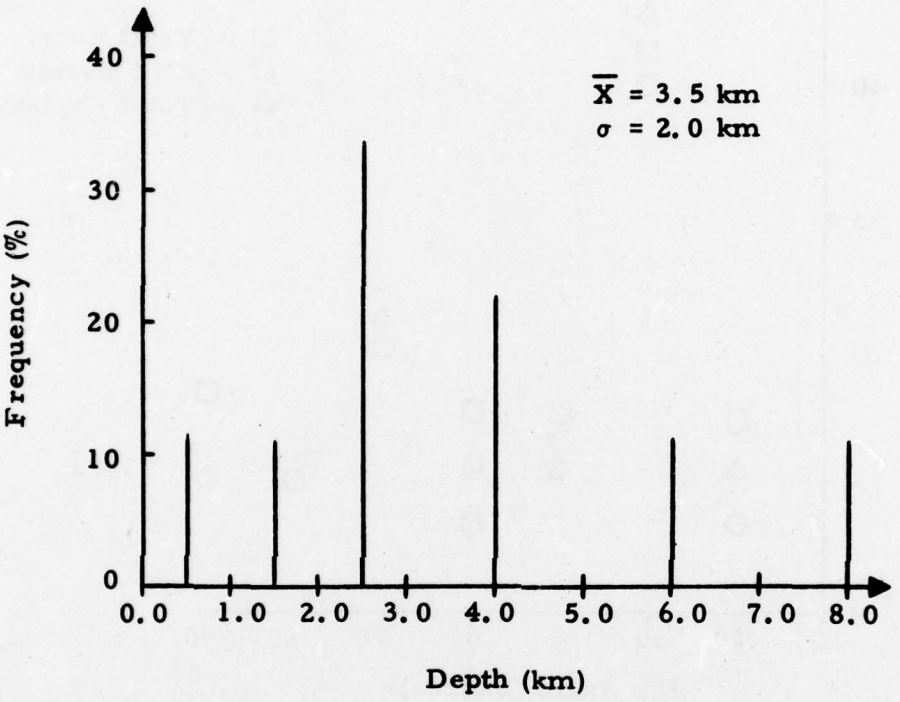

FIGURE IV-18

THE FREQUENCY DISTRIBUTION OF THE SELECTED EXPLOSIONS AT EACH DEPTH

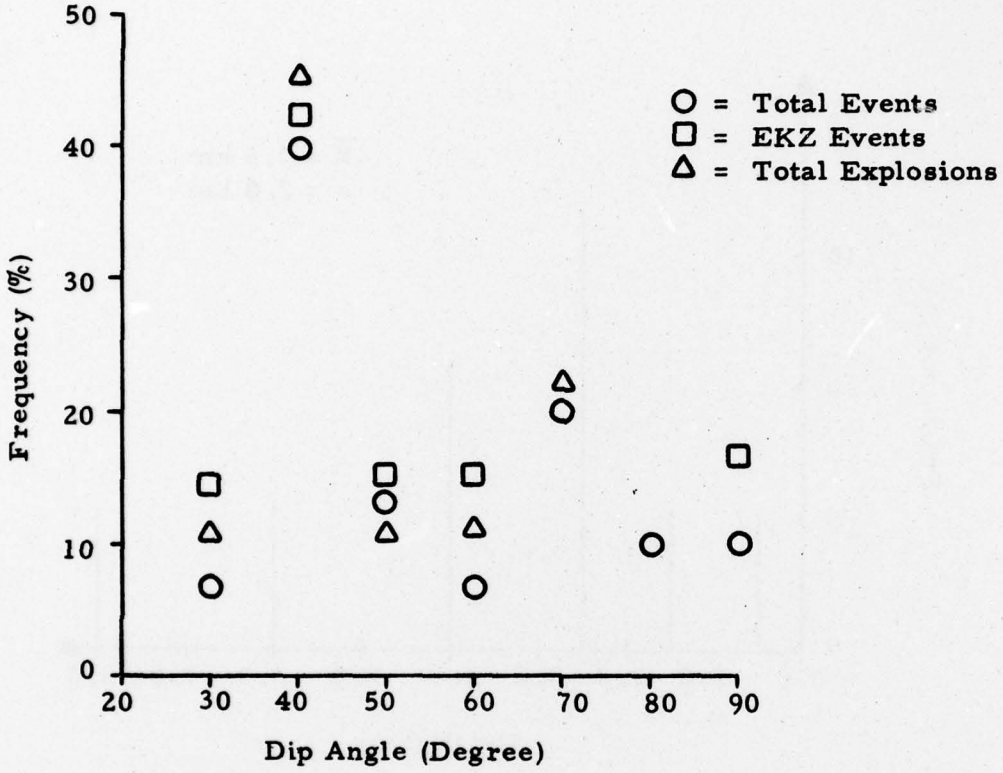

FIGURE IV-19

THE FREQUENCY DISTRIBUTIONS
OF TOTAL EVENTS, EXPLOSIONS,
AND EKZ EVENTS AT EACH DIP ANGLE

TABLE IV-7

MEAN VALUES AND STANDARD DEVIATIONS CORRESPONDING TO THE DIP ANGLES OF FIGURE IV-19

		Mean Value (Degree)	Standard Deviation (Degree)
Total Events	O	60	± 18.4
EKZ Events	□	50	± 18.5
Total Explosions	Δ	48.8	± 13.5

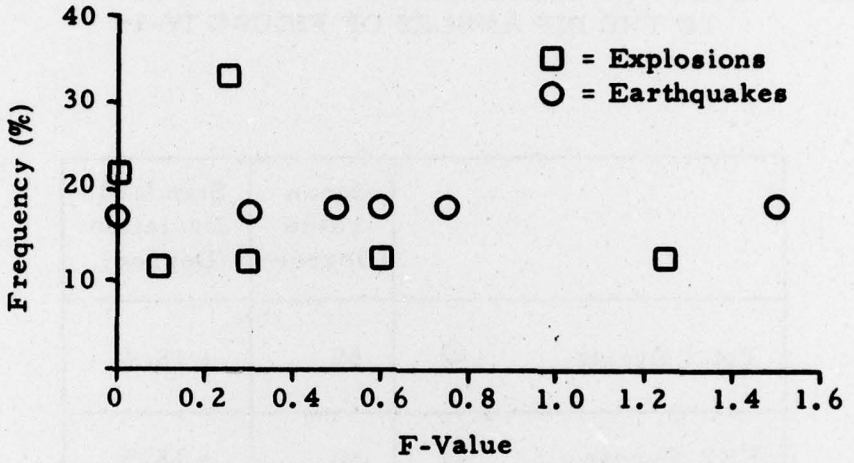

FIGURE IV-20

THE FREQUENCY DISTRIBUTIONS OF
EXPLOSIONS AND EARTHQUAKES AT EACH F-VALUE

and the earthquake population has been found. In general, the estimates of F-value of explosions are smaller than those of earthquakes. This result is quite different from what we expected. The large F-value of earthquakes, especially for the two deeper events ECU/02/03/72 and TZK/03/17/72, might be caused by the volume change during the rupture at deep focal depth. This change usually favors an explosive point source. The small F-value of explosions means that the double-couple source is dominant at the periods considered. The association of higher F-values with deeper earthquakes suggests that a higher dilatational component is required to overcome the overburden pressure. The lack of dilatation of explosions, random strike and deeper focus suggests that the double-couple source of explosions may be associated with large dislocations on a fracture zone surrounding the source. Radiation from the deeper part of the fracture zone is more visible due to the effect of the free surface. Compared with the previous results (Sun, 1977), less consistency and small values of the estimates of F-value have been found in this study. The reason for this difference is that we used the binary method to search through wider ranges and finer increments of parameters such as depth, F-value, and strike angle, without any constraint. Also, Sun's results were obtained by apparently limiting the search for minimum residual F-values to values greater than one. This explains his numerous occurrences of F=1 as edge phenomena in the exhaustive search.

SECTION V
RECOMMENDATIONS

It is recommended that future studies be directed toward the following points:

- Confirm the apparently universal surface wave moment versus m_b relationship with a much larger data base of earthquakes and explosions.
- Evaluate surface wave moment as a scaling parameter for estimating yields of explosions.
- Evaluate the sensitivity of source mechanism solutions to the distribution of stations and path corrections.
- Check the consistency of combined source mechanisms on a large earthquake and aftershock sequence.
- Develop feasible procedures for applying the combined source mechanism as an extended event identification technique.

SECTION VI
REFERENCES

Alexander, S. S., 1963; Surface Wave Propagation in the Western United States, Ph.D. Thesis, California Institute of Technology, Pasadena, California.

Ben-Menahem, A. and D. G. Harkrider, 1964; Radiation Patterns of Seismic Surface Waves from Buried Dipolar Point Source in a Flat Stratified Earth, J. Geophys. Res., 69, 2605-2620.

Harkrider, D. G., 1964; Surface Waves in Multilayered Elastic Media: I. Rayleigh and Love Waves from Buried Sources in A Multilayered Elastic Half-Space, Bull. Seismol. Soc. Am., 54, 627-680.

Lambert, D. G., A. I. Tolstoy, and E. S. Becker, 1974; Seismic Detection and Discrimination Capabilities of the Very Long-Period Experiment - Final Report; Technical Report No. 7, Texas Instruments Report No. ALEX (01)-TR-74-07, AFTAC Contract Number F08606-74-C-0033, Texas Instruments Incorporated, Dallas, TX.

Schmidt, A. W., and K. S. Wilson, 1977; Seismic Data Preparation Procedures; Technical Report No. 10, Texas Instruments Report No. ALEX(01)-TR-77-10, AFTAC Contract Number F08606-77-C-0004, Texas Instruments Incorporated, Dallas, TX.

Strauss, A. C., and L. C. Weltman, 1977; Continuation of the Seismic Research Observatories Evaluation; Technical Report No. 2, Texas Instruments Report No. ALEX(01)-TR-77-02, AFTAC Contract Number F08606-77-C-0004, Texas Instruments Incorporated, Dallas, TX.

Sun, D. 1977; Determination of Seismic Source Parameters from Long-Period Surface Wave Data; Technical Report No. 11, Texas Instruments Report

No. ALEX(01)-TR-77-11, AFTAC Contract Number F08606-77-C-0004, Texas Instruments Incorporated, Dallas, TX.

Sun, D., 1976; Source Studies in the Near- and Far-field, Semi-Annual Technical Report No. 6 Part A, Texas Instruments Report No. ALEX(02)-TR-76-01-Part A, AFOSR Contract Number F44620-73-C-0055, Texas Instruments Incorporated, Dallas, TX.

Sun, D. and J. S. Shaub, 1977; Analysis of Seismic Surface Waves Using PDP-15 Interactive Graphics, Proc. of the International Symposium on Computer Aided Seismic Analysis and Discrimination, Falmouth, Massachusetts.

Toksöz, M. N., A. Ben-Menahem, and D. G. Harkrider, 1964; Determination of Source Parameters of Explosions and Earthquakes by Amplitude Equalification of Seismic Surface Waves: 1. Underground Nuclear Explosions, J. Geophys. Res., 69, 4355-4366.

Tryggvason, E., 1965; Dissipation of Rayleigh Wave Energy, J. Geophys. Res., 70, 1449-1455.

Tsai, Y. B., 1972a; Utility of Tsai's Method for Seismic Discrimination; Semi-Annual Technical Report No. 1, AFOSR Contract Number F44620-71-C-0112, Texas Instruments Incorporated, Dallas, TX.

Tsai, Y. B., 1972b; Utility of Tsai's Method for Seismic Discrimination; Semi-Annual Technical Report No. 2, AFOSR Contract Number F44620-71-C-0112, Texas Instruments Incorporated, Dallas, TX.

Tsai, Y. B. and K. Aki, 1969; Simultaneous Determination of the Seismic Moment and Attenuation of Seismic Surface Waves, Bull. Seismol. Soc. Am., 59, 275-287.

Tsai, Y. B. and K. Aki, 1970; Precise Focal Depth Determination from Amplitude Spectra of Surface Wave, J. Geophys. Res., 75, 5729-5743.